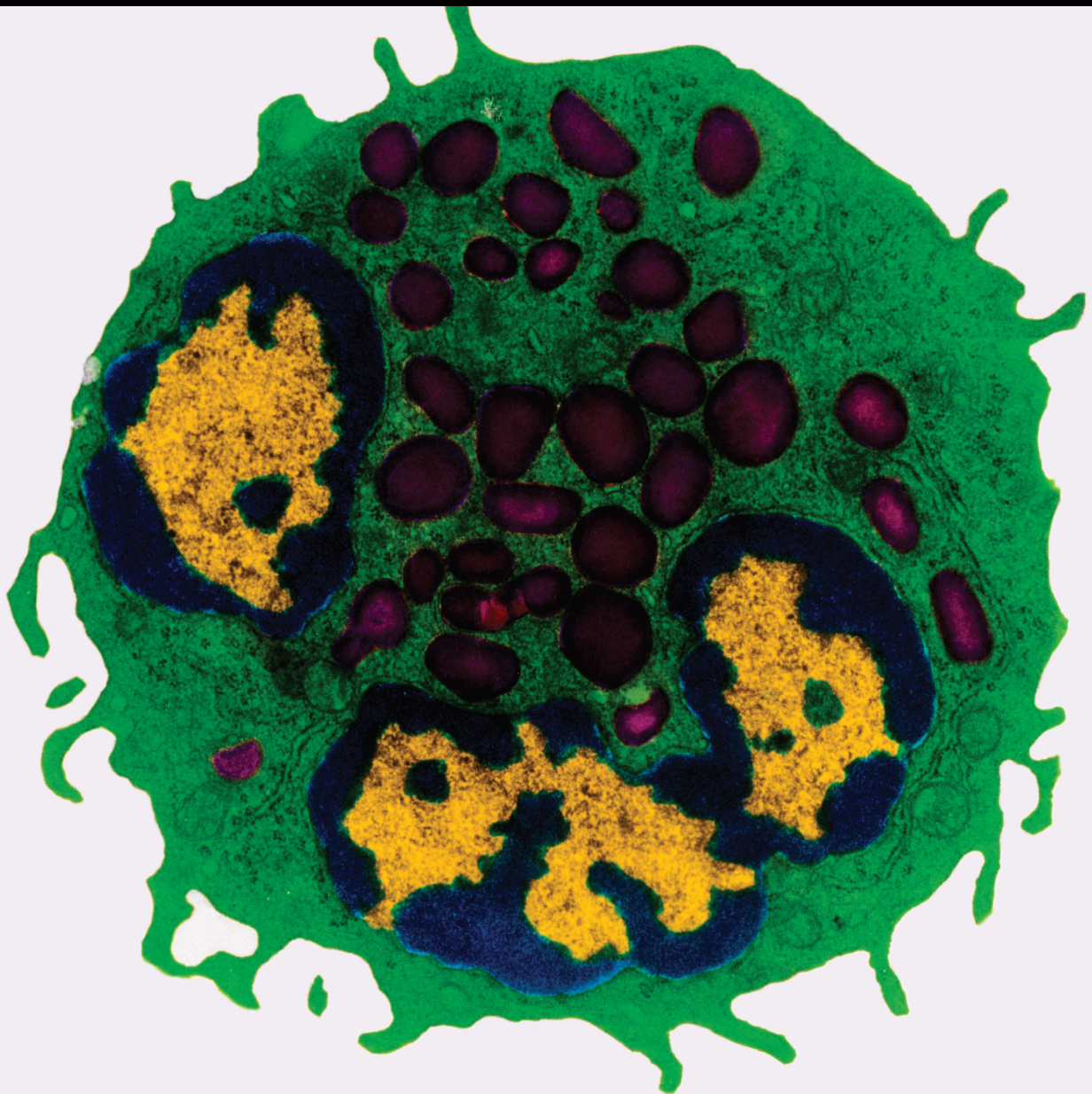


Inflammation in Musculoskeletal Diseases

Lead Guest Editor: Zhenhan Deng

Guest Editors: Chaofan Zhang, Fangjie Zhang, Yusheng Li, and Zeyu Huang





Inflammation in Musculoskeletal Diseases

Mediators of Inflammation

Inflammation in Musculoskeletal Diseases

Lead Guest Editor: Zhenhan Deng

Guest Editors: Chaofan Zhang, Fangjie Zhang,
Yusheng Li, and Zeyu Huang



Copyright © 2021 Hindawi Limited. All rights reserved.

This is a special issue published in “Mediators of Inflammation.” All articles are open access articles distributed under the Creative Commons Attribution License, which permits unrestricted use, distribution, and reproduction in any medium, provided the original work is properly cited.

Chief Editor

Anshu Agrawal , USA

Associate Editors

Carlo Cervellati , Italy
Elaine Hatanaka , Brazil
Vladimir A. Kostyuk , Belarus
Carla Pagliari , Brazil

Academic Editors

Amedeo Amedei , Italy
Emiliano Antiga , Italy
Tomasz Brzozowski , Poland
Daniela Caccamo , Italy
Luca Cantarini , Italy
Raffaele Capasso , Italy
Calogero Caruso , Italy
Robson Coutinho-Silva , Brazil
Jose Crispin , Mexico
Fulvio D'Acquisto , United Kingdom
Eduardo Dalmarco , Brazil
Agnieszka Dobrzyn, Poland
Ulrich Eisel , The Netherlands
Mirvat El-Sibai , Lebanon
Giacomo Emmi , Italy
Claudia Fabiani , Italy
Fabíola B Filippin Monteiro , Brazil
Antonella Fioravanti , Italy
Tânia Silvia Fröde , Brazil
Julio Galvez , Spain
Mirella Giovarelli , Italy
Denis Girard, Canada
Markus H. Gräler , Germany
Oreste Gualillo , Spain
Qingdong Guan , Canada
Tommaso Iannitti , United Kingdom
Byeong-Churl Jang, Republic of Korea
Yasumasa Kato , Japan
Cheorl-Ho Kim , Republic of Korea
Alex Kleinjan , The Netherlands
Martha Lappas , Australia
Ariadne Malamitsi-Puchner , Greece
Palash Mandal, India
Joilson O. Martins , Brazil
Donna-Marie McCafferty, Canada
Barbro N. Melgert , The Netherlands

Paola Migliorini , Italy
Vinod K. Mishra , USA
Eeva Moilanen , Finland
Elena Niccolai , Italy
Nadra Nilsen , Norway
Sandra Helena Penha Oliveira , Brazil
Michal A. Rahat , Israel
Zoltan Rakonczay Jr. , Hungary
Marcella Reale , Italy
Emanuela Roscetto, Italy
Domenico Sergi , Italy
Mohammad Shadab , USA
Elena Silvestri, Italy
Carla Sipert , Brazil
Helen C. Steel , South Africa
Saravanan Subramanian, USA
Veendamali S. Subramanian , USA
Taina Tervahartiala, Finland
Alessandro Trentini , Italy
Kathy Triantafilou, United Kingdom
Fumio Tsuji , Japan
Maria Letizia Urban, Italy
Giuseppe Valacchi , Italy
Kerstin Wolk , Germany
Soh Yamazaki , Japan
Young-Su Yi , Republic of Korea
Shin-ichi Yokota , Japan
Francesca Zimetti , Italy

Contents

Butyrate Inhibits Osteoclast Activity *In Vitro* and Regulates Systemic Inflammation and Bone Healing in a Murine Osteotomy Model Compared to Antibiotic-Treated Mice

Alexandra Wallimann , Walker Magrath , Brenna Pugliese , Nino Stocker , Patrick Westermann , Anja Heider, Dominic Gehweiler , Stephan Zeiter , Marcus J. Claesson , R. Geoff Richards , Cezmi A. Akdis , Christopher J. Hernandez , Liam O'Mahony , Keith Thompson , and T. Fintan Moriarty 

Research Article (17 pages), Article ID 8817421, Volume 2021 (2021)

Systemic Inflammatory Markers for Predicting Overall Survival in Patients with Osteosarcoma: A Systematic Review and Meta-Analysis

Xiaotong Song, Hao Zhang, Fanxing Yin, Panpan Guo, Xiaocheng Yang, Jinzhu Liu, Yanshuo Han , and Zhaozhou Ren 

Review Article (16 pages), Article ID 3456629, Volume 2021 (2021)

The Upregulation of COX2 in Human Degenerated Nucleus Pulposus: The Association of Inflammation with Intervertebral Disc Degeneration

Chang Liu, Guoyan Liang, Zhantao Deng, Jing Tan, Qiuqian Zheng, and Feng-Juan Lyu 

Research Article (10 pages), Article ID 2933199, Volume 2021 (2021)

Tryptophan-Kynurenine Pathway in COVID-19-Dependent Musculoskeletal Pathology: A Minireview

Sagar Vyavahare, Sandeep Kumar, Nicholas Cantu, Ravindra Kolhe, Wendy B. Bollag, Meghan E. McGee-Lawrence, William D. Hill, Mark W. Hamrick , Carlos M. Isales, and Sadanand Fulzele 

Review Article (6 pages), Article ID 2911578, Volume 2021 (2021)

Extracorporeal Shockwave Therapy Modulates the Expressions of Proinflammatory Cytokines IL33 and IL17A, and Their Receptors ST2 and IL17RA, within the Articular Cartilage in Early Avascular Necrosis of the Femoral Head in a Rat Model

Jai-Hong Cheng , Shun-Wun Jhan, Chieh-Cheng Hsu, Hung-Wen Chiu, and Shan-Ling Hsu 

Research Article (10 pages), Article ID 9915877, Volume 2021 (2021)

Research Article

Butyrate Inhibits Osteoclast Activity *In Vitro* and Regulates Systemic Inflammation and Bone Healing in a Murine Osteotomy Model Compared to Antibiotic-Treated Mice

Alexandra Wallimann ^{1,2}, Walker Magrath ¹, Brenna Pugliese ¹, Nino Stocker ²,
Patrick Westermann ², Anja Heider², Dominic Gehweiler ¹, Stephan Zeiter ¹,
Marcus J. Claesson ³, R. Geoff Richards ¹, Cezmi A. Akdis ²,
Christopher J. Hernandez ^{4,5}, Liam O'Mahony ⁶, Keith Thompson ¹,
and T. Fintan Moriarty ¹

¹AO Research Institute Davos, Davos, Switzerland

²Swiss Institute of Allergy and Asthma Research (SIAF), University of Zurich, Davos, Switzerland

³SeqBiome Ltd., 3 Castleheights, Bandon, County Cork, Ireland

⁴Sibley School of Mechanical and Aerospace Engineering, Cornell University, Ithaca, NY, USA

⁵Hospital for Special Surgery, New York, NY, USA

⁶Departments of Medicine and Microbiology, APC Microbiome Ireland, University College Cork, College Road, Cork, Ireland

Correspondence should be addressed to T. Fintan Moriarty; fintan.moriarty@aofoundation.org

Received 11 June 2021; Revised 8 October 2021; Accepted 12 November 2021; Published 10 December 2021

Academic Editor: Chaofan Zhang

Copyright © 2021 Alexandra Wallimann et al. This is an open access article distributed under the Creative Commons Attribution License, which permits unrestricted use, distribution, and reproduction in any medium, provided the original work is properly cited.

Short-chain fatty acids (SCFAs) produced by the gut microbiota have previously been demonstrated to play a role in numerous chronic inflammatory diseases and to be key mediators in the gut-bone signaling axis. However, the role of SCFAs in bone fracture healing and its impact on systemic inflammation during the regeneration process has not been extensively investigated yet. The aim of this study was to first determine the effects of the SCFA butyrate on key cells involved in fracture healing *in vitro*, namely, osteoclasts and mesenchymal stromal cells (MSCs), and second, to assess if butyrate supplementation or antibiotic therapy impacts bone healing, systemic immune status, and inflammation levels in a murine osteotomy model. Butyrate significantly reduced osteoclast formation and resorption activity in a dose-dependent manner and displayed a trend for increased calcium deposits in MSC cultures. Numerous genes associated with osteoclast differentiation were differentially expressed in osteoclast precursor cells upon butyrate exposure. *In vivo*, antibiotic-treated mice showed reduced SCFA levels in the cecum, as well as a distinct gut microbiome composition. Furthermore, circulating proinflammatory TNF α , IL-17a, and IL-17f levels, and bone preserving osteoprotegerin (OPG), were increased in antibiotic-treated mice compared to controls. Antibiotic-treated mice also displayed a trend towards delayed bone healing as revealed by reduced mineral apposition at the defect site and higher circulating levels of the bone turnover marker PINP. Butyrate supplementation resulted in a lower abundance of monocyte/macrophages in the bone marrow, as well as reduced circulating proinflammatory IL-6 levels compared to antibiotic- and control-treated mice. In conclusion, this study supports our hypothesis that SCFAs, in particular butyrate, are important contributors to successful bone healing by modulating key cells involved in fracture healing as well as systemic inflammation and immune responses.

1. Introduction

The gut microbiota, comprising bacteria, archaea, viruses, and fungi, has been shown to have a significant role in human health through regulation of host physiology and metabolism [1]. Disruptions in the gut microbiota, as may occur through antibiotic therapy, stress, or an unbalanced diet [2], have been linked with numerous diseases including inflammatory bowel disease [3], metabolic syndrome [4], asthma [5], cardiovascular diseases [6], and bone-associated pathologies, such as osteoporosis [7, 8] and osteoarthritis [9, 10]. Conversely, positive interventions, in the form of prebiotics, probiotics, or postbiotics, have proven health benefits to the host if administered in appropriate amounts [11, 12]. Many of the beneficial effects of the microbiota are mediated by the postbiotic short-chain fatty acids (SCFAs) acetate, propionate, butyrate, and valerate, which are generated by the gut bacteria upon fermentation of dietary fibers [13]. These postbiotics have been extensively studied in relation to chronic inflammatory diseases due to their ability to induce regulatory T cell (Treg) differentiation [14] and secretion of anti-inflammatory cytokines such as IL-10 and TGF β , while inhibiting secretion of proinflammatory cytokines, such as IFN γ , TNF α , IL-1 β , IL-6, and IL-8 [15]. However, to date, they have been much less studied in relation to bone healing.

Probiotic bacteria themselves have been shown to prevent bone loss by promoting anti-inflammatory immune responses, by increasing mineral absorption in the gut, and through production of endocrine bone signaling factors (e.g., incretins and serotonin) [16]. For example, rats supplemented with the probiotic *Bifidobacterium longum* ATCC 15707 showed increased calcium and magnesium content in their bones [17] and exopolysaccharides from *Bifidobacterium longum* 35624[®] were shown to inhibit osteoclast formation by a TLR2-dependent mechanism [18]. Another prominent probiotic strain, *Lactobacillus reuteri* ATCC PTA 6475, was shown to prevent ovariectomy-induced bone loss by suppressing CD4⁺ T cell expansion in bone marrow [19] and to prevent postantibiotic bone loss by reducing microbial dysbiosis and restoring barrier function in the intestine [20]. In fact, broad-spectrum antibiotics followed by four weeks of recovery led to dysbiosis and reduced trabecular femoral bone density, which was dependent on lymphocytes [20, 21].

Although several studies have already investigated the role of the gut microbiota in preventing bone loss, only a limited number of studies have focused on its role in bone fracture healing. Bone healing complications, including delayed healing or nonunions, occur in 5-10% of all long-bone fractures, which lead to pain and functional impairment [22, 23]. Chronic, nonresolving inflammation is a reason for impaired bone healing [24]. Immune cells, including T cells, B cells, and monocytes/macrophages, are crucial players during the fracture healing process and can affect osteoclast formation and activity. The increased prevalence of proinflammatory CD8⁺/CD57⁺ T cells in peripheral blood was significantly correlated with delayed bone fracture healing in humans [25]. CD4⁺ T cells present a heteroge-

nous population with different subpopulations including Th17 and Treg cells. Secretion of proinflammatory IL-17 from Th17 cells is known to stimulate osteoclast formation, whereas increased Treg cell numbers were correlated with higher bone mass and decreased bone resorption in mice [26, 27]. B cells have been shown to secrete OPG, a factor regulating osteoclast differentiation and activity [26]. Circulating CD14⁺ monocytes/macrophages can serve as osteoclast precursors cells, which migrate to bone to further differentiate to osteoclasts [28, 29].

Two studies recently highlighted the potential of probiotics in bone healing. *Bifidobacterium adolescentis* [30] and *Akkermansia muciniphila* [31] were shown to accelerate bone healing in mice by modulating levels of systemic inflammatory cytokines and gut-epithelial barrier function. Due to the broad effect of SCFAs on different cell types involved in fracture healing, such as mesenchymal stromal cells (MSCs), osteoclasts, and fibroblasts [32], and also their ability to modulate immunity, there is considerable potential of not only probiotics but also postbiotics, in affecting bone healing. However, the role of SCFAs in affecting bone healing and its impact on systemic inflammation during the regeneration process has not been investigated to date.

The aim of this study was to first investigate the effects of SCFA butyrate on key cells involved in fracture healing *in vitro* and, second, to assess if butyrate supplementation impacts bone healing and systemic immune and inflammation levels in a murine osteotomy model. Deficiency in SCFA production was induced by rifampicin and levofloxacin treatment, a common antibiotic regimen administered to fracture patients with staphylococcal bone infections.

2. Material and Methods

2.1. PBMC Isolation and Osteoclast Differentiation Assay. Peripheral blood mononuclear cells (PBMCs) were isolated from healthy human donors ($n = 3$) via density gradient centrifugation using Histopaque[®]-1077 reagent (Sigma-Aldrich, Merck KGaA, Darmstadt, Germany) and centrifugation at 800 g for 20 min at room temperature (RT). PBMCs were collected and further cultured under standard conditions (37°C, 5% CO₂) in α MEM supplemented with 10% (*v/v*) fetal bovine serum (FBS; Gibco), 100 U/mL penicillin, 100 μ g/mL streptomycin, and 20 ng/mL of recombinant human macrophage-colony stimulating factor (M-CSF; R&D Systems, Abingdon, UK) to induce differentiation of osteoclast precursor cells (monocytes/macrophages). Fresh cytokines were added every 2 days, and adherent M-CSF-dependent osteoclast precursors were detached after 5-7 days using trypsin-EDTA solution (Gibco) and a cell scraper, which were then plated into 96-well plates at 1×10^4 cells/well. Recombinant murine receptor activator of NF κ B ligand (RANKL; 10 ng/mL; R&D Systems) was added to the cultures to induce the fusion of osteoclast precursors into multinucleated osteoclasts. Additionally, 0.1 mM, 0.25 mM, 0.5 mM, and 1 mM of SCFAs acetate, propionate, butyrate, or valerate were added to investigate the effect of SCFAs on osteoclast differentiation. Likewise, 0.5 μ g/mL, 5 μ g/mL, and 50 μ g/mL rifampicin and/or levofloxacin were

added to investigate the effect of antibiotics on osteoclast formation. Medium, cytokines, SCFAs, and antibiotics were replaced every 2 days, and after 7-10 days, cells were fixed using a 4% formaldehyde solution in PBS for 15 min at RT. To determine osteoclast formation, cells were stained using a tartrate-resistant acid phosphatase (TRAcP) staining kit (Sigma-Aldrich, Buchs, Switzerland). Multinucleated (≥ 3 nuclei) TRAcP-positive cells were classified as osteoclasts, and the total number of osteoclasts per well was quantified using a Zeiss Axiovert A1 light microscope (Zeiss).

2.2. Resorption Assay. To assess the effects of butyrate on mature osteoclasts, osteoclasts were first generated by seeding 300,000 osteoclast precursor cells/well in 6-well plates and stimulated with M-CSF and RANKL as described above. Once cell fusion was observed (typically 3-4 days following RANKL addition), mature osteoclasts were detached by trypsinization and gentle scraping, then resuspended into a complete medium (containing 20 ng/mL M-CSF and 10 ng/mL RANKL; 2 mL/well) before seeding into Osteoassay 96-well plates (Corning) at 100 μ L cell suspension/well. After allowing the cells to attach to the Osteoassay substrate for 4 hours, 0.1 mM, 0.25 mM, 0.5 mM, or 1 mM butyrate was added to the respective wells. After 72 hours, cells were washed twice with PBS and were then fixed using 4% (*v/v*) formaldehyde solution for 15 min at RT. To assess osteoclast resorption, the cells were removed using 10% (*v/v*) bleach, and a von Kossa silver nitrate staining was performed.

2.3. Cell Viability Assay. Effects of butyrate on cell viability of osteoclast precursors and MSCs were assessed using CellTiter-Blue reagent (Promega AG, Dübendorf, Switzerland), according to the manufacturer's instructions.

2.4. Functional Osteoclast Formation Assays. To check whether GPR43 and GPR183 are required for osteoclast formation, human osteoclast precursor cells were isolated and cultured as described above but additionally treated with either 75 nM, 750 nM, or 7500 nM of GPR43 (FFA2) agonist (Sigma-Aldrich) or 5 nM, 50 nM, or 500 nM of inverse GPR183 agonist (GSK682753A, MedChemExpress). Compounds were dissolved in dimethylsulfoxide (DMSO, Sigma). Osteoclast quantification was performed with the TRAcP staining kit, as described above.

2.5. Isolation and Expansion of Human Bone Marrow-Derived Mesenchymal Stromal Cells. Human bone marrow aspirates were obtained with informed consent of all donors and with full approval from the Ethics Committee of the University of Freiburg Medical Centre (EK-Freiburg: 135/14) and the ethical commission of Graubünden (KEK-ZH-NR: 2016-00141). Human bone marrow-derived mesenchymal stromal cells (BM-MSCs) were isolated by density gradient centrifugation using Histopaque-1077 and cultured as previously described [33, 34]. BM-MSCs were seeded at 3×10^3 cells/cm² in α -MEM supplemented with 10% (*v/v*) MSC-qualified FBS (Sera-Plus, PAN-Biotec GmbH, Aidenbach, Germany), 100 U/mL penicillin, 100 μ g/mL streptomycin, and 5 ng/mL basic fibroblast growth factor-2 (bFGF-2; Fitzgerald Industries, USA), under standard condi-

tions of 37°C and 5% CO₂ in a humidified atmosphere. For osteogenesis and chondrogenesis assays, culture-expanded MSCs were used up to passage 5.

2.6. In Vitro MSC Osteogenic Differentiation Assay. To assess the impacts of butyrate on MSC osteogenic differentiation, human BM-MSCs ($n = 3$) were plated at 3×10^4 cells/well on Thermanox coverslips in 24-well plates and grown until confluent. At this point, cell monolayers were treated with either control medium (1 g/L glucose DMEM, 10% FBS, 100 U/mL penicillin, and 100 μ g/mL streptomycin) or osteogenic medium: control medium additionally supplemented with 50 μ g/mL ascorbic acid 2-phosphate (AA2P; Sigma), 5 mM β -glycerophosphate (Sigma), and 10 nM dexamethasone (Sigma). Culture medium was exchanged three times per week, and the cells were cultured for a total period of 28 days. Butyrate (0.5 mM) was added to the wells and was replenished at each medium change. Cells were then washed twice with PBS, fixed with 4% formaldehyde for 15 min at RT, and washed three times in distilled water. The cell monolayer was then stained using a 40 mM solution of Alizarin red solution (pH 4.2) for 1 hour on a rocking platform. The cells were then washed five times with distilled water, and Alizarin red staining was imaged using an inverted light microscope.

To quantify mineralization, Alizarin red was extracted by incubating in 10% (*v/v*) acetic acid at RT for 30 min. After removal of the monolayer by scraping, the samples were then heated at 85°C for 10 min and cooled on ice. After centrifugation at 13,000 g for 10 min the supernatant was collected, then the pH was altered to 4.3 using 10% (*v/v*) ammonium hydroxide. Quantification was assessed in comparison to known Alizarin red concentrations by measuring the absorbance of the standards/samples at 405 nm with a Multiskan™ GO 3.2 microplate spectrophotometer and analyzed using SkanIt™ Software (Thermo Fisher Scientific, Waltham, MA, USA).

2.7. In Vitro MSC Chondrogenic Differentiation Assay. Human BM-MSCs ($n = 5$) were culture expanded as described above. BM-MSCs were then harvested using trypsin-EDTA (Gibco) and resuspended in chondropermissive media consisting of Dulbecco's Modified Eagle Serum (DMEM) 4.5 g/L glucose, 50 μ g/mL AA2P, 1% (*v/v*) nonessential amino acids, 100 U/mL penicillin, 100 μ g/mL streptomycin, 1% (*v/v*) ITS supplement (Corning), and 100 nM dexamethasone. Cells were seeded in quadruplicates into a 96-well V-bottomed plate at a density of 2×10^5 cells/well. The plate was then centrifuged (400 g, 5 min), and pellets were allowed to form for 24 hours. Fresh chondropermissive medium or chondrogenic medium (chondropermissive medium supplemented with 10 ng/mL TGF β 1 (Fitzgerald Industries)) was then added to the cell pellets (day 0). To assess the impacts of SCFA supplementation on chondrogenesis of MSCs, pellets cultured under chondropermissive and chondrogenic conditions were also treated with 0.5 mM butyrate. Growth medium was replaced every 2-3 days, with conditioned medium collected and stored for subsequent assessment of sulphated glycosaminoglycan (sGAG)

content. Cell pellets were harvested at day 24. Two pellets per condition were subsequently processed for histological assessment, and the remaining 2 pellets were processed for sGAG content analysis. Chondrogenic differentiation was assessed using Safranin O/Fast Green to visualize proteoglycans and collagen. Pellets were fixed using 4% formaldehyde then dehydrated in an ascending ethanol series prior to embedding in paraffin. Sections cut at 6 μm were then stained with Safranin O/Fast Green and visualized using light microscopy. Content of sGAG content in the pellets was assessed using 1,9-dimethyl-methylene blue (DMMB), following overnight digestion of the pellets at 56°C in 0.5 mg/mL Proteinase K (Roche) solution. Absorbance was measured immediately at 535 nm using a Victor³ Microtitre plate reader (Perkin Elmer®), using a standard curve of known concentrations of chondroitin sulphate. Results were expressed after normalization to DNA content of cell pellets using Hoechst 33258 and calf thymus DNA as a standard.

2.8. Bulk RNA Sequencing. To characterize gene expression changes in osteoclast precursor cells upon butyrate stimulation, PBMCs from five healthy human donors were isolated as described above. Magnetic-activated cell sorting (MACS) using CD14 MicroBeads (130-050-201, Miltenyi Biotec), positive selection columns (MS+ column 120-000-472, Miltenyi Biotec), and OctoMACS™ separator (Miltenyi Biotec) was performed on isolated PBMCs to recover CD14+ monocytes/macrophages. Purity of positively selected CD14+ monocytes/macrophages was assessed using flow cytometry and was $\geq 95\%$. CD14+ monocytes/macrophages were further cultured in αMEM supplemented with 10% (*v/v*) FBS, 100 U/mL penicillin, 100 $\mu\text{g}/\text{mL}$ streptomycin, and 20 ng/mL of human M-CSF until confluency. After 5-7 days, adherent M-CSF-dependent osteoclast precursors were detached using trypsin-EDTA solution and a cell scraper and subsequently seeded in 6-well plates (3×10^5 cells/2 mL) and stimulated with 20 ng/mL human M-CSF. The following day, 20 ng/mL murine RANKL and 0.5 mM butyrate were added to the osteoclast precursor cells. After 6 h and 24 h of stimulation with 0.5 mM butyrate and RANKL, whole RNA was isolated by means of RNeasy® plus micro kit (Qiagen, Hilden, Germany) according to manufacturer's instructions. Purity and integrity of isolated RNA were assessed using a spectrophotometer (NanoDrop, Thermo Fisher Scientific) and Agilent 2200 TapeStation (Agilent Technologies, Waldbronn, Germany), respectively. RNA library processing (poly A selection) and Illumina Hiseq single end (150 bp) sequencing were performed at the Functional Genomics Center Zurich. Data was analyzed within the sushi data analysis framework launched by Functional Genomics Center Zurich and by MetaCore software (ClariVate™ Analytics). False discovery rate (FDR) threshold was set to < 0.01 and fold change ratio to ± 0.5 .

2.9. In Vivo Experimental Design. The *in vivo* experiment was approved by the Tierversuchskommission Graubünden (Approval Nr. 2019_25). Healthy male C57BL/6J mice ($n = 55$, including reserves), free of orthopedic disease, were obtained from Charles River (Germany). Mice were acclima-

tized for two weeks and were housed at a 12 h dark/12 h light cycle in groups of 2-6 in individually ventilated cages. Single housing was deemed necessary for certain mice due to aggression and hierarchy fights within cages. Mice were fed *ad libitum* and had constant access to water. Mice were randomly allocated to one of the following experimental groups ($n = 12$ per group): group 1, the control group, was orally gavaged with vehicle (sterile water) in the morning and afternoon (8 hours later); group 2 was orally gavaged with the vehicle in the morning and with 30 mM butyrate in the afternoon; group 3 received a 25 mg/kg rifampicin plus 20 mg/kg levofloxacin (Rif + Levo) antibiotic mixture in the morning and vehicle in the afternoon. An additional fourth group was administered Rif + Levo antibiotic mixture in the morning and 30 mM butyrate in the afternoon. However, after suffering from a greater than anticipated drop-out rate, the results of this experiment are not presented (see Discussion). Mice were orally gavaged with the corresponding treatment (administration volume 200 μL) for five consecutive days per week during the whole study duration (21 days), starting the gavage the morning of osteotomy. At 20 weeks of age, mice were placed under general anesthesia and a 0.44 mm femoral osteotomy was performed, under aseptic conditions, in the left hind limb using a 4-hole jig and Gigli wire (Mouse Fix Drill & Saw guide, RIS.301.107). A 4-hole polyether ether ketone (PEEK) plate (RISystem MouseFix Plate 4-hole, PEEK RIS.601.001), 0.31 mm drill bit (RIS.592.202), and 4 self-cutting angular stable screws (MouseFix Screw, length 2 mm, RIS. 401.100) were used to fix the osteotomy. Mice were operated group by group, and surgeons were therefore not blinded. Mice were subcutaneously injected with calcein green (5 mg/kg) at 10 days and with xylenol orange (90 mg/kg) at 18 days after osteotomy to investigate calcium apposition retrospectively.

2.10. Anesthesia, Analgesia, and Euthanasia. Mice were anesthetised with sevoflurane (1.5-3% in O_2 , flow rate 0.6-0.8 L/min) during the surgery and CT scans, and before euthanasia, which was done by cervical dislocation. Intraoperative analgesia consisted of buprenorphine (1 : 10 dilution of 0.3 mg/mL solution; 0.1 mL subcutaneously (*s.c.*)) and carprofen (1 : 10 dilution of 50 mg/mL solution; 0.1 mL *s.c.*) immediately after anesthetic induction. To prevent loss of body temperature, the mice were placed on a temperature-controlled heating mat pre- and intraoperatively. Postoperative analgesia consisted of tramadol added to the drinking water (25 mg/L, 1 drop per 100 mL tap water) for 7 days.

2.11. MicroCT Imaging. MicroCT scans of the operated femora were performed using VivaCT40 (SCANCO Medical AG, Brüttisellen, Switzerland). Images were acquired using a voxel resolution of 10.5 μm and a beam energy and intensity of 70 kVp and 114 μA , respectively. Scans were performed at three different timepoints: immediately following surgery, and at 10 and 21 days postsurgery (at euthanasia).

2.12. Blood Collection and Serum Preparation. Blood was collected on the day of osteotomy (preoperatively) and at 10 days postoperatively from the lateral tail vein and at 21

days (at euthanasia) from the retrobulbar vessels. The collected blood was allowed to clot at RT for 30 min, then centrifuged for 10 min at 6000 g at RT. Serum was collected and frozen at -20°C until further analysis.

2.13. Quantification of Serum Inflammatory and Bone Turnover Markers. Rat/Mouse PINP EIA kit (ids®, UK) was used to assess levels of type I procollagen (PINP) in mouse serum, according to the manufacturer's protocol. Data were collected using a Multiskan™ GO 3.2 microplate spectrophotometer and analyzed using SkanIt™ Software. A V-PLEX Mouse Proinflammatory Panel kit (Meso Scale Diagnostics, Rockville, MD, USA) was used to test a panel of inflammatory markers including IL-6, IL-10, IL-1 β , TNF α , and KC/GRO, in the serum of mice. The assay was performed according to the manufacturer's protocol.

2.14. Olink® Targeted Proteomics. An Olink® Target 96 Mouse Exploratory panel (Olink Proteomics, SE-751 83 Uppsala, Sweden) was used to assess 92 protein biomarkers in the murine serum samples. Data were analyzed using the Olink® Insights Stat Analysis app and with GraphPad Prism software (GraphPad Software 8.1.0, Inc., La Jolla, CA, USA).

2.15. Histological Processing and Morphometric Analysis. Operated femora ($n = 5$ per group), with the 4-hole PEEK-plate attached, were fixed in methanol and subsequently embedded in methyl methacrylate (MMA). Slices of 50–70 μm were cut and imaged on an Olympus BX63F light microscope. Upon fluorescence imaging, slices were stained with a 15% (v/v) Giemsa and a 1% (v/v) Eosin solution and imaged with an Olympus BX63F light microscope. Images of fluorescent mouse femora were analyzed using ImageJ (NIH, Bethesda, USA) and scaled using a 500 μm scale bar. The region of interest (ROI) was a rectangular area surrounding the tissue between the two middle screws and the osteotomy. The red and green channels were used to quantify the mean fluorescent intensity (mean pixel value) of xylenol orange and calcein green, respectively, in each image.

2.16. Biomechanical Testing of Femora. To measure stiffness of the newly formed callus and the mechanical properties of unoperated femora, four-point bending (destructive testing) was performed. PEEK implants were carefully dissected from operated femora ($n = 7$ per group), and femora were moistened with Ringer's solution, wrapped in gauze, and frozen at -20°C until testing was performed. Unoperated, contralateral femora were collected and stored in the same manner. Duration of frozen storage was kept consistent for all samples. On the day of measurement, mouse femora were removed from Ringer's solutions and nonbone tissue was carefully removed from each sample. An Instron® 5866 machine (Norwood MA, US) with a 100 N loadcell was used for the mechanical testing. All samples were placed in the same orientation on two bending points. Preload between 0 and 0.05 N was applied to the samples, and testing was performed with a speed of 0.5 mm/min. Measurement was aborted as soon as femora samples broke. Plots of force ver-

sus displacement were derived from the four-point bending test. Failure load was extrapolated from each curve.

2.17. 16S rRNA Sequencing and Data Analysis. Cecal content of mice was harvested on the day of euthanasia and frozen at -20°C until further processing. DNA of cecal content of mice was isolated using QIAmp® PowerFecal Pro DNA kit (Qiagen). Samples were sequenced and analyzed by SeqBiome Ltd. (County Cork, Ireland). DADA2 R package was used for data analysis using the SILVA 138 as reference database for taxonomy assignment.

2.18. SCFA Measurement in Murine Cecal Water. Cecal water from residual cecal content, which was not used for DNA isolation, was prepared to measure SCFAs. Sulfuric acid (0.15 mM) was added to cecal content in a ratio of 1 mL per 0.3 g. Samples were rigorously vortexed and then centrifuged at 14,000 g for 30 min at 4°C. Supernatant was collected and again centrifuged at the same speed. Samples were sequentially filtered through a 0.45 μm and 0.2 μm filter. The filtered supernatants were analyzed on an ACQUITY UPLC H-Class Bio System (Waters Corp, Milford, MA, USA). The separation was carried out on an Aminex HPX-87H ion exchange column (300 mm \times 7.8 mm, 9 μm particle, Bio-Rad Laboratories Inc.) together with a Micro-Guard Cation H+ refill cartridge (Bio-Rad Laboratories Inc.) at a flow rate of 0.35 mL/min at 40°C with 10 mmol/L H₂SO₄ as an eluent solution. Injection volume was 20 μL , and the detection wavelength was 210 nm. The samples were quantified in relation to standards measured in parallel.

2.19. Flow Cytometric Analysis. Spleen, inguinal lymph node (iLN) from the operated site, and tibial bone marrow were collected on the day of euthanasia. Single-cell suspensions were prepared from all tissues using a 40 μm cell strainer, followed by staining for the following surface markers: PE anti-mouse CD3 antibody (clone: 17A2, isotype: rat IgG2b), Alexa Fluor® 700 anti-mouse CD4 antibody (clone: GK1.5, isotype: rat IgG2b, κ), PE/Dazzle™ 594 anti-mouse CD8a antibody (clone:53-6.7, isotype: Rat IgG2a, κ), Brilliant Violet 510™ anti-mouse CD45 (clone:30-F11, isotype: rat IgG2b, κ), PE-Cy5 anti-mouse CD19 (clone: 6D5, isotype: rat IgG α , κ), and FITC anti-mouse CD14 (clone: Sa14-2, isotype: rat IgG2a, κ). Cell viability was assessed using fixable viability dye eFluor™ 780. Antibodies were all purchased from BioLegend and the viability dye from eBioscience. Samples were acquired using a BD FACSAria™ III Cell Sorter (BD Biosciences, New Jersey, US) and analyzed with Kaluza Software (Beckman Coulter GmbH, Germany).

2.20. Statistical Analysis. Data is reported as mean \pm SEM unless stated otherwise. One-way ANOVA was used to determine statistical significance between experimental groups, using Tukey's post hoc analysis. Threshold for statistical significance was $p < 0.05$. Unless stated otherwise, all analyses were performed using GraphPad Prism software (GraphPad Software 8.1.0, Inc., La Jolla, CA, USA).

3. Results

3.1. Butyrate Inhibits Formation and Resorption Activity of Human Osteoclasts and Affects Osteogenic Differentiation of Human MSCs. To investigate the impact of butyrate on osteoclast formation, osteoclast precursor cells were generated from human PBMCs. These osteoclast precursor cells were treated with RANKL alone or with butyrate at concentrations from 0.1 mM to 1 mM. Quantification of osteoclasts by means of TRAcP staining revealed a significant ($p < 0.0001$) reduction of osteoclast formation in the presence of 0.1 mM (54% reduction), 0.25 mM (59% reduction), 0.5 mM (76% reduction), and 1 mM of butyrate (89% reduction) (Figure 1(a)). Similar inhibitory effects could also be detected with other SCFAs, including acetate, propionate, and valerate (Supplementary Figure 1A). However, the presence of 0.5 $\mu\text{g/mL}$, 5 $\mu\text{g/mL}$, and 50 $\mu\text{g/mL}$ rifampicin or levofloxacin did not significantly affect osteoclast formation (Supplementary Figure 1B). The resorption activity of mature osteoclasts was also significantly ($p < 0.05$) reduced in the presence of 0.5 mM (40% reduction) and 1 mM butyrate (66% reduction) (Figure 1(b)). Concentrations below 0.25 mM had no effect on cell viability, and less than 30% reduction was observed at higher concentrations after 72 hours of treatment (Supplementary Figure 1C) without obvious signs of toxicity as seen in Figure 1(a). In contrast to the inhibitory effects of butyrate on osteoclast formation and resorption activity, 0.5 mM butyrate displayed a trend for increased calcium deposits in MSCs cultured in osteogenic media (Figure 1(c), $p = 0.0503$) as revealed by Alizarin red staining. However, no significant change was observed in sGAG content of pellet culture of MSCs in chondrogenic media in the presence of 0.5 mM butyrate (Supplementary Figure 1B). Cell viability of MSCs treated with 0.5 mM butyrate was not significantly affected (Supplementary Figure 1D). Overall, these *in vitro* experiments show that butyrate influences both the differentiation and the activity of bone-resorbing osteoclasts and the osteogenic differentiation of MSCs, in a manner expected to be beneficial for bone remodeling and healing.

3.2. Butyrate Affects Pathways and Expression of Genes Relevant for Bone Healing and Osteoclast Differentiation. By means of bulk RNA sequencing, we further explored potential pathways and genes involved in butyrate-mediated inhibition of osteoclast formation. The transcriptome of osteoclast precursor cells (CD14⁺ monocytes/macrophages) of five healthy human donors was analyzed in the absence and presence of 0.5 mM butyrate at 6 and 24 hours. Following 6 h of butyrate stimulation, 2718 genes were upregulated and 2342 genes downregulated (Figure 2(a)). Following 24 h of butyrate treatment, only four genes passed the FDR threshold (LAD1, CCR7, HTR2B, and ANKRD1, data not shown). Pathway enrichment analysis by means of MetaCore™ software revealed several pathways relevant for bone healing were significantly altered. Immune response pathway related to IFN-alpha/beta signaling, ROS-induced oxidative stress cellular signaling, and endo-

plasmic reticulum- (ER-) associated protein degradation were the top three statistically significant downregulated pathways in osteoclast precursor cells upon butyrate stimulation (Figure 2(b)). Upregulated pathways included signal transduction of angiotensin II via p38, ERK, and PI3K, pathways associated with chemotaxis signaling via GPCR, and signal transduction of bone-related WNT5A signaling (Figure 2(c)). As part of GPCR signaling, stimulation of GPR43 with an agonist lead to a significant ($p < 0.01$) reduction in osteoclast formation (Supplementary Figure 2A). DMSO, which served as solvent for the GPR43 agonist, did not influence osteoclast formation (data not shown).

Investigation of individual genes involved in osteoclast differentiation and fusion revealed a significant downregulation of GPR183, ELF1, FCER1G, SBNO2, CHUK, SNX10, TRAF6, and TCIRG1 in butyrate-treated osteoclast precursor cells (Figure 2(d)). Inhibition of GPR183 using a selective inverse agonist (GSK682753A) only slightly affected osteoclast formation (Supplementary Figure 2B). In contrast, EPHA2, CA2, TNFRSF11A (also known as the RANK receptor), FARP2, CTNBN1, TYROBP, CD300LF, TNF, NFATC1, MAPK14, TGFB1, and GLO1 were significantly upregulated in butyrate-treated osteoclast precursor cells (Figure 2(e)). To summarize, butyrate induces marked changes in the transcriptome of osteoclast precursors involving pathways relevant for bone healing and genes crucial for osteoclast differentiation and fusion.

3.3. Rifampicin- and Levofloxacin-Treated Mice Show Reduced Cecal SCFA Levels and a Change in Gut Microbiome Composition Compared to Butyrate- and Control-Treated Mice. Based on our *in vitro* data, which demonstrates the potential beneficial effects of butyrate on key cells involved in bone remodeling and healing, namely, osteoclasts and MSCs, we further investigated this in a murine osteotomy model (overview provided in Figure 3(a)). Control mice were compared with mice receiving oral butyrate supplementation and mice receiving oral Rif + Levo. Rif + Levo-treated mice show up to a three-fold reduction of acetate, propionate, and butyrate in cecal water compared to butyrate- and control-treated mice (Figure 3(b), $p < 0.05$). Butyrate supplementation did not impact the gut microbiome composition of mice compared to controls; however, Rif + Levo administration had marked effects as revealed by Principle Coordinate Analysis (PCoA) using Bray-Curtis distances (Supplementary Figure 2A). Considering bacterial phylum abundance, Rif + Levo-treated mice show higher *Firmicutes* abundance, whereas butyrate- and control-treated mice show higher *Bacteroidata* abundance (Figure 3(c)). Furthermore, Rif + Levo-treated mice show higher relative abundances of *Prevotellaceae*, *Rikenellaceae*, and *Deferribacteraceae* families (Supplementary Figure 2B) and have higher relative proportions of *Clostridiodes* genera compared to control- and butyrate-treated mice (Supplementary Figure 2C). Taken together, butyrate supplementation did not impact gut microbiota or SCFA production; however, administration of an antibiotic regimen involving Rif + Levo strongly reduced SCFA levels in the cecal water and

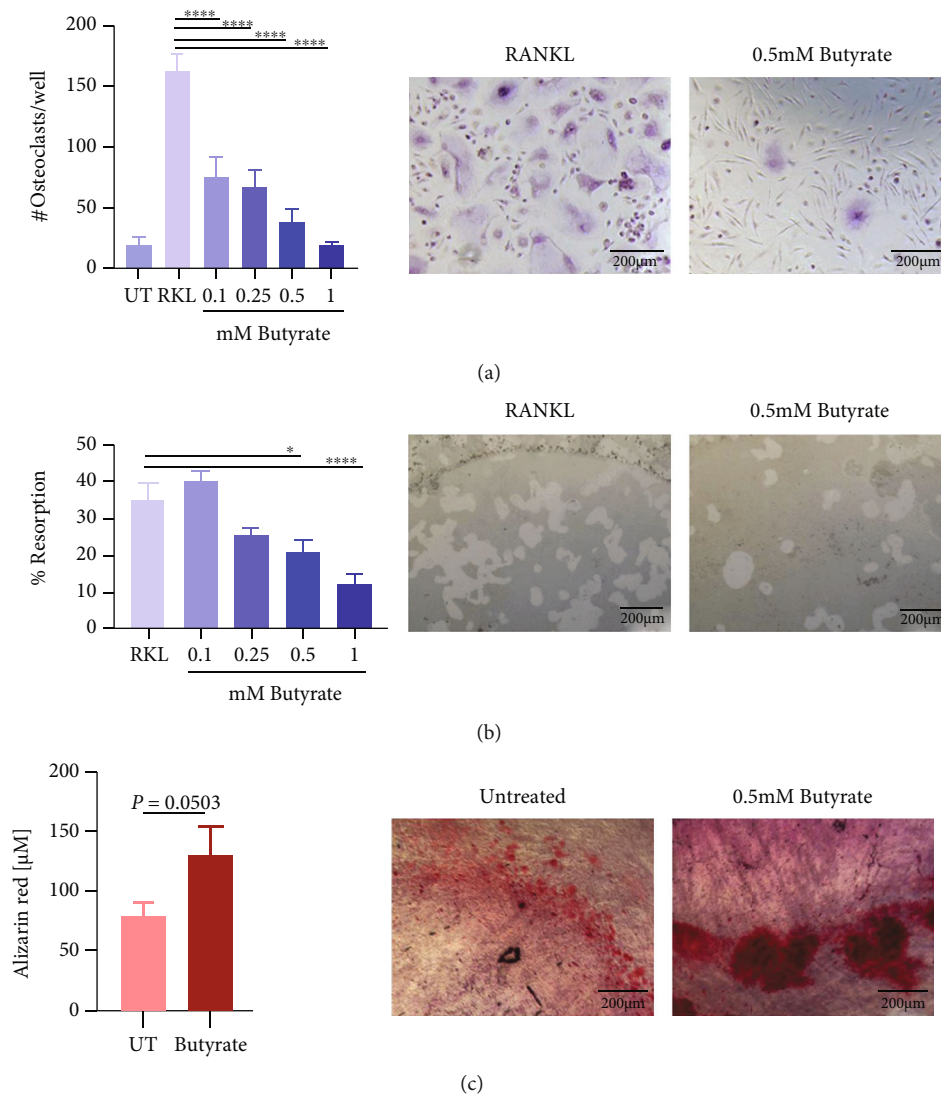


FIGURE 1: Butyrate inhibits human osteoclast formation and resorption. Impact of butyrate on cells involved in bone healing. (a) Osteoclast precursor cells were cultured with 20 ng/mL M-CSF and 10 ng/mL RANKL and with 0.1 mM, 0.25 mM, 0.5 mM, or 1 mM butyrate, respectively. Osteoclast formation was quantified by means of TRACP staining. Data shown are means ($n = 3$ independent donors, triplicates per donor were used) \pm SEM. Representative images showing TRACP-stained osteoclasts in the absence (left image) and presence of 0.5 mM butyrate (right image). (b) Mature osteoclasts were cultured on a hydroxyapatite-coated plate in the presence and absence of butyrate with concentrations as indicated above. Resorption areas were quantified by means of von Kossa staining. Data shown are means \pm SEM ($n = 1$ donor, performed in triplicate, and two pictures per well were taken and quantified). Representative images showing resorbed areas of hydroxyapatite-coated wells in the absence (left image) and presence of 0.5 mM butyrate (right image). (c) MSCs were cultured in osteogenic media and calcium deposits were quantified by means of Alizarin red staining in the absence and presence of 0.5 mM butyrate. Data shown are means ($n = 3$ independent donors) \pm SEM. Representative images of Alizarin red staining in the absence (left image) and presence of 0.5 mM butyrate (right image). Scale bar in all images = 200 μ m; UT = untreated; RKL = RANKL; **** $p < 0.0001$; * $p < 0.05$.

induced a marked change in the gut microbiome composition.

3.4. Butyrate Induces a Reduction of Proinflammatory Mediators, Whereas Rifampicin and Levofloxacin Increase Proinflammatory and Bone-Preserving Markers in Serum. To determine the systemic effects of butyrate and antibiotic treatment, a variety of (proinflammatory) cytokines and a broad range of protein biomarkers were further assessed in the serum of mice (Figure 4). Proinflammatory IL-6 was sig-

nificantly reduced in butyrate-treated mice compared to Rif + Levo-treated mice 10 days after osteotomy ($p < 0.05$), but this effect was diminished at 21 days due largely to a reduction in the levels of antibiotic-treated mice at this timepoint (Figure 4(a)). Levels of the proinflammatory TNF α were similar for control- and butyrate-treated mice at both timepoints; however, they were significantly increased in Rif + Levo-treated mice (Figure 4(b)). Proinflammatory IL-1 β levels and KC/GRO, the murine IL-8 homologue, were not significantly affected at either timepoint by butyrate or

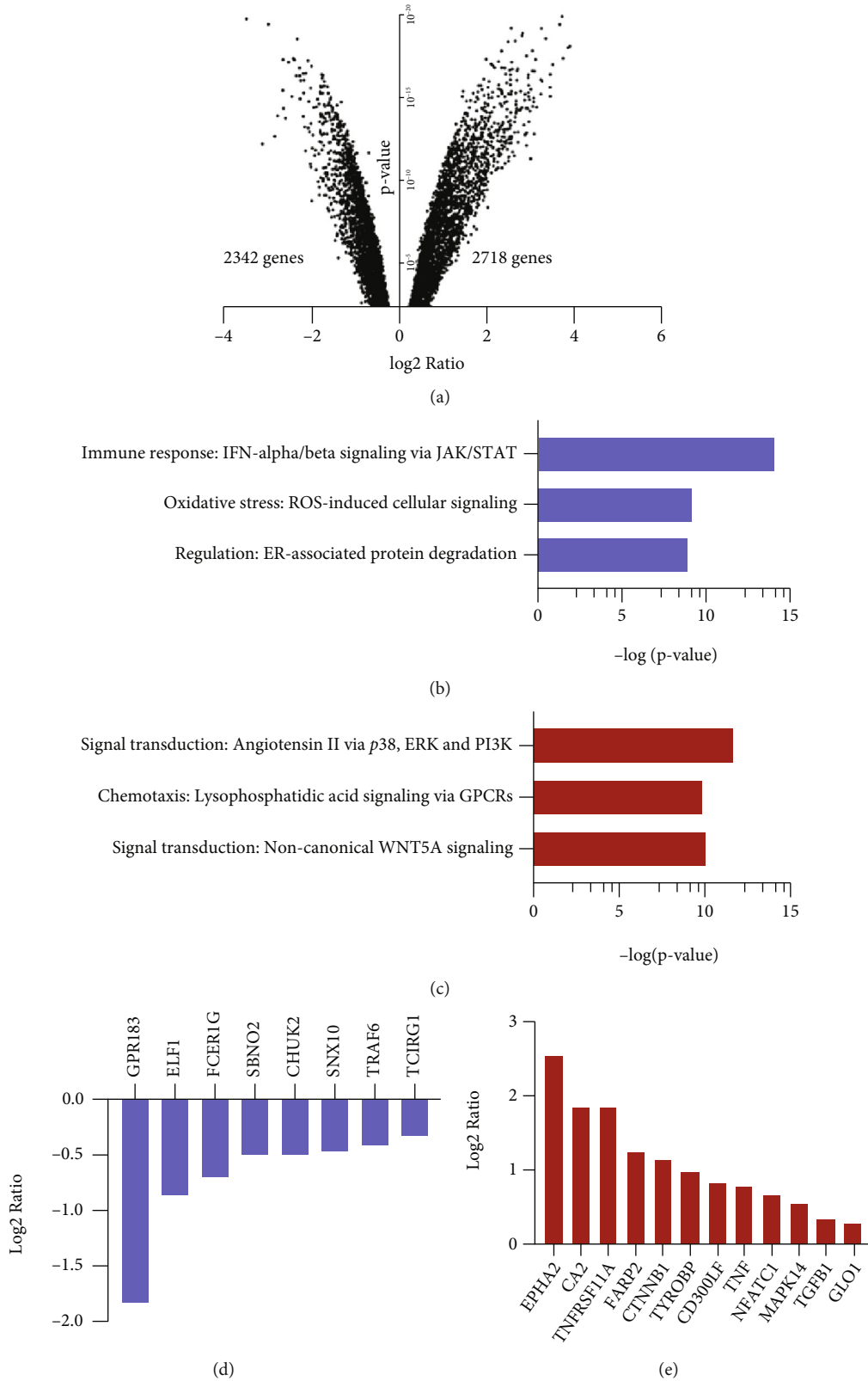


FIGURE 2: Butyrate regulates pathways and expression of genes relevant for bone healing and osteoclast differentiation. RNA sequencing of human osteoclast precursor cells following 6 h of butyrate treatment. (a) Volcano plot showing number of upregulated and downregulated genes in osteoclast precursor cells following 6 h stimulation with 0.5 mM butyrate. Functional enrichment analysis showing the three most significantly downregulated (b) and upregulated (c) pathways following 6 h of 0.5 mM butyrate treatment. (d) Downregulation and (e) upregulation of genes involved in osteoclast differentiation following 6 h 0.5 mM butyrate treatment. Fold change threshold = 0.5 and FDR threshold < 0.01 for all charts.

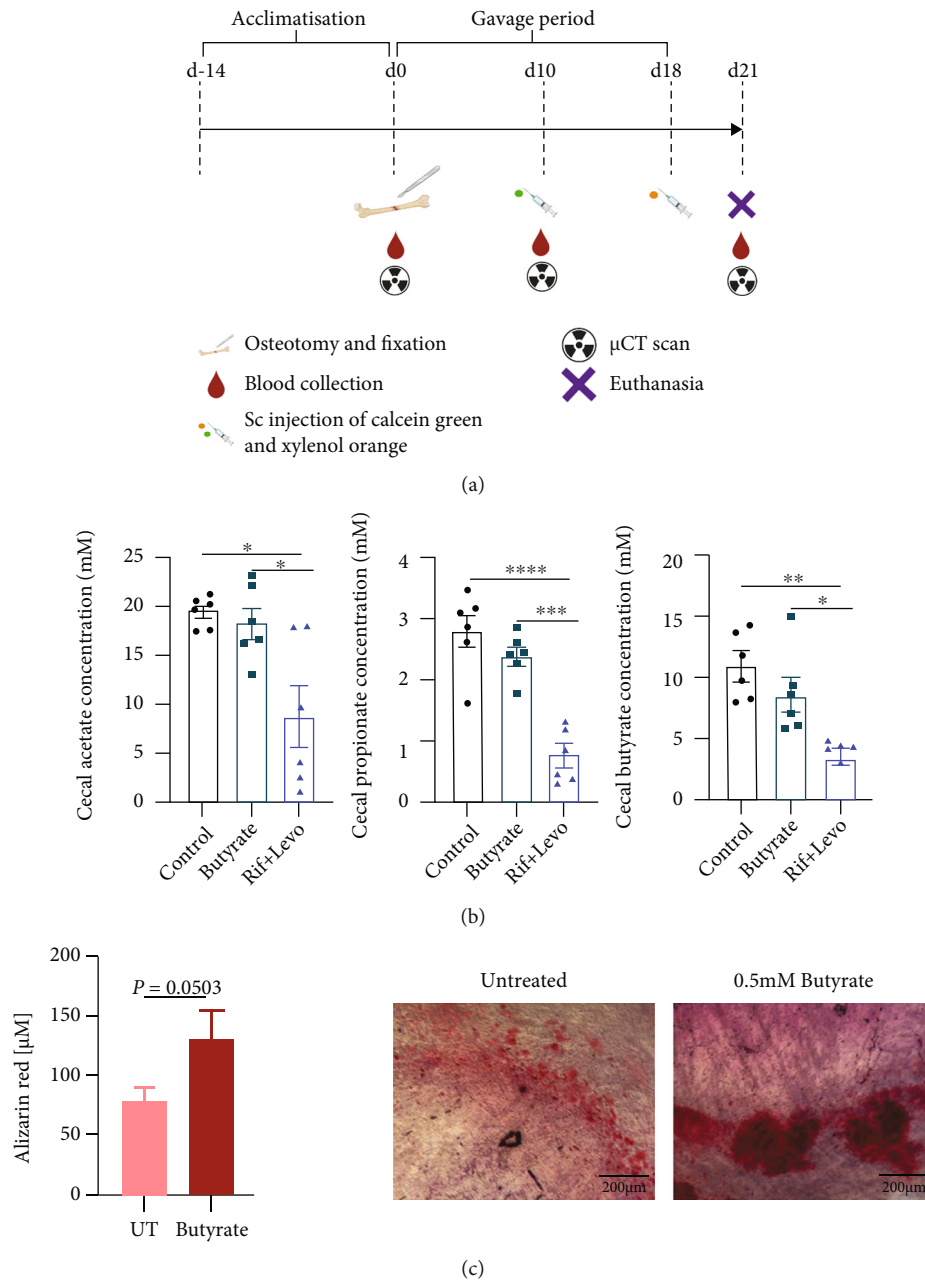


FIGURE 3: Rifampicin- and levofloxacin-treated mice show reduced cecal SCFA levels and a change in gut microbiome composition compared to butyrate- and control-treated mice. The effect of butyrate on the gut microbiome, systemic immunity, and bone healing was assessed in a murine osteotomy model. (a) Experimental outline of *in vivo* study indicating interventions and time frame. The figure was created with <http://BioRender.com/>. (b) Cecal concentrations of acetate, propionate, and butyrate were measured by means of UPLC. Data shown are means ($n = 6$) and \pm SEM. **** $p < 0.0001$, *** $p < 0.001$, ** $p < 0.01$, and * $p < 0.05$. (c) DNA of murine cecal content was isolated, and 16s rRNA sequencing was performed to determine microbiome composition. Percent abundance of bacterial phyla in the murine cecum ($n = 10$ Rif + Levo-treated animals, $n = 8$ butyrate-treated animals, and $n = 7$ control-treated animals).

antibiotic therapy (Figures 4(c) and 4(d)), although KC/GRO displayed a trend for increased levels in Rif + Levo-treated mice at 10 days ($p = 0.0976$) (Figure 4(d)). No clear differences between the groups were detected in terms of anti-inflammatory IL-10 levels at 10 days and 21 days (Supplementary Figure 3A).

Differential expression analysis of the 92 biomarkers tested with Olink® technology revealed that antibiotic treatment had a major impact on serum biomarkers with 11 pro-

teins being significantly affected ($p < 0.01$). Butyrate induced two significant changes: Flrt2, a marker for cell-cell adhesion and migration, and Tpp1, a lysosomal serine protease, were significantly downregulated in butyrate-treated mice compared to control mice (Figure 4(e)). In addition, trends for downregulation in the proinflammatory and osteoclastogenic IL-1 β (logFC = -0.7484 ; $p = 0.0130$), IL-6 (logFC = -0.6000 ; $p = 0.0622$), IL-17a (logFC = -0.4966 ; $p = 0.01127$), and Tnfrsf11b (=OPG, logFC = -0.2769 ; $p =$

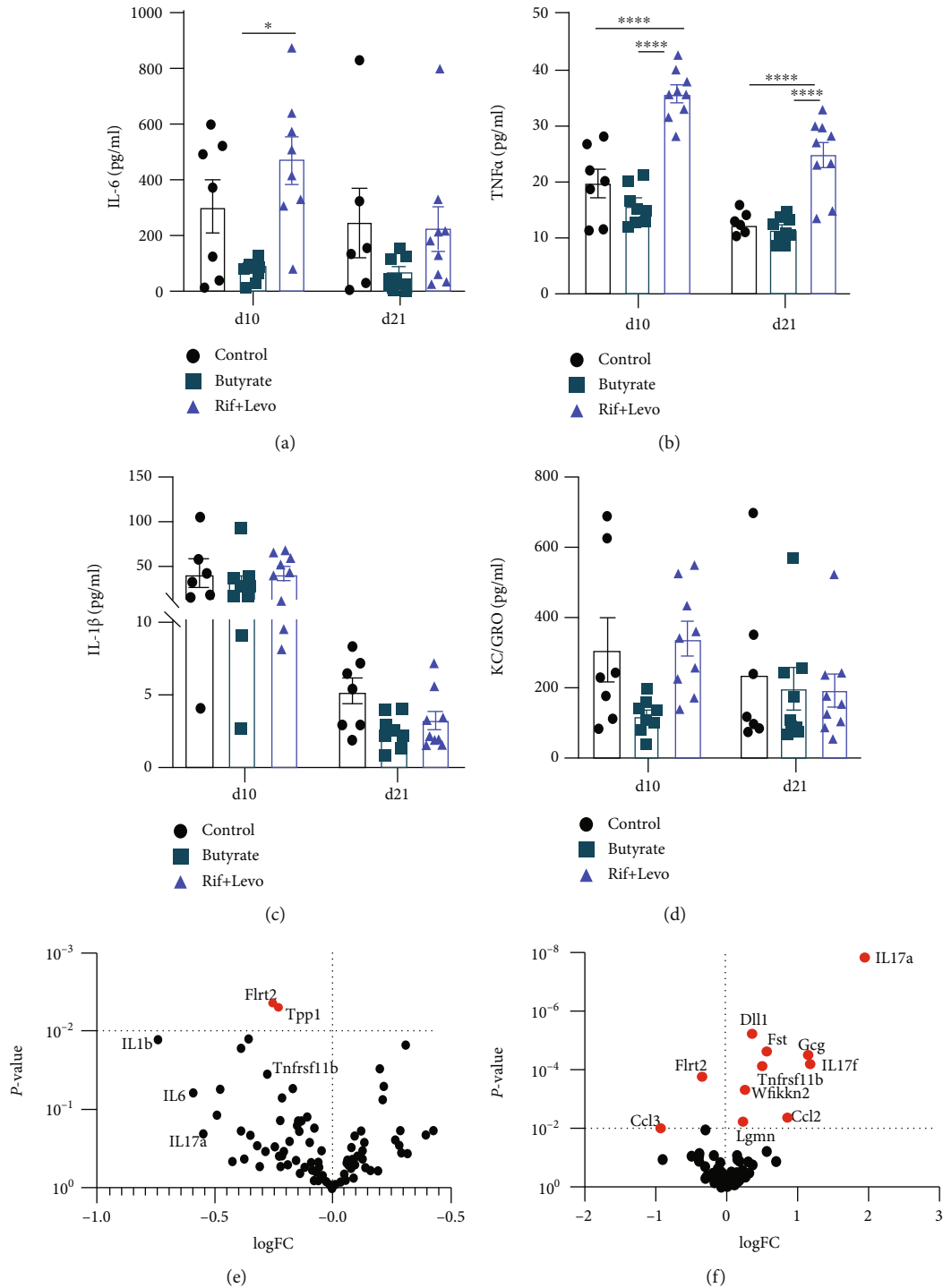


FIGURE 4: Butyrate induces a reduction of proinflammatory mediators, whereas rifampicin and levofloxacin increase proinflammatory and bone-preserving markers in serum. A variety of (pro-) inflammatory cytokines in serum of mice were assessed 10 days and 21 days following osteotomy using a multiplexed cytokine array and Olink targeted proteomics to investigate systemic biomarkers in serum of mice. Serum concentrations of (a) IL-6, (b) TNF α , (c) IL-1 β , and (d) of KC/GRO (murine IL-8 homologue) in the absence and presence of butyrate and Rif + Levo, respectively, 10 days and 21 days after osteotomy. Data shown are means ($n = 7-9$) \pm SEM. Differential expression of 92 biomarkers in (e) butyrate-treated mice compared to control mice and in (f) Rif + Levo-treated mice compared to control mice. Significance threshold $p < 0.01$. Significantly changed biomarkers are labelled in red. Flrt2 = leucine-rich repeat transmembrane protein; Tpp1 = tripeptidyl-peptidase 1; Ccl3 = C-C motif chemokine 3; Lgmn = legumain; Wfikkn2 = WAP, Kazal, immunoglobulin, Kunitz, and NTR domain-containing protein 2; Tnfrsf11b = tumor necrosis factor receptor superfamily member 11B (osteoprotegerin); Ccl2 = C-C motif chemokine 2; Dll1 = delta-like protein 1; Fst = follistatin; Gcg = glucagon. **** $p < 0.0001$; * $p < 0.05$.

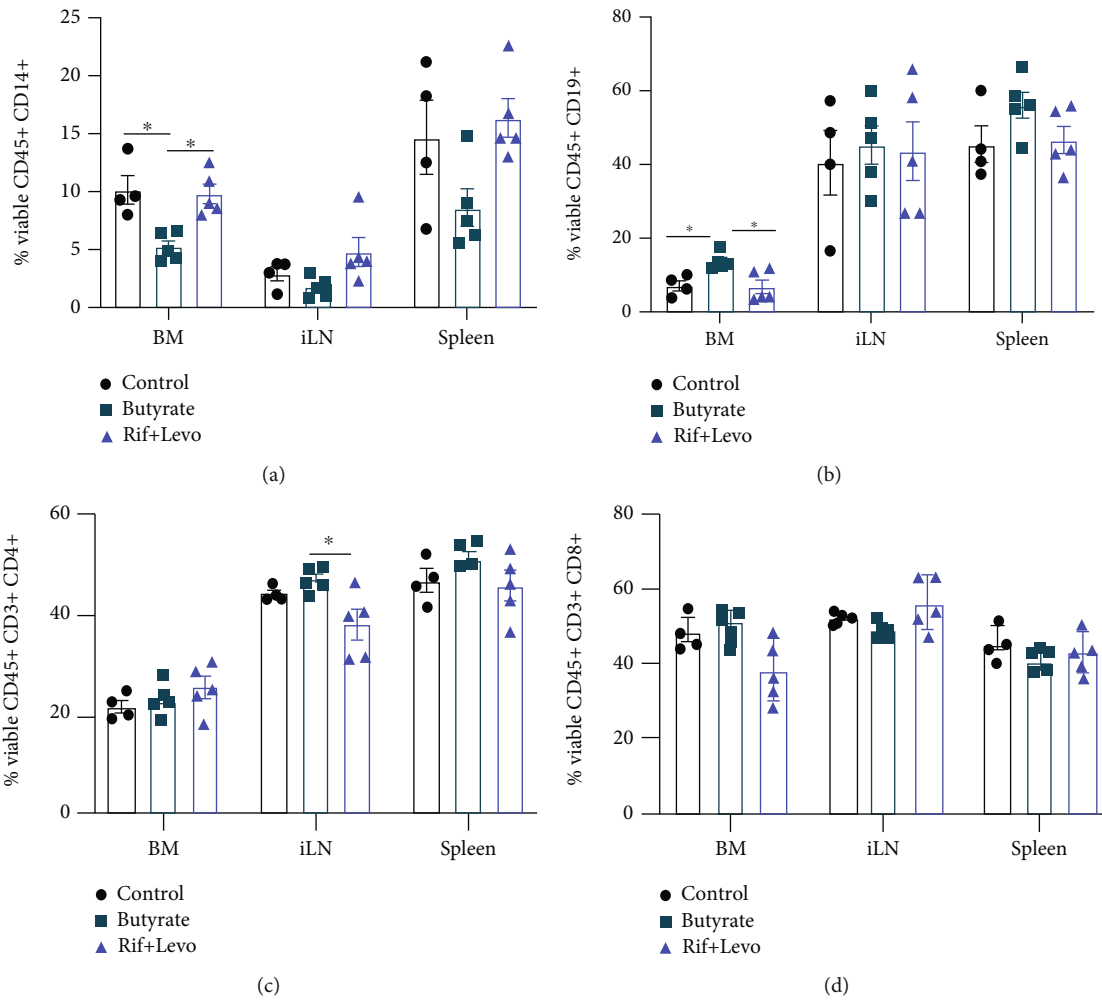


FIGURE 5: Butyrate treatment decreases the CD14+ monocyte/macrophage population but increases the CD19+ B cell population in bone marrow following osteotomy. Immunophenotyping of single-cell suspensions from bone marrow (BM), inguinal lymph node (iLN), and spleen from operated mice was performed. (a) Percent of viable CD45+ CD14+ monocytes/macrophages, (b) CD45+ CD19+ B cells, (c) CD45+ CD3+ CD4+ T cells, and (d) CD45+ CD3+ CD8+ T cells in spleen, iLN, and BM, in the absence and presence of butyrate and Rif + Levo, respectively. Data shown are means ($n = 4-5$) \pm SEM. * $p < 0.05$.

0.0346) were observed in butyrate-supplemented mice. In contrast, IL-17a, IL-17f, and Tnfrs11b were significantly upregulated in antibiotic-treated mice compared to control mice (Figure 4(f)). Other significantly upregulated proteins were as follows: DIII1, a regulator of adult stem cells; Fst (follicle-stimulating hormone (FSH); Gcg (glucagon), blood glucose regulator; Wfikn2, a protease inhibitor; and the chemokine Ccl2. Flrt2 and the chemokine Ccl3 were significantly downregulated in antibiotic-treated mice compared to control mice. Summarizing the serum analysis, antibiotic treated, SCFA-depleted mice show higher levels of the proinflammatory and proosteoclastogenic TNF α , IL-17a, and IL-17f as well as higher OPG levels compared to control mice. In contrast, butyrate-treated mice show the converse trend, i.e., lower levels of proinflammatory and proosteoclastogenic IL-6, IL-1 β , and IL-17a and lower OPG levels compared to control mice.

3.5. Butyrate Treatment Decreases CD14+ Monocyte/Macrophage Population but Increases CD19+ B Cell

Population in the Bone Marrow of a Mice with an Osteotomy. We used flow cytometry to perform immunophenotyping in the spleen, the left inguinal lymph node (iLN), which drained the operated bone area, and the left tibial bone marrow (BM) of the mice. The spleen was chosen to mirror a systemic immune response, whereby BM and iLN reflect the local immune response. Cell populations of interest were gated as shown in Supplementary Figure 3B. The percent of viable CD45+ CD14+ monocyte/macrophages was reduced by ~50% in BM of butyrate-treated mice compared to both control- and antibiotic-treated mice (Figure 5(a)). Similar trends for a reduction in CD14+ populations were observed in iLN ($p = 0.0900$) and spleen ($p = 0.0799$) of butyrate-treated mice compared to Rif + Levo-treated mice. In contrast, the percentage of the viable CD45+ CD19+ B cell population in BM of butyrate-treated mice was 2-fold higher compared to control- and Rif + Levo-treated mice but remained largely unchanged in iLN and spleen (Figure 5(b)). Regarding viable CD45+

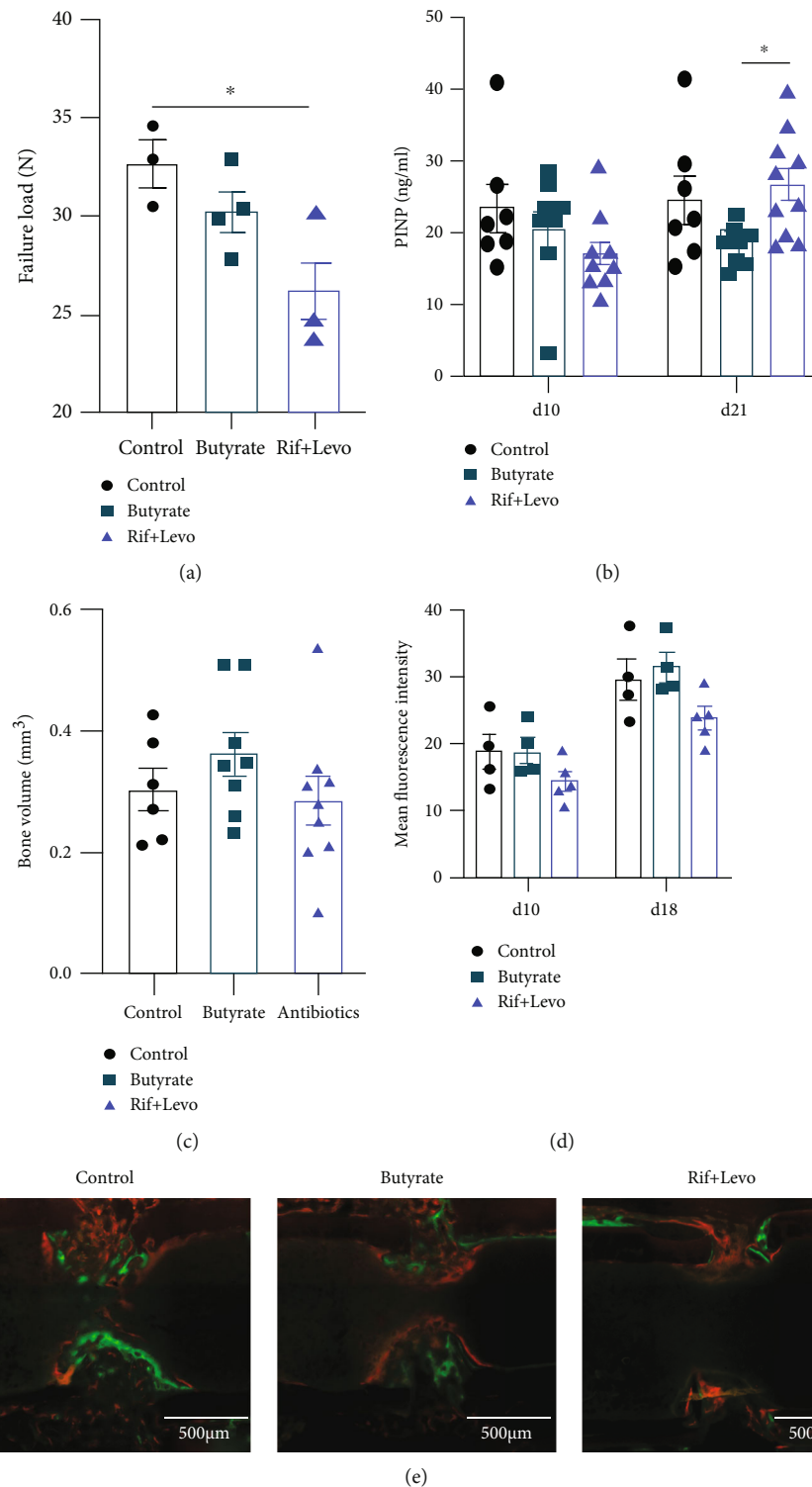


FIGURE 6: Butyrate does not significantly impact bone healing outcomes while rifampicin and levofloxacin may delay bone healing in a murine osteotomy model. Bone healing outcomes of operated mice were assessed 10 days, 18 days, and 21 days (euthanasia) following osteotomy. (a) Failure load of contralateral, unoperated femora was determined by a four-point-bending test. Data shown are means ($n = 3-4$) \pm SEM. (b) Procollagen type I C-terminal propeptide (PINP) in serum was determined 10 days and 21 days after osteotomy. Data shown are means ($n = 7-10$) \pm SEM. (c) Bone volume was measured by μ CT 21 days after osteotomy. Data shown are means ($n = 6-10$) \pm SEM. (d) Quantification of calcium deposition at osteotomy site 10 days after osteotomy (calcein green injection) and 18 days after osteotomy (xylenol orange injection). Data shown are mean fluorescent intensities ($n = 4-5$) \pm SEM. (e) Representative fluorescent images showing calcein green and xylenol orange labelling of exposed calcium at osteotomy site. Scale bar = 500 μ m, * $p < 0.05$.

CD3⁺ CD4⁺ T cells, butyrate-treated mice showed significantly higher percentages compared to Rif + Levo-treated mice in the iLN, whereas percentages in BM spleen remained largely unchanged between groups (Figure 5(c)). Viable CD45⁺ CD8⁺ T cell percentages trended higher in butyrate-treated mice compared to Rif + Levo-treated mice ($p=0.0713$) but did not significantly differ compared to the control group, and no large differences between groups were detected in iLN and spleen (Figure 5(d)). Taken together, butyrate mainly influences CD14⁺ monocytes/macrophages and CD19⁺ B cell population in BM of mice, therefore matching its potent effect on osteoclast precursor cells as shown *in vitro*.

3.6. Butyrate Does Not Significantly Impact Bone Healing Outcomes While Rifampicin and Levofloxacin May Delay Bone Healing in a Murine Osteotomy Model. Based on our *in vitro* findings showing butyrate's inhibitory effect on osteoclast formation and activity and its tendency to promote osteogenic differentiation of MSCs, we assessed whether butyrate impacts bone healing in a murine osteotomy model. Bone mechanical properties of the unoperated, contralateral femur of the mice were tested to determine the failure load. Failure load of butyrate-treated mice did not significantly differ from control mice, but Rif + Levo-treated mice showed a significant ($p < 0.05$) reduction in failure load 21 days after osteotomy (Figure 6(a)). Systemic PINP, a bone turnover marker, was significantly ($p < 0.05$) higher in Rif + Levo-treated mice compared to butyrate-treated mice at 21 days, but no significant difference between the groups was detected 10 days following osteotomy (Figure 6(b)). Bone volume of the newly formed callus at the osteotomy site was quantified 21 days following osteotomy by means of μ CT. No significant differences between the groups could be detected in terms of newly formed bone 21 days following osteotomy (Figure 6(c)). To determine the state of mineral apposition, as an indicator for bone remodeling and healing, fluorescently labelled calcium-binding agents were administered to mice 10 days (calcein green) and 18 days (xylenol orange) after osteotomy. Rif + Levo-treated mice show a slight reduction in mean fluorescent intensity at 10 and 18 days (Figures 6(d) and 6(e)). In addition, Giemsa-Eosin staining was performed to further visualize cartilaginous and bony callus formation at the osteotomy site 21 days after surgery. Rif + Levo-treated mice show a higher abundance of cartilaginous, rather than bony, mineralized callus, compared to control- and butyrate-treated mice (Supplementary Figure 5). This is in line with the finding of reduced mean fluorescent intensity, thus mineral apposition, in the Rif + Levo-treated mice. To conclude, butyrate does not significantly affect bone properties and healing outcomes in a murine osteotomy model. However, Rif + Levo-treated mice show a trend towards delayed bone remodeling and a change in bone properties as revealed by increased PINP levels in serum, reduced mineral apposition, and failure loads 21 days following osteotomy.

4. Discussion

The beneficial effects of probiotics and postbiotics on a variety of inflammatory diseases such as colitis and arthritis have raised the possibility that it may also play an important role in bone fracture healing. Postbiotic SCFAs have proven capacity to resolve hyperinflammatory responses [35], which may prevent delayed fracture union, resulting from a prolonged inflammatory healing phase. Conversely, disturbances in SCFA production, for example, via antibiotic therapy, may negatively impact fracture union, although this also remains largely unstudied to date.

Our initial *in vitro* studies showed that SCFAs are potent osteoclast inhibitors, by reducing osteoclast formation and their resorption activity. Mechanistic insights into this effect were revealed by RNA sequencing, whereby several pathways crucial for bone healing were highly affected in osteoclast precursor cells after exposure to butyrate. For example, the GPR-mediated chemotaxis pathway was upregulated in the presence of butyrate. GPR41, 43, and 109a and olfactory receptor 78 are well-known receptors for SCFAs, and, of particular relevance, GPR43 (also known as FFAR2) has previously been shown to be required for the inhibitory effects of SCFAs on osteoclasts [36]. We found that stimulation of GPR43 with a selective agonist led to a significant reduction in osteoclast formation, indicating the importance of GPR43 in the prevention of osteoclast formation. Lucas et al. found that the inhibitory effect of SCFAs on osteoclasts is largely independent of GPR43 but rather occurs as a consequence of a metabolic reprogramming of osteoclast precursor cells, leading to a downregulation of the essential osteoclast genes, TRAF6 and NFATc1 [37]. This discrepancy could be due to the differences in SCFA concentrations and mouse sexes used in these studies. In the context of GPR signaling, GPR183 (also known as EB12) was shown to be required for murine osteoclast precursor migration and osteoclast differentiation [38]. Although gene expression of GPR183 was significantly downregulated upon butyrate treatment in our study, inhibition of GPR183 signaling in human osteoclast precursor cells did not affect osteoclast formation. The upregulation of Wnt5a signaling in our gene enrichment analysis indicates another link between butyrate and bone healing, since Wnt5a was shown to be upregulated in fracture repair [39]. Regarding downregulated pathways, oxidative stress-related ROS signaling was one of the most affected pathways. High oxidative stress was shown to negatively influence bone remodeling by favoring osteoclastogenesis [40]. Tang et al. further demonstrated that butyrate protected from bone loss in rats by reducing ROS levels and promoting activity of mitochondrial antioxidant enzymes [41]. Although not particularly investigated in this study, it is worth mentioning that several *in vitro* studies highlighted the inhibitory effect of butyrate on osteoclast formation being attributed to inhibitory effects on histone deacetylase (HDAC) activity [42, 43]. Based on our transcriptome data and studies from others, it becomes obvious that the SCFA-mediated inhibition of osteoclast formation is a likely consequence of effects on multiple pathways including GPR signaling, HDAC inhibition, immune-related signaling, and metabolic changes.

The effect of butyrate on osteoclast precursor cells is also apparent in our *in vivo* osteotomy model. CD14⁺ monocytes/macrophages, which are precursor cells for osteoclasts, were significantly decreased in the BM following butyrate administration when compared to control- and antibiotic-treated mice. It was shown previously that butyrate directly affected CD45⁺ CD14⁺ cells by reducing CD14 receptor expression through posttranscriptional mechanisms [44]. Furthermore, SCFA propionate altered bone marrow hematopoiesis by mainly affecting macrophage and dendritic cell precursors in mice [45]. The butyrate-induced reduction of monocyte/macrophages in murine bone marrow is an additional proof of the potent impact of butyrate on osteoclast formation. The effect of SCFAs, in particular butyrate, on macrophages has previously been demonstrated, whereby SCFAs increased phagocytic capacity and antimicrobial activity in those cells [46, 47]. In contrast to the reduction of the monocytes/macrophage population, butyrate increased CD19⁺ B cell numbers in the BM compared to control- and antibiotic-treated mice. It has been recently described that butyrate supplementation suppressed arthritis in mice in a regulatory B cell- (Breg-) dependent manner [48]. Breg cells are also crucial in the bone union process by suppressing proinflammatory cytokines [49], and loss of Breg cell function has previously been associated with delayed healing in tibial fracture patients [50]. Although we did not assess the specific contributions of Breg and Treg cells to the observed effects of butyrate in our model, this is a likely potential mediator worthy of further investigation.

Besides butyrate's impact on a variety of immune cell populations, butyrate also impacted serum inflammatory maker, notably reducing proinflammatory IL-6 levels. IL-6 is not only secreted by immune cells such as macrophages but also by osteoblasts, which then promotes osteoclast formation [51]. Interestingly, pharmacological inhibition of soluble IL-6 improved compromised fracture healing after severe trauma in mice [52]. Other cytokines, which are also known to have osteoclastogenic capacity, are TNF α , IL-1 β , and IL-17 amongst others [53]. Here, Rif + Levo-treated mice show strongly increased TNF α , IL-17a, and IL-17f levels in the serum compared to control- and butyrate-treated mice. In fact, mice treated with Rif + Levo showed significantly reduced levels of SCFAs acetate, propionate, and butyrate in the cecal water, which was accompanied by a marked change in their gut microbiome composition [54]. The reduced levels of SCFAs might explain the high levels of circulating proinflammatory TNF α , IL-17a, and IL-17f levels in the serum of antibiotic-treated mice. In contrast, OPG (Tnfrsf11b) is an antiosteoclastogenic factor that preserves bone mass and is increased in antibiotic-treated mice but decreased in butyrate-treated mice compared to control mice. The correlation of TNF α and OPG in our study is in line with others describing TNF α as a promotor of OPG expression [54]. Indeed, TNF α was shown to upregulate OPG expression in dendritic cells, endothelial cells, smooth muscle cells, and fibroblasts [55] but also stimulated OPG secretion from human umbilical vein endothelial cells (HUVECs) [56]. Additionally, serum levels of both TNF α and OPG were higher in osteoarthritis patients compared to

healthy patients [57]. Thus, increased expression of OPG may counteract the proosteoclastogenic effects of increased TNF α levels to protect from excessive bone destruction. Interestingly, OPG treatment in rats impaired callus remodeling by reducing osteoclast numbers, although it did not influence early callus expansion [58]. Also, blockade of RANK signaling with the RANKL-targeted antibody denosumab, or treatment with the bisphosphonate alendronate, was shown to delay fracture callus remodeling but improved mechanical strength and bone mineral density in mice [59, 60]. Together, this highlights that a targeted and temporary activity of osteoclasts in the fracture healing is required for successful callus remodeling. Butyrate could be a candidate compound to optimally support fracture healing by preventing overactivity of osteoclasts at the remodeling stage and to support effective resolution of the initial inflammatory phase in fracture healing.

The high levels of circulating TNF α , IL-6, IL-17a, and IL-17f in SCFA depleted antibiotic-treated mice are indicative of a prolonged and unresolved systemic inflammatory phase in those mice. This could explain the tendency for delayed bone healing in the antibiotic-treated mice as revealed by increased PINP levels 21 days upon osteotomy and the trend towards reduced mineral apposition at the defect site. Since PINP is produced upon cleavage of procollagen during matrix formation prior to mineralization, this could indicate that bone remodeling and mineralization is at an early stage in the antibiotic-treated mice, whereas it is further advanced in the control- and butyrate-treated mice. Furthermore, the chronic elevation of TNF α , IL-6, IL-17a, and IL-17f can lead to excessive and prolonged osteoclast activity, which then results in net bone loss and decreased bone stability [61]. Indeed, antibiotic-treated mice showed reduced failure load values in the contralateral, unoperated femora in this study indicating a negative systemic effect on bone turnover. The measurement of IL-17a, IL-17f, and other cytokines in this study was performed in the mid and late phase of fracture repair (10 days and 21 days upon surgery), at which the osteoclasts are key players [24]. In the early phase of fracture repair (<7 days), it has been shown that both IL-17a and IL-17f promote osteoblast maturation and accelerate osteogenesis [62, 63]. Thus, depending on the fracture healing stage, IL-17a and IL-17f might have different functions and impact on both osteoclasts and osteoblasts. Such a bimodal role of cytokines in fracture healing has also been described for IL-6 [64].

Based on our findings, an interesting aspect for further study would be to investigate if butyrate supplementation could reverse the negative effects of antibiotic treatment on bone healing. Indeed, we tested a combined regime by administering both butyrate and antibiotics in an additional study group. However, after suffering from a greater than anticipated drop-out rate, the limited findings from this experimental group are not presented. The main reason for exclusions, which were present in all groups, was screw loosening; this may be partially attributed to the flexible fixation method and likely compounded by the use of male mice, which typically are heavier and display more pronounced barbering behavior than female mice. Flexible fixation methods are known to induce higher inflammatory callus

formation and so were selected for this study to reveal the potential for SCFAs to modulate healing in a positive direction. In order to test this combination of butyrate and antibiotics, refinement of the model may be required, through the use of a more rigid fixation approach, for example. The impact of butyrate in combination with antibiotics may also be tested in a bone infection model where significant inflammatory osteolysis is expected.

5. Conclusion

In conclusion, butyrate significantly reduced osteoclast formation and resorption activity in a dose-dependent manner and displayed a trend for increased calcium deposits in MSC cultures. *In vivo*, butyrate reduced monocyte/macrophages in the bone marrow and systemic IL-6 levels in a murine osteotomy model compared to control- and antibiotic-treated mice. In contrast, antibiotic-treated mice showed reduced SCFA levels in the cecum and higher circulating proinflammatory TNF α , IL-17a, and IL-17f levels. Antibiotic-treated mice also displayed a trend towards delayed bone healing compared to control- and butyrate-treated mice.

This study highlights the potential of the gut microbiota and its associated SCFAs as potential contributors to successful bone healing.

Data Availability

Fastq data files of RNA sequencing and 16s rRNA sequencing will be deposited on <http://ncbi.nlm.nih.gov/> upon manuscript publication. Other data is available upon request to authors.

Conflicts of Interest

All authors declare that they have no conflicts of interest.

Acknowledgments

The authors would like to thank all the members of the pre-clinical facility at ARI Davos for their help with the animal study, in particular the animal caretakers, Caroline Constant for performing surgeries, Karen Mys for support in μ CT analysis, and Mauro Bluvol and Nora Goudsouzian for histological sample processing. Pamela Furlong, Ge Tan, Susanne Bärtil, Ciara Ferris, and Samson Arveladze are also acknowledged for support in the performance of this study. This study was funded by AO Trauma as part of the Clinical Priority Program Bone Infection (AR2017_06).

Supplementary Materials

Supplementary Figure 1: (A, B) impact of acetate, propionate, butyrate, valerate (A), and antibiotics (B) on osteoclast formation. Osteoclast precursor cells were cultured with 20 ng/mL M-CSF and 10 ng/mL RANKL and with 0.1 mM, 0.25 mM, 0.5 mM, or 1 mM of the different SCFA classes, or 0.5 μ g/mL, 5 μ g/mL, or 50 μ g/mL rifampicin and/or levofloxacin, respectively. Osteoclast formation was quantified by means

of TRAcP staining. Shown are means ($n = 3$ independent donors, triplicates per donor) \pm SEM. (C) MSCs were cultured in chondrogenic media, and sulphated glycosaminoglycan (sGAG) content in cell pellets was assessed and normalized to DNA content. Data shown are means ($n = 5$ independent donors) with \pm SEM. Representative images of Safranin O and Fast Green staining in the absence (left image) and presence of 0.5 mM butyrate (right image). (D, E) Effects of butyrate on cell viability of osteoclast precursors (D) and MSCs (E) were assessed using CellTiter-Blue reagent. Data shown are means ($n = 3$ independent donors, triplicates per donor) \pm SEM. Percent cell viability was normalized to untreated osteoclast precursor cells and MSCs, respectively. **** $p < 0.0001$, *** $p < 0.001$, ** $p < 0.01$, and * $p < 0.05$. Supplementary Figure 2: (A, B) impact of GPR43 agonist and GPR183 inverse agonist (inhibitor) on osteoclast formation. Human osteoclast precursor cells were cultured with 20 ng/mL M-CSF and 10 ng/mL RANKL and with 75 nM, 750 nM, or 7500 nM GPR43 agonist (A) or 5 nM, 50 nM, or 500 nM inverse GPR183 agonist (B). Osteoclast formation was quantified by means of TRAcP staining. Shown are means ($n = 3$ independent donors, triplicates per donor) \pm SEM. ** $p < 0.01$; UT = untreated; RKL = RANKL. (C) Representative images of TRAcP staining of untreated (UT), RANKL-stimulated cells (RKL), and upon treatment with either 500 nM GPR183 inhibitor or 7500 nM GPR43 agonist. Scale bar in all images = 100 μ m. Supplementary Figure 3: (A) Principle Coordinate Analysis (PCoA) was performed on filtered ribosomal sequence variants (RSVs) using Bray-Curtis distances. (B) Percent abundances of 50 most abundant RSVs grouped by taxonomic family. (C) Heat map of the 50 most abundant genera as assigned by DADA2 analysis pipeline. Supplementary Figure 4: (A) serum concentrations of IL-10 in the absence and presence of butyrate and Rif + Levo, respectively, 10 days and 21 days upon osteotomy. (B) Gating strategy of flow cytometric immunophenotyping. Viable (eFluor 780 negative cells) were selected, and CD45+ cells were further gated from this population. CD19+, CD14+, CD3+ CD4+, and CD3+ CD8+ cells were selected as presented. Supplementary Figure 5: representative images of osteotomy sites 21 days after surgery stained with Giemsa-Eosin. Images were chosen based on bone volume median of each treatment group measured by μ CT 21 days upon surgery. Scale bar = 500 μ m. (*Supplementary Materials*)

References

- [1] S. V. Lynch and O. Pedersen, "The human intestinal microbiome in health and disease," *The New England Journal of Medicine*, vol. 375, no. 24, pp. 2369–2379, 2016.
- [2] J. A. Hawrelak and S. P. Myers, "The causes of intestinal dysbiosis: a review," *Alternative Medicine Review*, vol. 9, no. 2, pp. 180–197, 2004.
- [3] E. A. Franzosa, A. Sirota-Madi, J. Avila-Pacheco et al., "Gut microbiome structure and metabolic activity in inflammatory bowel disease," *Nature Microbiology*, vol. 4, no. 2, pp. 293–305, 2019.
- [4] K. Dabke, G. Hendrick, and S. Devkota, "The gut microbiome and metabolic syndrome," *The Journal of Clinical Investigation*, vol. 129, no. 10, pp. 4050–4057, 2019.

- [5] W. Barcik, R. C. T. Boutin, M. Sokolowska, and B. B. Finlay, "The role of lung and gut microbiota in the pathology of asthma," *Immunity*, vol. 52, no. 2, pp. 241–255, 2020.
- [6] M. Witkowski, T. L. Weeks, and S. L. Hazen, "Gut microbiota and cardiovascular disease," *Circulation Research*, vol. 127, no. 4, pp. 553–570, 2020.
- [7] K. Ding, F. Hua, and W. Ding, "Gut microbiome and osteoporosis," *Aging and Disease*, vol. 11, no. 2, pp. 438–447, 2020.
- [8] J. D. Guss, M. W. Horsfield, F. F. Fontenele et al., "Alterations to the gut microbiome impair bone strength and tissue material properties," *Journal of Bone and Mineral Research*, vol. 32, no. 6, pp. 1343–1353, 2017.
- [9] J. M. Berthelot, J. Sellam, Y. Maugars, and F. Berenbaum, "Cartilage-gut-microbiome axis: a new paradigm for novel therapeutic opportunities in osteoarthritis," *RMD Open*, vol. 5, no. 2, article e001037, 2019.
- [10] J. D. Guss, S. N. Ziemian, M. Luna et al., "The effects of metabolic syndrome, obesity, and the gut microbiome on load-induced osteoarthritis," *Osteoarthritis and Cartilage*, vol. 27, no. 1, pp. 129–139, 2019.
- [11] Y. L. Tsai, T. L. Lin, C. J. Chang et al., "Probiotics, prebiotics and amelioration of diseases," *Journal of Biomedical Science*, vol. 26, no. 1, p. 3, 2019.
- [12] C. J. Hernandez, "Musculoskeletal microbiology: the utility of the microbiome in orthopedics," *Journal of Orthopaedic Research*, vol. 39, no. 2, pp. 251–257, 2021.
- [13] J. Żółkiewicz, M. Ruszczyński, W. Feleszko, and W. Feleszko, "Postbiotics—a step beyond pre- and probiotics," *Nutrients*, vol. 12, no. 8, p. 2189, 2020.
- [14] N. Arpaia, C. Campbell, X. Fan et al., "Metabolites produced by commensal bacteria promote peripheral regulatory t-cell generation," *Nature*, vol. 504, no. 7480, pp. 451–455, 2013.
- [15] H. Liu, J. Wang, T. He et al., "Butyrate: a double-edged sword for health?," *Advances in Nutrition*, vol. 9, no. 1, pp. 21–29, 2018.
- [16] J. D. Schepper, R. Irwin, J. Kang et al., "Probiotics in gut-bone signaling," *Advances in Experimental Medicine and Biology*, vol. 1033, pp. 225–247, 2017.
- [17] F. C. Rodrigues, A. S. B. Castro, V. C. Rodrigues et al., "Yacon flour and bifidobacterium longum modulate bone health in rats," *Journal of Medicinal Food*, vol. 15, no. 7, pp. 664–670, 2012.
- [18] A. Wallimann, M. Hildebrand, D. Groeger et al., "An exopolysaccharide produced by *Bifidobacterium longum* 35624® inhibits osteoclast formation via a tlr2-dependent mechanism," *Calcified Tissue International*, vol. 108, no. 5, pp. 654–666, 2021.
- [19] R. A. Britton, D. Quach, R. Irwin et al., "Probiotic *L. reuteri* treatment prevents bone loss in a menopausal ovariectomized mouse model," *Journal of Cellular Physiology*, vol. 229, no. 11, pp. 1822–1830, 2014.
- [20] J. D. Schepper, F. L. Collins, N. D. Rios-Arce et al., "Probiotic *Lactobacillus reuteri* prevents postantibiotic bone loss by reducing intestinal dysbiosis and preventing barrier disruption," *Journal of Bone and Mineral Research*, vol. 34, no. 4, pp. 681–698, 2019.
- [21] N. D. Rios-Arce, J. D. Schepper, A. Dagenais et al., "Post-antibiotic gut dysbiosis-induced trabecular bone loss is dependent on lymphocytes," *Bone*, vol. 134, article 115269, 2020.
- [22] M. Rupp, C. Biehl, M. Budak, U. Thormann, C. Heiss, and V. Alt, "Diaphyseal long bone nonunions - types, aetiology, economics, and treatment recommendations," *International Orthopaedics*, vol. 42, no. 2, pp. 247–258, 2018.
- [23] C. Tzioupis and P. V. Giannoudis, "Prevalence of long-bone non-unions," *Injury*, vol. 38, Suppl 2, pp. S3–S9, 2007.
- [24] C. S. Bahney, R. L. Zondervan, P. Allison et al., "Cellular biology of fracture healing," *Journal of Orthopaedic Research*, vol. 37, no. 1, pp. 35–50, 2019.
- [25] S. Reinke, S. Geissler, W. R. Taylor et al., "Terminally differentiated cd8⁺ t cells negatively affect bone regeneration in humans," *Science Translational Medicine*, vol. 5, no. 177, 2013.
- [26] G. S. Baht, L. Vi, and B. A. Alman, "The role of the immune cells in fracture healing," *Current Osteoporosis Reports*, vol. 16, no. 2, pp. 138–145, 2018.
- [27] C. Schlundt, H. Schell, S. B. Goodman, G. Vunjak-Novakovic, G. N. Duda, and K. Schmidt-Bleek, "Immune modulation as a therapeutic strategy in bone regeneration," *Journal of experimental orthopaedics*, vol. 2, no. 1, p. 1, 2015.
- [28] M. Kotani, J. Kikuta, F. Klauschen et al., "Systemic circulation and bone recruitment of osteoclast precursors tracked by using fluorescent imaging techniques," *Journal of Immunology*, vol. 190, no. 2, pp. 605–612, 2013.
- [29] L. Kindle, L. Rothe, M. Kriss, P. Osdoby, and P. Collin-Osdoby, "Human microvascular endothelial cell activation by il-1 and tnf-alpha stimulates the adhesion and transendothelial migration of circulating human cd14+ monocytes that develop with rankl into functional osteoclasts," *Journal of Bone and Mineral Research*, vol. 21, no. 2, pp. 193–206, 2006.
- [30] J. L. Roberts, G. Liu, T. M. Darby et al., "*Bifidobacterium adolescentis* supplementation attenuates fracture-induced systemic sequelae," *Biomedicine & Pharmacotherapy*, vol. 132, article 110831, 2020.
- [31] J. H. Liu, T. Yue, Z. W. Luo et al., "*Akkermansia muciniphila* promotes type h vessel formation and bone fracture healing by reducing gut permeability and inflammation," *Disease Models & Mechanisms*, vol. 13, no. 11, 2020.
- [32] A. Wallimann, W. Magrath, K. Thompson et al., "Gut microbial-derived short-chain fatty acids and bone: a potential role in fracture healing," *European Cells & Materials*, vol. 41, pp. 454–470, 2021.
- [33] M. F. Pittenger, A. M. Mackay, S. C. Beck et al., "Multilineage potential of adult human mesenchymal stem cells," *Science*, vol. 284, no. 5411, pp. 143–147, 1999.
- [34] J. O. Voss, C. Loebel, J. J. Bara et al., "Effect of Short-Term Stimulation with Interleukin-1 β and Differentiation Medium on Human Mesenchymal Stromal Cell Paracrine Activity in Coculture with Osteoblasts," *BioMed Research International*, vol. 2015, Article ID 714230, 16 pages, 2015.
- [35] K. M. Maslowski, A. T. Vieira, A. Ng et al., "Regulation of inflammatory responses by gut microbiota and chemoattractant receptor gpr43," *Nature*, vol. 461, no. 7268, pp. 1282–1286, 2009.
- [36] C. C. Montalvany-Antonucci, L. F. Duffles, J. A. A. de Arruda et al., "Short-chain fatty acids and ffar2 as suppressors of bone resorption," *Bone*, vol. 125, pp. 112–121, 2019.
- [37] S. Lucas, Y. Omata, J. Hofmann et al., "Short-chain fatty acids regulate systemic bone mass and protect from pathological bone loss," *Nature Communications*, vol. 9, no. 1, p. 55, 2018.
- [38] E. Nevius, F. Pinho, M. Dhodapkar et al., "Oxysterols and ebi2 promote osteoclast precursor migration to bone surfaces and regulate bone mass homeostasis," *The Journal of Experimental Medicine*, vol. 212, no. 11, pp. 1931–1946, 2015.

- [39] K. S. Houschyar, C. Tapking, M. R. Borrelli et al., “Wnt pathway in bone repair and regeneration - what do we know so far,” *Frontiers in Cell and Development Biology*, vol. 6, p. 170, 2018.
- [40] V. Domazetovic, G. Marcucci, T. Iantomasi, M. L. Brandi, and M. T. Vincenzini, “Oxidative stress in bone remodeling: role of antioxidants,” *Clinical Cases in Mineral and Bone Metabolism*, vol. 14, no. 2, pp. 209–216, 2017.
- [41] X. Tang, S. Ma, Y. Li et al., “Evaluating the activity of sodium butyrate to prevent osteoporosis in rats by promoting osteal GSK-3 β /Nrf2 signaling and mitochondrial function,” *Journal of Agricultural and Food Chemistry*, vol. 68, no. 24, pp. 6588–6603, 2020.
- [42] M. M. Rahman, A. Kukita, T. Kukita, T. Shobuike, T. Nakamura, and O. Kohashi, “Two histone deacetylase inhibitors, trichostatin a and sodium butyrate, suppress differentiation into osteoclasts but not into macrophages,” *Blood*, vol. 101, no. 9, pp. 3451–3459, 2003.
- [43] D. S. Kim, J. E. Kwon, S. H. Lee et al., “Attenuation of rheumatoid inflammation by sodium butyrate through reciprocal targeting of hdac2 in osteoclasts and hdac8 in t cells,” *Frontiers in Immunology*, vol. 9, p. 1525, 2018.
- [44] F. Lasitschka, T. Giese, M. Paparella et al., “Human monocytes downregulate innate response receptors following exposure to the microbial metabolite n-butyrate,” *Immunity, Inflammation and Disease*, vol. 5, no. 4, pp. 480–492, 2017.
- [45] A. Trompette, E. S. Gollwitzer, K. Yadava et al., “Gut microbiota metabolism of dietary fiber influences allergic airway disease and hematopoiesis,” *Nature Medicine*, vol. 20, no. 2, pp. 159–166, 2014.
- [46] J. Schulthess, S. Pandey, M. Capitani et al., “The short chain fatty acid butyrate imprints an antimicrobial program in macrophages,” *Immunity*, vol. 50, no. 2, pp. 432–445.e7, 2019.
- [47] T. Wu, H. Li, C. Su et al., “Microbiota-derived short-chain fatty acids promote lamtor2-mediated immune responses in macrophages,” *mSystems*, vol. 5, no. 6, 2020.
- [48] E. C. Rosser, C. J. M. Piper, D. E. Matei et al., “Microbiota-derived metabolites suppress arthritis by amplifying aryl-hydrocarbon receptor activation in regulatory b cells,” *Cell Metabolism*, vol. 31, no. 4, pp. 837–851.e10, 2020.
- [49] G. Sun, Y. Wang, Y. Ti, J. Wang, J. Zhao, and H. Qian, “Regulatory b cell is critical in bone union process through suppressing proinflammatory cytokines and stimulating foxp3 in treg cells,” *Clinical and Experimental Pharmacology & Physiology*, vol. 44, no. 4, pp. 455–462, 2017.
- [50] S. Yang, W. Ding, D. Feng et al., “Loss of b cell regulatory function is associated with delayed healing in patients with tibia fracture,” *APMIS*, vol. 123, no. 11, pp. 975–985, 2015.
- [51] T. Wang and C. He, “TNF- α and il-6: the link between immune and bone system,” *Current Drug Targets*, vol. 21, no. 3, pp. 213–227, 2020.
- [52] K. Kaiser, K. Prystaz, A. Vikman et al., “Pharmacological inhibition of il-6 trans-signaling improves compromised fracture healing after severe trauma,” *Naunyn-Schmiedeberg's Archives of Pharmacology*, vol. 391, no. 5, pp. 523–536, 2018.
- [53] D. S. Amarasekara, H. Yun, S. Kim, N. Lee, H. Kim, and J. Rho, “Regulation of osteoclast differentiation by cytokine networks,” *Immune network*, vol. 18, no. 1, article e8, 2018.
- [54] A. Kubota, K. Hasegawa, T. Suguro, and Y. Koshihara, “Tumor necrosis factor-alpha promotes the expression of osteoprotegerin in rheumatoid synovial fibroblasts,” *The Journal of Rheumatology*, vol. 31, no. 3, pp. 426–435, 2004.
- [55] P. Reid and I. Holen, “Pathophysiological roles of osteoprotegerin (opg),” *European Journal of Cell Biology*, vol. 88, no. 1, pp. 1–17, 2009.
- [56] A. C. Zannettino, C. A. Holding, P. Diamond et al., “Osteoprotegerin (opg) is localized to the weibel-palade bodies of human vascular endothelial cells and is physically associated with von willebrand factor,” *Journal of Cellular Physiology*, vol. 204, no. 2, pp. 714–723, 2005.
- [57] S. Min, C. Wang, W. Lu et al., “Serum levels of the bone turnover markers dickkopf-1, osteoprotegerin, and TNF- α in knee osteoarthritis patients,” *Clinical Rheumatology*, vol. 36, no. 10, pp. 2351–2358, 2017.
- [58] M. Ulrich-Vinther and T. T. Andreassen, “Osteoprotegerin treatment impairs remodeling and apparent material properties of callus tissue without influencing structural fracture strength,” *Calcified Tissue International*, vol. 76, no. 4, pp. 280–286, 2005.
- [59] L. C. Gerstenfeld, D. J. Sacks, M. Pelis et al., “Comparison of effects of the bisphosphonate alendronate versus the rankl inhibitor denosumab on murine fracture healing,” *Journal of Bone and Mineral Research*, vol. 24, no. 2, pp. 196–208, 2009.
- [60] L. M. Flick, J. M. Weaver, M. Ulrich-Vinther et al., “Effects of receptor activator of nfkappab (rank) signaling blockade on fracture healing,” *Journal of Orthopaedic Research*, vol. 21, no. 4, pp. 676–684, 2003.
- [61] K. A. Tompkins, “The osteoimmunology of alveolar bone loss,” *Connective Tissue Research*, vol. 57, no. 2, pp. 69–90, 2016.
- [62] T. Ono, K. Okamoto, T. Nakashima et al., “IL-17-producing $\gamma\delta$ T cells enhance bone regeneration,” *Nature Communications*, vol. 7, no. 1, article 10928, 2016.
- [63] D. Nam, E. Mau, Y. Wang et al., “T-lymphocytes enable osteoblast maturation via il-17f during the early phase of fracture repair,” *PLoS One*, vol. 7, no. 6, article e40044, 2012.
- [64] K. Prystaz, K. Kaiser, A. Kovtun et al., “Distinct effects of il-6 classic and trans-signaling in bone fracture healing,” *The American Journal of Pathology*, vol. 188, no. 2, pp. 474–490, 2018.

Review Article

Systemic Inflammatory Markers for Predicting Overall Survival in Patients with Osteosarcoma: A Systematic Review and Meta-Analysis

Xiaotong Song,¹ Hao Zhang,¹ Fanxing Yin,¹ Panpan Guo,¹ Xiaocheng Yang,¹ Jinzhu Liu,² Yanshuo Han ¹, and Zhaozhou Ren ³

¹School of Life and Pharmaceutical Sciences, Dalian University of Technology, Panjin 124001, China

²Department of Orthopedic Surgery, The Third People's Hospital of Shenzhen, Shenzhen 518000, China

³Department of Orthopaedic Surgery, Shengjing Hospital of China Medical University, Shenyang 110001, China

Correspondence should be addressed to Yanshuo Han; yanshuohan@dlut.edu.cn and Zhaozhou Ren; zhaozhou.ren@yahoo.com

Received 2 June 2021; Revised 6 September 2021; Accepted 25 September 2021; Published 21 October 2021

Academic Editor: zhenhan deng

Copyright © 2021 Xiaotong Song et al. This is an open access article distributed under the Creative Commons Attribution License, which permits unrestricted use, distribution, and reproduction in any medium, provided the original work is properly cited.

Background. Inflammatory markers are associated with tumor genesis and progression, but their prognostic significance in osteosarcoma remains unclear. Therefore, we discussed the prognostic value of related inflammatory markers in osteosarcoma through a meta-analysis and systematic review. These inflammatory markers include C-reactive protein (CRP), neutrophil to lymphocyte ratio (NLR), lymphocyte to monocyte ratio (LMR), platelet to lymphocyte ratio (PLR), and Glasgow prognostic score (GPS). **Methods.** The Chinese National Knowledge Infrastructure (CNKI), Wanfang, Chinese Scientific Journals (VIP), PubMed, Embase, and Cochrane libraries were searched. The design of meta-analysis was made based on the PICOS (population, intervention/exposure, control, outcomes, and study design) principles, and STATA 15.1 was used to analyze the data. The Newcastle-Ottawa scale (NOS) was used to assess the quality of included studies. Hazard ratios (HRs) for overall survival (OS) and disease-specific survival (DPS) were extracted for the investigation of the prognostic value of inflammatory markers. **Results.** Twelve researches with 2162 osteosarcoma patients were included in total. The pooled results showed that elevated NLR, CRP, and GPS are all greatly related to shortening of OS among patients with osteosarcoma (HR = 1.68, $P = 0.007$, 95% CI: 1.15-2.45; HR = 1.96, $P = 0.002$, 95% CI: 1.28-3.00; HR = 2.54, $P < 0.0001$, 95% CI: 1.95-3.31, respectively), and CRP level is significantly associated with shortening of DPS among patients with osteosarcoma (HR = 2.76, 95% CI: 2.01-3.80, $P < 0.0001$), additionally. However, the correlation between LMR or PLR and the prognosis of osteosarcoma is not statistically significant (HR = 0.60, 95% CI: 0.30-1.18, $P = 0.138$; HR = 1.13, 95% CI: 0.85-1.49, $P = 0.405$, respectively). The outcomes of subgroup analysis to NLR and CRP suggested that histology, ethnicity, metastasis, and sample size all have an impact on its prognosis of patients with osteosarcoma. **Conclusion.** Worsened prognosis may be related to high levels of NLR, CRP, and GPS before treatment rather than LMR or PLR, which can provide the basis for clinicians to judge the outcomes of prognosis. **Trial Registration.** PROSPERO (CRD42021249954), https://www.crd.york.ac.uk/prospero/display_record.php?RecordID=249954.

1. Introduction

As a greatly malignant bone tumor, osteosarcoma mainly influences adolescents and young adults, accounting for about 45% of all bone sarcomas [1]. The development of integrated chemotherapy in the 1970s increased the overall survival rates by about 50% [2]. Among them, the incidence

of osteosarcoma in Europe is 7.3 per million person-years, while 12.2 per 1 million person-years in Asia [3]. In addition, the 5-year survival rate for osteosarcoma in Europe is 61% and 75% in Asia [4]. With the gradual development of clinical practice, the inaccuracy and inadequacy of traditional prognostic elements, such as the presence of tumor grade, metastasis, tumor location, and histological subtypes,

have gradually been exposed [5]. Therefore, identifying more effective prognostic factors will be valuable for stratifying patients with different treatment options and improving survival.

In recent years, according to emerging evidence, systemic inflammatory response is an independent prognostic biomarker among different tumors. Moreover, according to increasing studies, there is a clear association between inflammatory markers and lower survival rates for some tumors such as neutrophil to lymphocyte ratio (NLR), Glasgow prognostic score (GPS), C-reactive protein (CRP), platelet to lymphocyte ratio (PLR), and lymphocyte to monocyte ratio (LMR) [6–9]. However, the predictive effect of these inflammatory indicators on the prognosis of osteosarcoma is unclear. The research of Liu et al. [10] and Xia et al. [11] believed that enhanced NLR is significantly related to the shortening of OS among patients with osteosarcoma, but the study of Huang et al. [12] suggested that NLR can be used as a protective factor for osteosarcoma. In addition, there is no significant relationship between CRP and the prognosis of osteosarcoma from the point of Li et al. [13] and Liu et al. [10]. Hence, the association between systemic inflammatory marker (e.g., NLR, CRP, LMR, GPS, and PLR) levels and the overall survival of patients with osteosarcoma was explored by a meta-analysis, aiming to assess these biomarkers as prognostic factors for overall survival and disease-specific survival.

2. Methods

The registration of systematic inspection at PROSPERO (<http://www.crd.york.ac.uk/PROSPERO>) as CRD42021249954 was made on basis of the associated items of the PRISMA statement [14].

2.1. Search Strategy. The English literatures of PubMed, Embase, and Cochrane libraries and the Chinese literature of CNKI, Wanfang, and VIP from their establishment to April 2021 will be comprehensively and systematically searched. PubMed, Cochrane Library, and Embase were searched through the subject words and keywords retrieval method using the following keywords: “Osteosarcoma” [MeSH], “C-reactive protein” [MeSH], “neutrophil to lymphocyte ratio” [MeSH], “Glasgow prognostic score” [MeSH], “lymphocyte to monocyte ratio” [MeSH], and “platelet to lymphocyte ratio” [MeSH] (Supplementary File 1). The manual retrieve of other associated articles was made from the reference lists or citations in the primary search or applying “Similar Articles” PubMed option. The CNKI, Wanfang, and VIP were searched using the general Chinese translation of the above search terms: C-reactive protein (CRP), neutrophil to lymphocyte ratio (NLR), lymphocyte to monocyte ratio (LMR), Glasgow prognostic score (GPS), and platelet to lymphocyte ratio (PLR).

2.2. Literature Inclusion and Exclusion Criteria. The eligibility criteria were mainly conducted in accordance with the PICOS (population, intervention/exposure, control, out-

comes, and study design) principle limited to Chinese and English study.

The inclusion standards were shown below:

(a) *Population.* Patients with primary osteosarcoma who have survived radiation therapy, surgery, and chemotherapy

(b) *Exposure.* Risk factor (inflammatory marker), including NLR, CRP, GPS, PLR, and LMR level

(c) *Comparators.* Normal levels of inflammatory markers in normal subjects

(d) *Outcomes.* Survival outcomes or clinicopathological characteristics of osteosarcoma cases, such as recurrence and metastasis

(e) *Study design.* Case-control study or cohort study

The following exclusion criteria were utilized: (a) papers which were meta-analysis, reviews, animal experiments, case reports, conference abstracts, non-English/Chinese literature, mechanism researches or other diseases/cancers, or lacking the full text; (b) duplicate publication or overlapped data which was offered in the prior article; (c) study provided insufficient information on survival outcomes about HR, or no data presented for CRP, NLR, GPS, PLR, and LMR level.

2.3. Literature Screening and Data Extraction. Independently, all eligibility surveys for inclusion in the study were conducted by two authors (X.S. and H.Z.), and any differences that arose during the screening process were discussed, negotiated, and resolved by the two authors together. In case of questions or controversies, the decision was made after discussing or consulting with a third person (Y.H.). For the data extraction, the author, publication year, study area, research type, number of cases, follow-up, and hazard ratios (Table 1) are for evaluating neutrophil-to-lymphocyte ratio (NLR), Glasgow prognostic score (GPS), C-reactive protein (CRP), platelet to lymphocyte ratio (PLR), and lymphocyte-monocyte ratio (LMR) of overall survival (OS) and disease-specific survival (DPS).

2.4. Literature Quality Assessment. Two researchers (X.S. and F.Y.) separately made literature quality evaluations applying the Newcastle-Ottawa Scale (NOS) for cohort study [15] in Table 2. There are 4 items (4 points) for “Research Subject Selection,” 1 item (2 points) for “Comparability between Groups,” and 3 items (3 points) for “Result Measurement” in NOS, with a full score of 9 points and ≥ 7 is regarded as high-quality literature, less than 7 is classified as low-quality literature.

2.5. Data Synthesis and Statistical Analysis. STATA version 15.1 statistical software (StataCorp LP, College Station, TX) was used to analyze the data. The association of associated inflammatory factors with OS and DPS was evaluated by using hazard ratios (HR) and 95% confidence intervals (CI). Heterogeneity was assessed by Cochran’s Q statistic and I^2 . If the heterogeneity test is $P \geq 0.1$ and $I^2 \leq 50\%$, indicating the existence of homogeneity among the studies, and the combined analysis was made by the fixed-effect model; if $P < 0.1$, $I^2 > 50\%$, it indicates whether there is heterogeneity in the study. The source of heterogeneity was found by

TABLE 1: Baseline characteristics and quality assessment of the included studies.

Study	Year	Location	Sample size	Type	Metastasis	Follow-up*	Gender (m/f)	Treatment	Outcomes	Inflammatory markers
Funovics et al. [18]	2011	Austria	79	Osteosarcoma	30/49	33 (1-126) months	42/37	Chemotherapy; surgery	DPS/OS	CRP
Nakamura et al. [19]	2013	British	318	Osteosarcoma; Ewing's sarcoma; chondrosarcoma	NO	40 (1-109) months	176/142	Radiotherapy; surgery; chemotherapy	OS	CRP
Liu et al. [20]	2015	China	327	Osteosarcoma	130/197	24 (3-60) months	235/92	Surgery; chemotherapy	OS	LMR
Liu et al. [10]	2016	China	162	Osteosarcoma	78/162	NA	96/66	Chemotherapy; surgery	OS	CRP, GPS, LMR, NLR, PLR
Aggerholm-Pedersen et al. [21]	2016	Denmark	172	Chondrosarcoma; Ewing's sarcoma; osteosarcoma	NO	8.8 (4.3-19) years	98/74	Radiotherapy; surgery; chemotherapy	DPS/OS	CRP, GPS, NLR
Xia et al. [11]	2016	China	359	Osteosarcoma	132/227	40 (3-60) months	258/101	Surgery; chemotherapy	OS	NLR, PLR,
Li et al. [22]	2017	China	215	Osteosarcoma	30/49	NA	122/94	Surgery; chemotherapy	OS	GPS, NLR, PLR
Li et al. [13]	2015	China	85	Osteosarcoma	37/85	NA	43/42	Chemotherapy	OS	CRP
Jattoo et al. [23]	2019	British	79	Osteosarcoma; chondrosarcoma; Ewing's sarcoma	14/63	45 (1-172) months	44/35	Surgery; chemotherapy	DPS/OS	CRP
Huang et al. [24]	2018	China	103	Osteosarcoma	13/90	43 months	63/40	Surgery; chemotherapy	OS	GPS, NLR
Huang et al. [12]	2019	China	126	Osteosarcoma	7/119	44 (7-81) months	78/48	Surgery; chemotherapy	OS	NLR, PLR
Hu et al. [25]	2020	China	137	Osteosarcoma	61/76	55 (4-112) months	80/57	Surgery; chemotherapy	OS	LMR

Note: “*” median (minimum-maximum) follow-up time; NA: data were not provided in the publication.

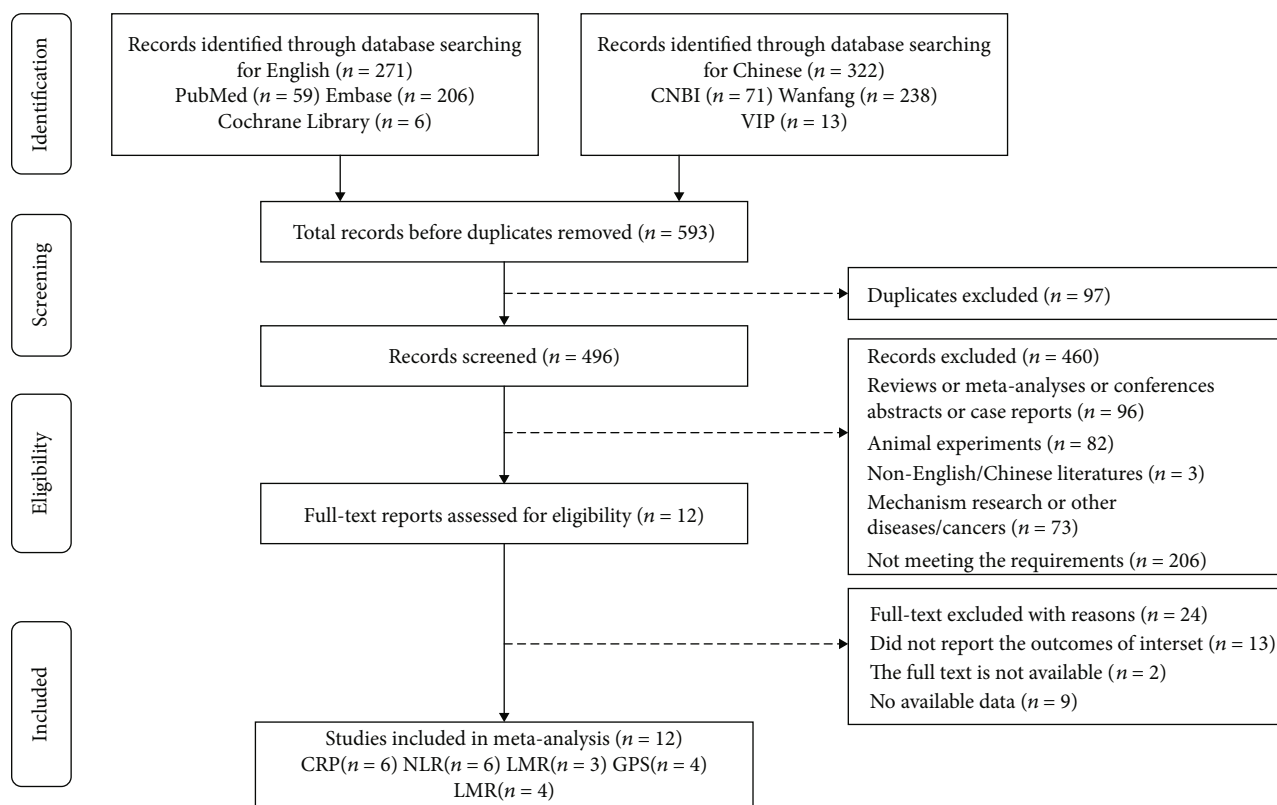


FIGURE 1: Flow chart of the study selection.

subgroup analysis based on race, histology, metastasis, and sample size. If the heterogeneity is still large, the random effects model was adopted or the combination of results was abandoned and descriptive analysis was adopted. Begg's test [16] and Egger's test [17] were utilized to estimate publication bias. Sensitivity analysis was utilized to estimate the robustness and reliability of the combined results influenced by a single included study.

3. Results

3.1. The Results of Literature Search. In this study, 593 studies were retrieved from the database in total. After eliminating duplicate studies, 97 were obtained. After browsing titles and abstracts, 36 researches were obtained. Finally, 12 articles meeting the requirements were brought into the meta-analysis (Figure 1), and there were 8 studies in China, 2 studies in British, 1 study in Denmark, and 1 study in Austria. The type of study included was a cohort study with a maximum follow-up time of 19 years (Table 1).

3.2. Systemic Inflammatory Markers and Overall Survival. 6 studies reported an association between neutrophil-to-lymphocyte ratio (NLR) and overall survival among patients with osteosarcoma. With a meta-analysis conducted through a random-effects model, the pooled results show that elevated NLR is significantly associated with shortening of OS

in patients with osteosarcoma (HR = 1.68, 95% CI: 1.15-2.45, $P = 0.007$; $I^2 = 84.7\%$, $P < 0.0001$; Figure 2(a)).

6 studies reported an association between C-reactive protein (CRP) and OS among patients with osteosarcoma. With a meta-analysis conducted through a random-effects model, the pooled results show that elevated CRP is significantly associated with shortening of OS in patients with osteosarcoma (HR = 1.96, 95% CI: 1.28-3.00, $P = 0.002$; $I^2 = 60.0\%$, $P = 0.028$; Figure 2(b)).

3 studies reported an association between lymphocyte-monocyte ratio (LMR) and OS among patients with osteosarcoma. With a meta-analysis conducted through a random effects model, the pooled results show that there is no significantly relationship between LMR and OS of patients with osteosarcoma (HR = 0.60, 95% CI: 0.30-1.18, $P = 0.138$; $I^2 = 82.7\%$, $P = 0.003$; Figure 2(c)).

4 studies reported an association between Glasgow prognostic score (GPS) and OS among patients with osteosarcoma. With a meta-analysis conducted through a fixed effects model, the pooled results show that GPS is significantly associated with shortening of OS among patients suffering from osteosarcoma (HR = 2.54, 95% CI: 1.95-3.31, $P < 0.0001$; $I^2 = 0.0\%$, $P = 0.496$; Figure 2(d)).

4 studies reported an association between platelet to lymphocyte ratio (PLR) and OS among patients with osteosarcoma. A meta-analysis was conducted through a random effects model, and the pooled results show that there is no significant relationship between PLR and OS of patients with

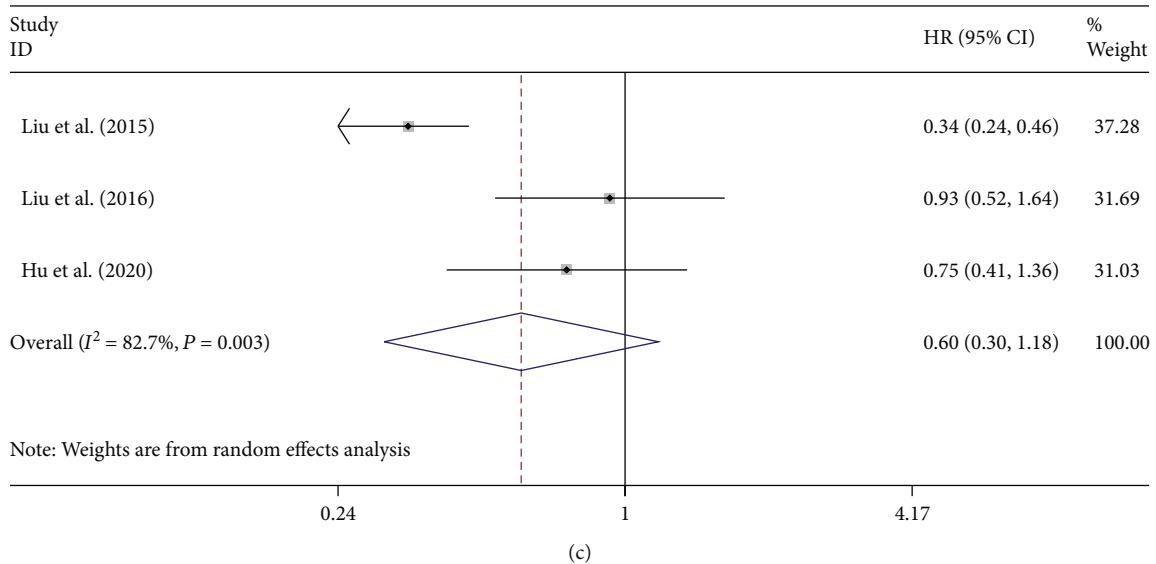
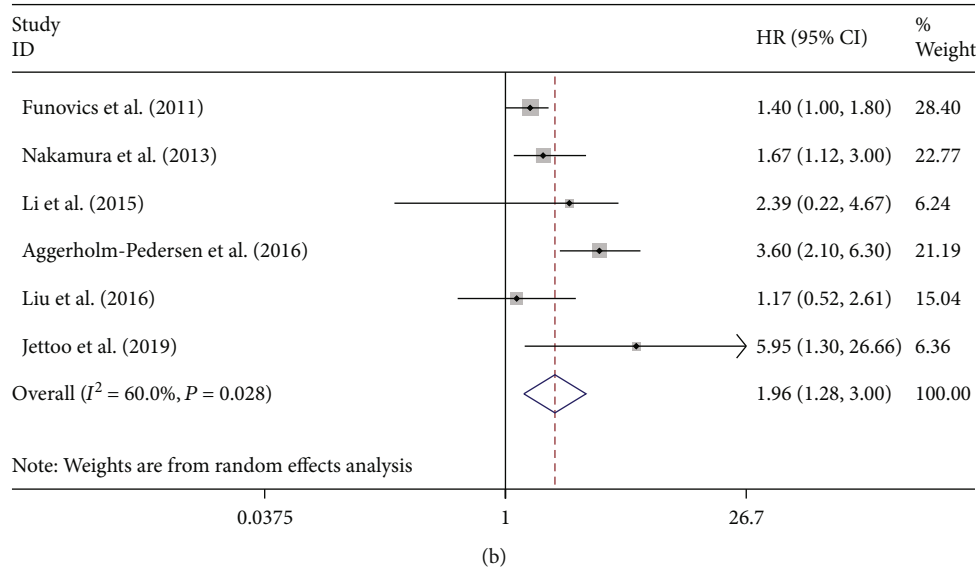
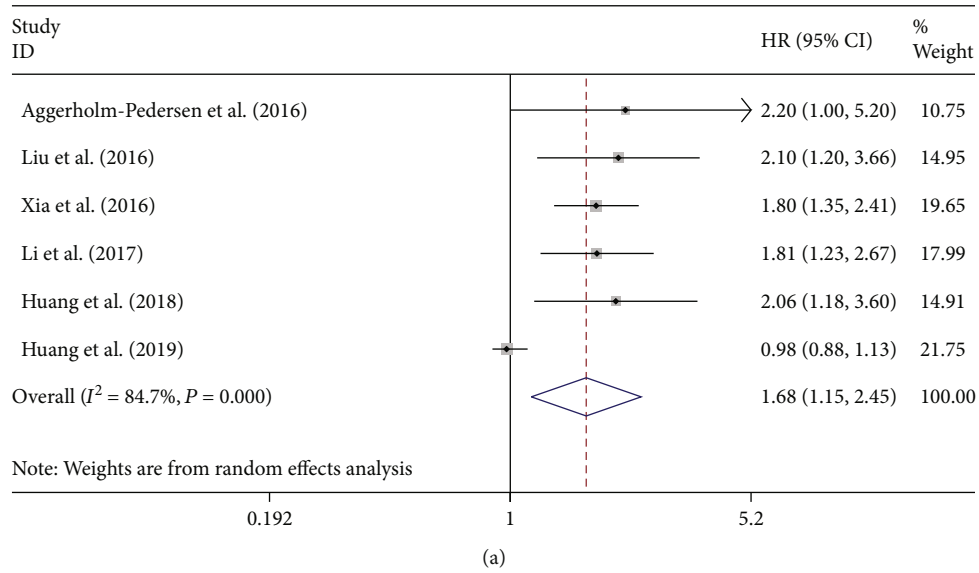


FIGURE 2: Continued.

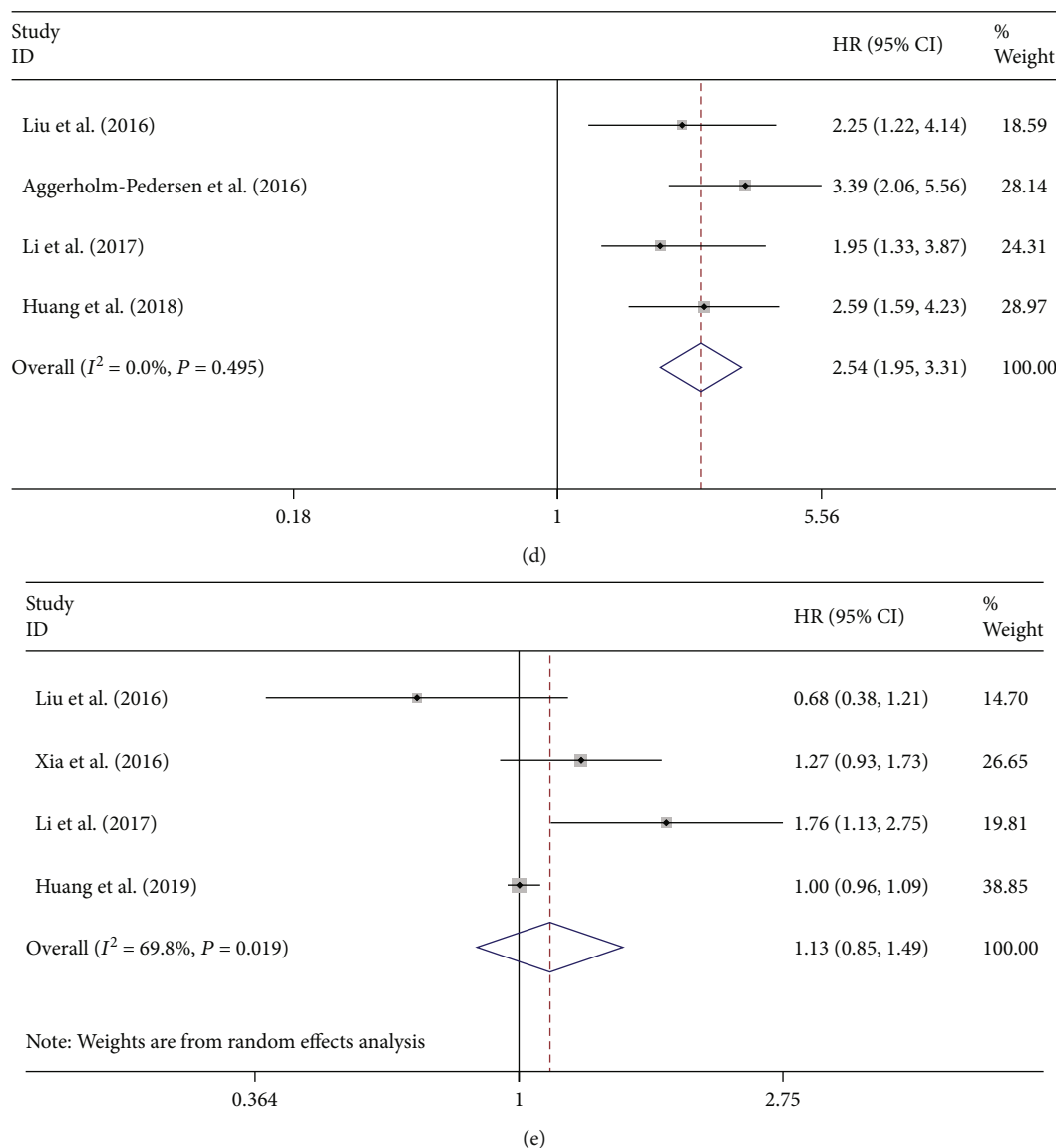


FIGURE 2: The association of NLR (a), CRP (b), LMR (c), GPS (d), and PLR (e) levels with the OS of patients with osteosarcoma.

osteosarcoma (HR = 1.13, 95% CI: 0.85-1.49, $P = 0.405$; $I^2 = 69.8\%$, $P = 0.003$; Figure 2(e)).

3.3. Systemic Inflammatory Markers and Disease-Specific Survival. There were 3 studies that reported the relationship between C-reactive protein level and disease-specific survival (DPS). Additionally, the pooled results show that CRP is greatly related to the shortening of DPS among patients suffering from osteosarcoma (HR = 2.76, 95% CI: 2.01-3.80, $P < 0.0001$; $I^2 = 0.0\%$, $P = 0.549$; Figure 3).

3.4. Subgroup Analysis for Neutrophil-to-Lymphocyte Ratio. For the detection of the potential source of heterogeneity in analyzing the relation between NLR and OS, ethnicity, metastasis, histology, and sample size were applied to stratify the subgroup analysis. The pooled results show that the elevated NLR predicts poorer OS in Asian populations (HR = 1.63, 95% CI: 1.09-2.43, $P = 0.017$; Figure 4(a)), while the relationship between the level of NLR and OS was not

significant in European populations (HR = 2.20, 95% CI: 0.96-5.02, $P = 0.067$; Figure 4(a)).

Subgroup analyses were also performed on histology and metastasis to further explain. Among patients suffering from osteosarcoma, growing NLR was related to shortened OS (HR = 1.63, 95% CI: 1.09-2.43, $P = 0.017$; Figure 4(b)). However, according to the pooled outcomes, there is no great relation between NLR and OS of patients suffering from osteosarcoma and other bone cancers (HR = 2.20, 95% CI: 0.96-5.02, $P = 0.061$; Figure 4(b)).

An enhanced level of NLR was related to reduced survival among patients with metastasis (HR = 1.63, 95% CI: 1.09-2.43, $P = 0.017$; Figure 4(c)), while the association between the level of NLR and OS was not evident in patients without metastasis (HR = 2.20, 95% CI: 0.96-5.02, $P = 0.061$; Figure 4(c)).

3.5. Subgroup Analysis for C-Reactive Protein. Subgroup analysis for the detection of the potential source of

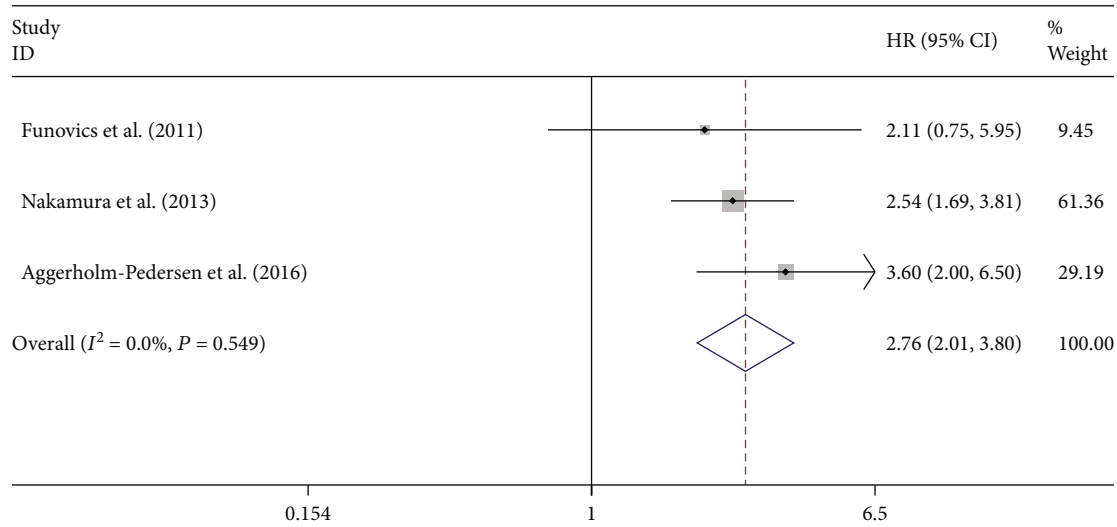


FIGURE 3: The association of CRP levels with the disease-specific survival of patients with osteosarcoma.

heterogeneity in analyzing the association between CRP and OS was made by stratification by ethnicity, histology, metastasis, and sample size. The pooled results show that poorer OS in European populations (HR = 2.19, 95% CI: 1.28-3.74, $P = 0.004$; Figure 5(a)) can be predicted by the enhanced CRP level, while there was no great relationship between the level of CRP and OS in Asian populations (HR = 1.36, 95% CI: 0.67-2.78, $P = 0.394$; Figure 5(a)). Sub-group analyses on metastasis, histology, and sample size were performed for further explanation to further explain. Among patients suffering from osteosarcoma, increased CRP level was correlated with shortened OS (HR = 1.39, 95% CI: 1.06-1.83, $P = 0.016$; Figure 5(b)), and patients with bone sarcomas encountered the same situation (HR = 2.78; 95% CI: 1.40-5.49, $P = 0.003$; Figure 5(b)). An enhanced level of CRP was related to reduced survival among patients with or without metastasis (Figure 5(c)). Additionally, the pooled outcomes displayed that in studies with a sample size of greater than or equal to 100 patients, elevated CRP predicted poor OS (HR = 1.99, 95% CI: 1.06-3.74, $P = 0.032$; Figure 5(d)). However, in a sample size less than 100, relationship between CRP and OS was not significant (HR = 2.10, 95% CI: 0.92-4.81, $P = 0.080$; Figure 5(d)).

3.6. Sensitivity Analysis. Sensitivity analysis eliminated every included research successively and performed a summary discussion on the remaining researches to evaluate whether a single included research excessively influenced on the overall outcomes of the meta-analysis. The outcomes of the sensitivity analysis are shown in Supplementary file 2, indicating that no research exerted an excessive impact on the outcomes of the meta-analysis, and that the outcomes of the remaining researches are stable and credible.

3.7. Publication Bias. The Begg's funnel plot of this study is shown in Supplementary file 3. It could be seen that the funnel plot was basically symmetrical, and the P value of Egger's test for NLR was 0.115 (Figure 6), for CRP was 0.762, for

GPS was 0.130, indicating that no obvious publication bias in this study.

4. Discussion

This meta-analysis pooled 12 researches, including 2,162 patients, to examine the relation between C-reactive protein (CRP), neutrophil to lymphocyte ratio (NLR), lymphocyte to monocyte ratio (LMR), Glasgow prognostic score (GPS), and platelet to lymphocyte ratio (PLR) levels with the OS of patients suffering from osteosarcoma, aiming to assess these biomarkers as prognostic elements for overall survival and disease-specific survival.

Inflammation is essential for human tumors, malignant transformation, and antitumor immunity [26]. It is increasingly recognized that systemic inflammation exerts a vital effect on the occurrence and growth of cancer [27, 28]. Inflammatory factors can directly provide free radicals to attack normal DNA mechanisms and cause cancer or indirectly damage DNA and regulate gene expression by affecting the epigenetic characteristics of cells [29]. Neoplastic cells often excessively express proinflammatory mediators such as proteases, cytokines, and chemokines [30]. Various types of oncogenes are activated through mutation, chromosomal rearrangement, or amplification. Transformed cells undergoing this process produce inflammatory mediators that activate the expression of transcription factors. Then, activated transcription factors further coordinate the production of inflammatory mediators and ultimately form cancer-related microenvironments [27]. It is not surprising to detect increased levels of CRP, NLR, or GPS in cancer because of the importance of the inflammation in the development of cancer.

It is known that NLR values increase in acute pancreatitis [31], cardiac events [32], and atherosclerosis [33]. As a marker of systemic inflammation, NLR can also be considered as a potential prognostic factor for different tumors. Pretreatment NLR was utilized as a prognostic indicator of long-term mortality in patients with breast cancer by Azab

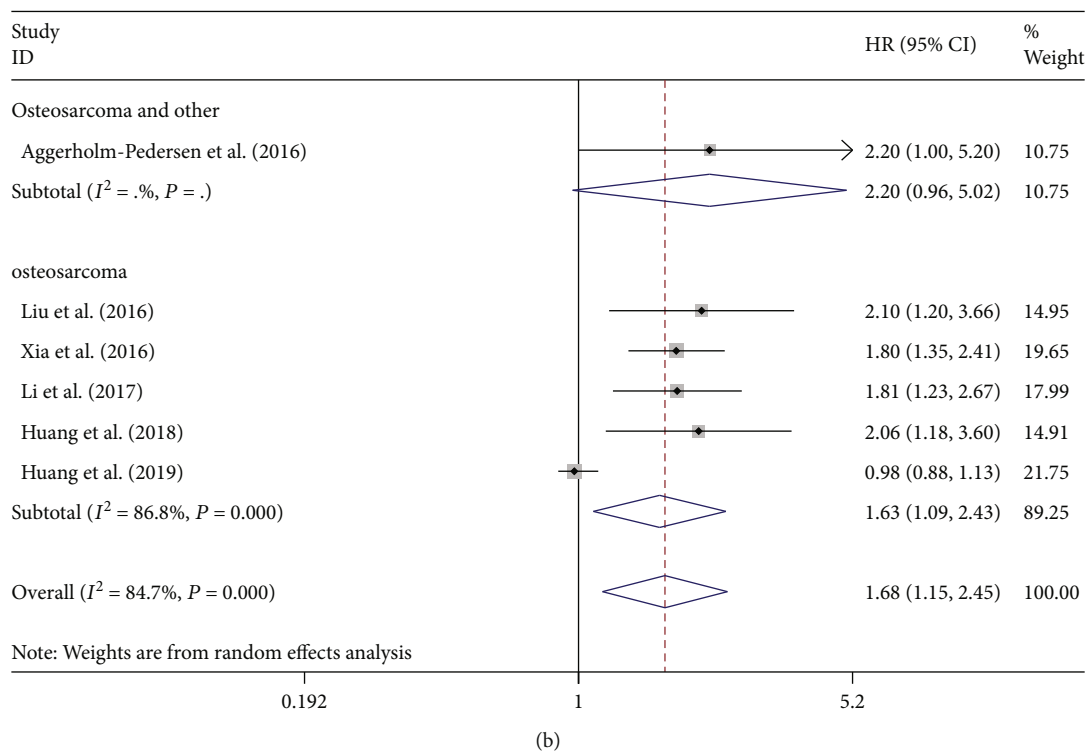
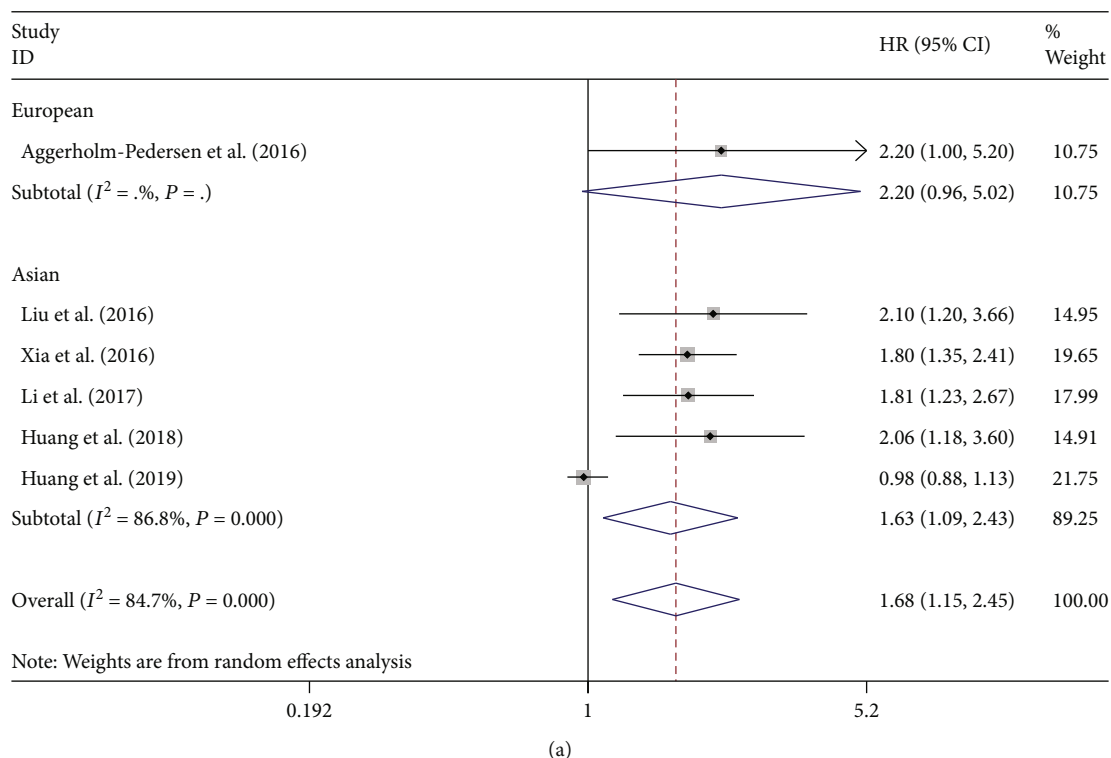


FIGURE 4: Continued.

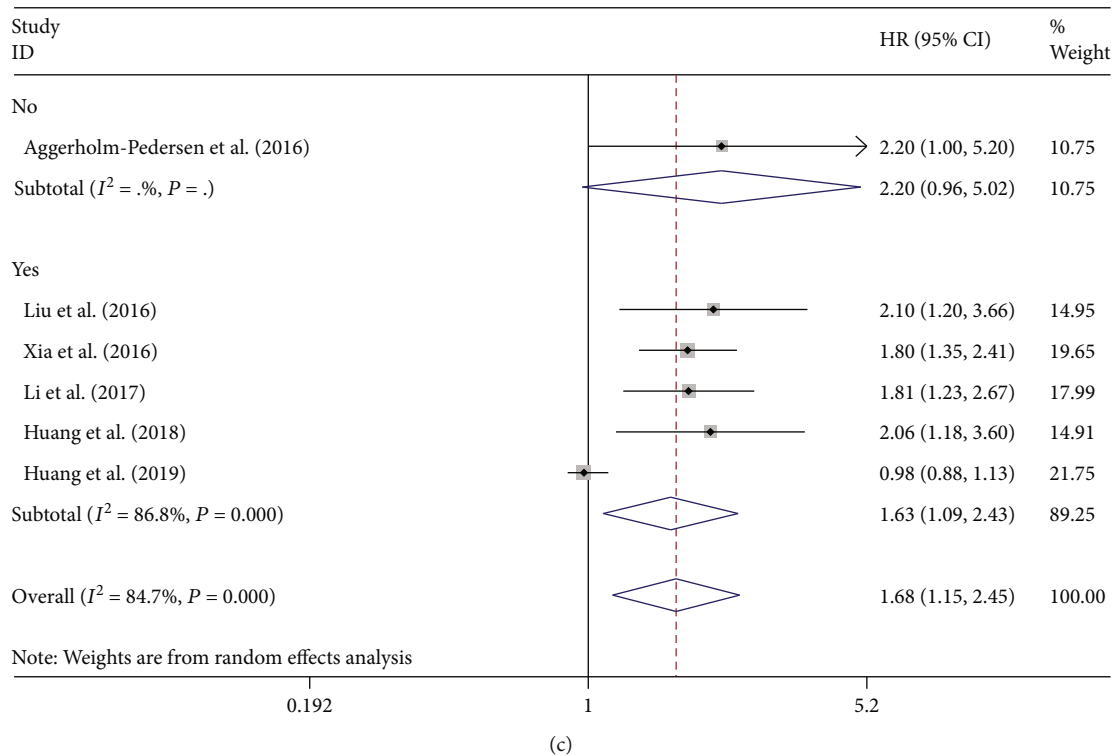


FIGURE 4: Subgroup analysis of the association of NLR levels with the OS of patients with osteosarcoma. The association of overall survival within European or Asian patients (a), osteosarcoma or other bone sarcomas (b), metastasis or nonmetastasis patients (c), and NLR levels with the OS of patients with osteosarcoma.

et al. [34]. According to Deng et al., preoperative NLR is a separate prognostic factor specific to cancer survival among patients undergoing gastric cancer surgery [9]. However, the relation between NLR and the prognosis of patients suffering from osteosarcoma remains controversial. The pooled outcomes showed that enhanced NLR is greatly related to the shortening of OS in patients with osteosarcoma, showing that great serum levels of NLR before treatment may be a negative prognostic element for patients suffering from bone cancers.

It has been also shown that increased levels of systemic inflammation are related to lower survival rates in patients with solid tumors [35, 36]. CRP is a nonspecific but sensitive marker of systemic inflammation synthesized by liver cells replying microbial invasion or tissue damage [37]. It is well known that during inflammation, acute infection, and tissue damage, CRP levels will rise rapidly. In addition, enhanced CRP levels are also regarded as a significant risk element for atherosclerosis [38], stroke [39–41], and myocardial infarction [42]. Importantly, it has been confirmed that the preoperative level of serum CRP is related to the prognosis of hepatocellular carcinoma [43] and pancreatic cancer [44]. Our pooled results also found that elevated levels of CRP are greatly related to the shortening of OS in patients with osteosarcoma (HR = 1.96, 95% CI: 1.28–3.00) which conforms to the outcomes of most researches [13, 18, 19, 21]. Additionally, pooled result showed that CRP is significantly associated with shortening of DPS in patients with osteosarcoma (HR = 2.76, 95% CI: 2.01–3.80). These all suggested that

CRP is a risk factor for the prognosis of osteosarcoma. To improve the prognosis of the patients with elevated CRP, NLR, and GPS, it is urgently needed a management protocol for systemic inflammatory response via the tumor-host interaction during the postoperative course is urgently needed to improve their prognosis [45].

Simultaneously, no great association between the level of NLR and OS in Europe patients was found in the stratified analysis (HR = 2.20, 95% CI: 0.96–5.02) and no significant association between CRP levels and OS in Asia patients (HR = 1.36, 95% CI: 0.67–2.78). This may be due to the differences in the susceptibility genes, treatment options, and CRP measurement methods of bone tumors in Asia and Europe. Subgroup analyses on metastasis, histology, and sample size were made for the explanation of heterogeneity. In the analysis of NLR, the pooled results showed that there is no significant relationship between NLR and OS of patients suffering from osteosarcoma and other bone cancers (HR = 2.20, 95% CI: 0.96–5.02). The similar result also appeared in nonmetastasis osteosarcoma, indicating that histology and metastasis may be the cause of high heterogeneity. In the analysis of CRP, enhanced CRP was related to shortened OS in patients with osteosarcoma (HR = 1.39, 95% CI: 1.06–1.83), and patients with other bone cancers encountered the same situation. Similarly, the pooled results showed that an enhanced level of CRP was related to reduced OS in patients with osteosarcoma regardless of metastasis. The results suggested that this high heterogeneity may be independent of histology and metastasis.

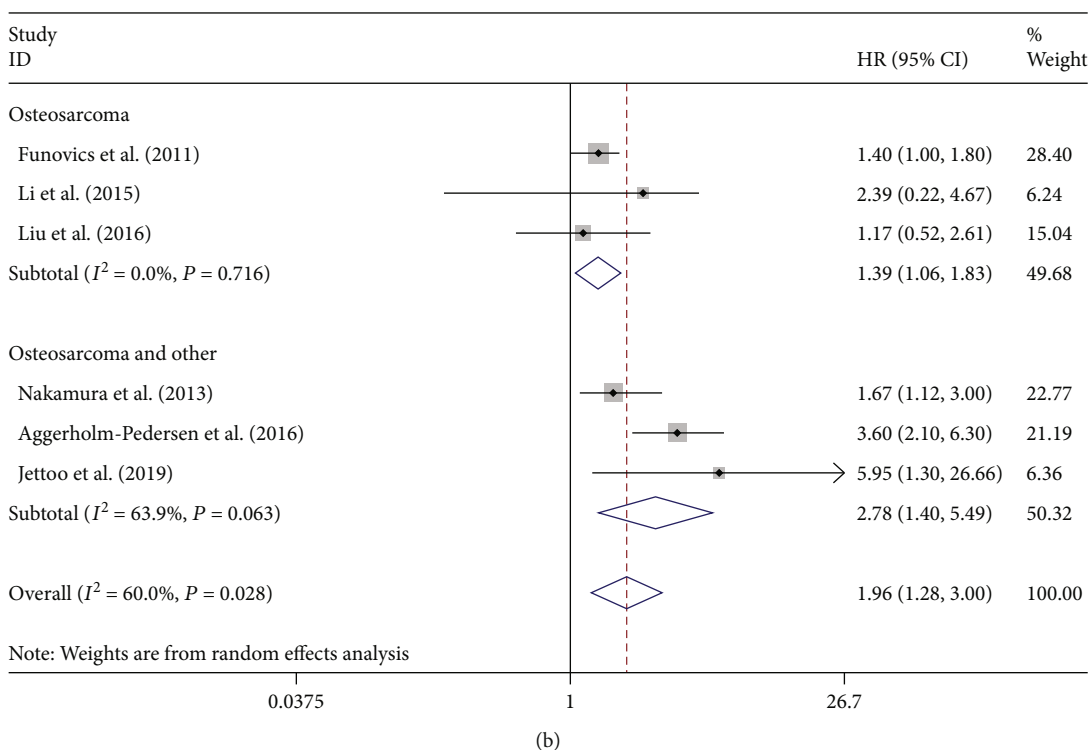
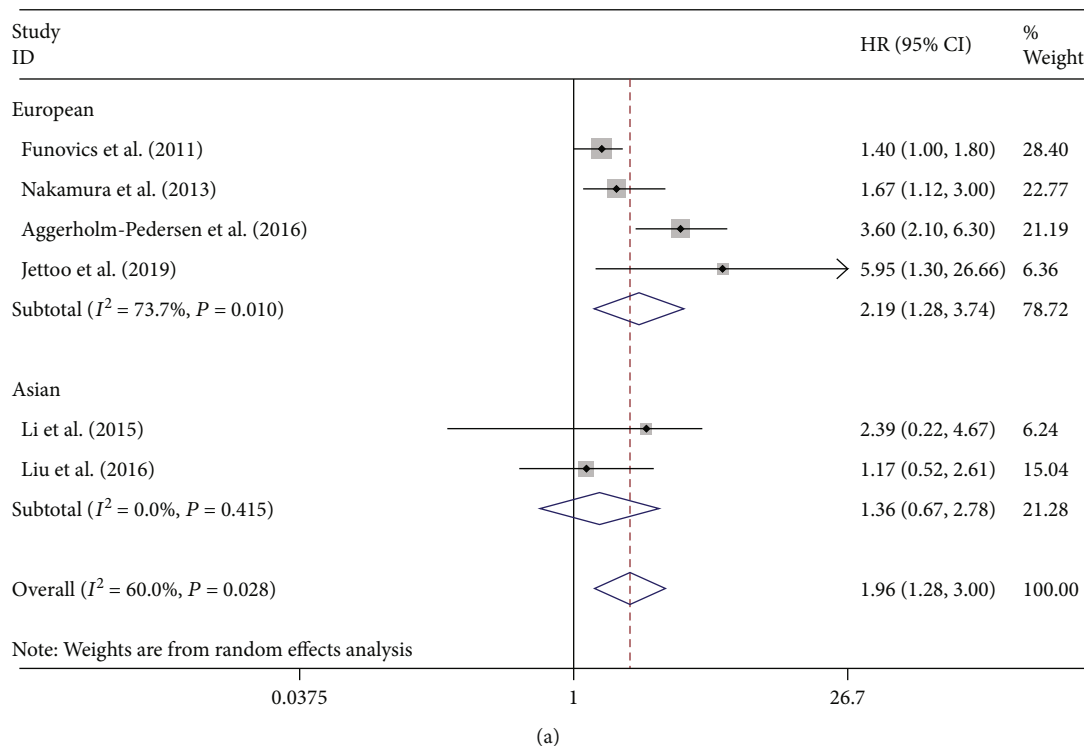


FIGURE 5: Continued.

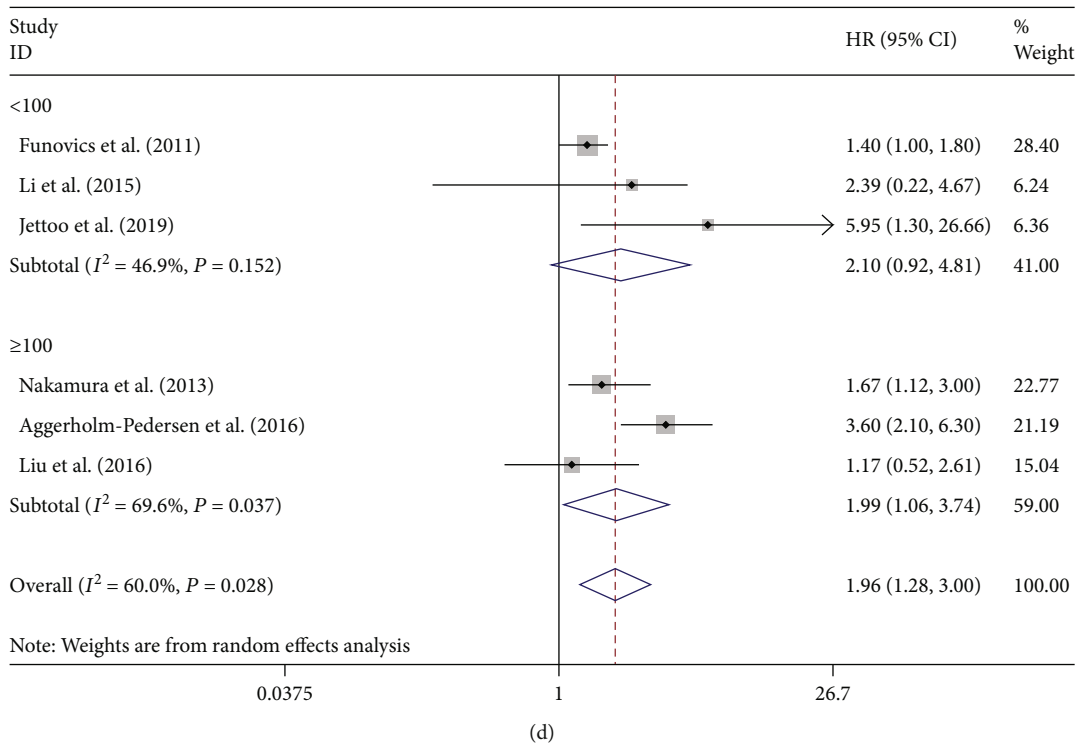
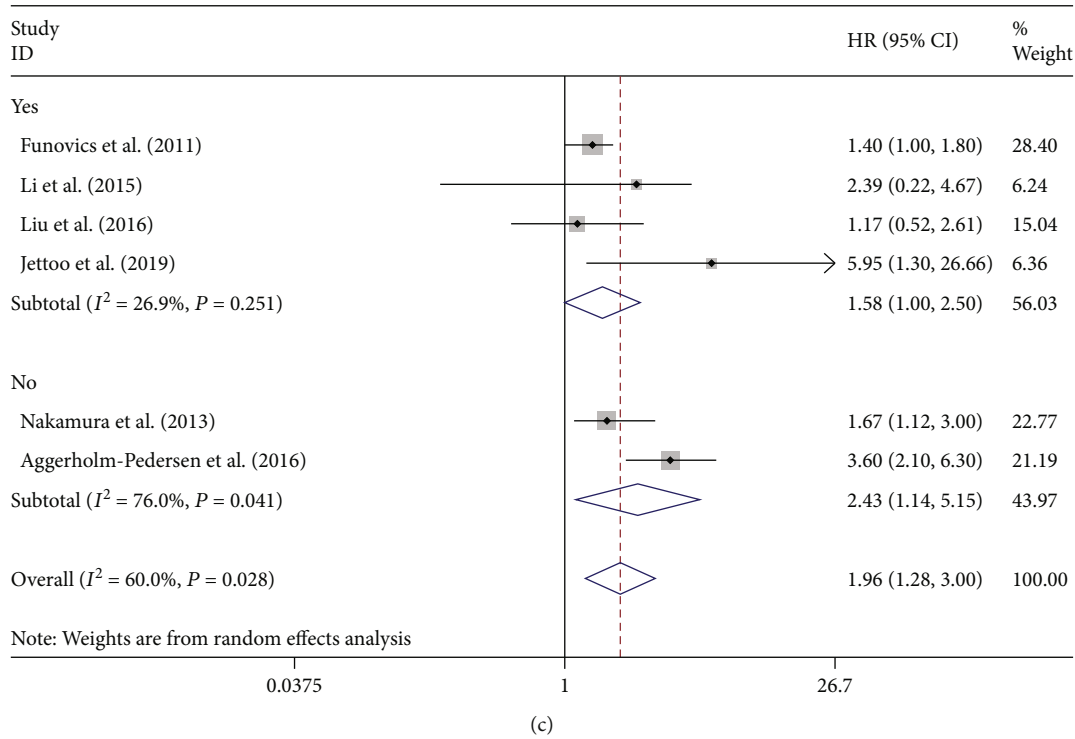
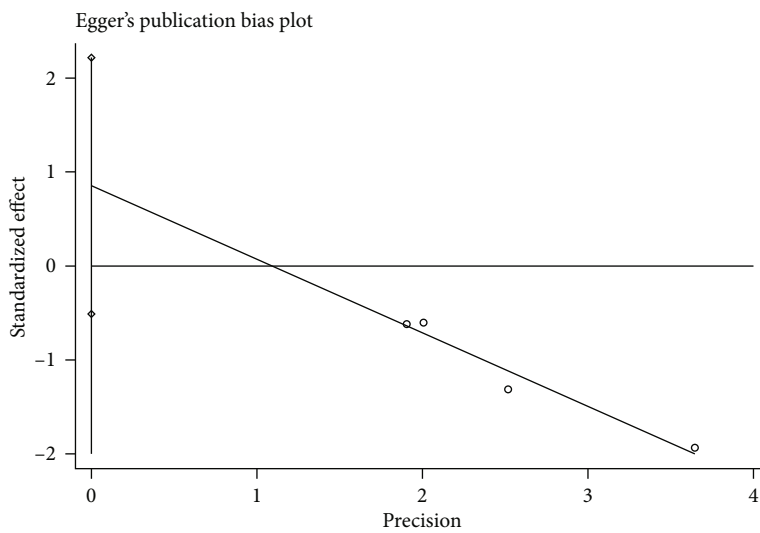


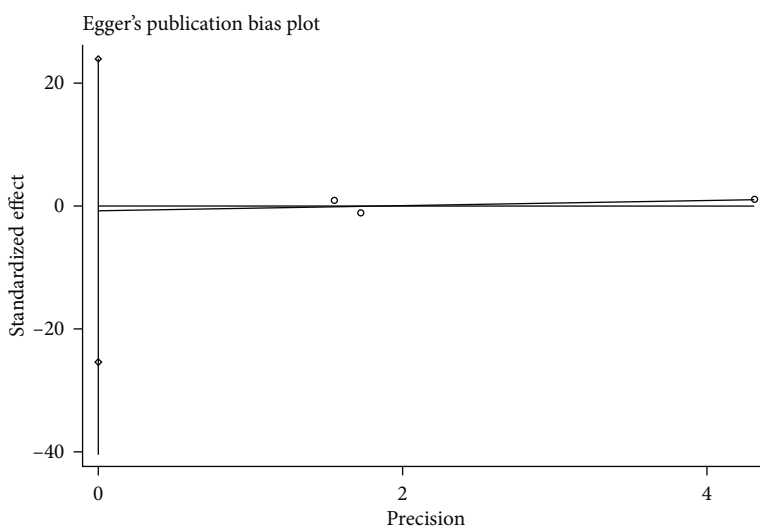
FIGURE 5: Subgroup analysis of the association of CRP levels with the OS of patients with osteosarcoma. The association of CRP level and overall survival within European or Asian patients (a), osteosarcoma or other bone sarcomas (b), metastasis or nonmetastasis patients (c), sample size (d) in patients with osteosarcoma.

The definition of GPS was carried out on the basis of the presence of hypoalbuminemia (<35 g/L) and enhanced CRP (>10 mg/L): if both were abnormal, the score was 2; if either was abnormal, the score was 1; if there were no exceptions, the score was 0 [46, 47]. According to increasing researches,

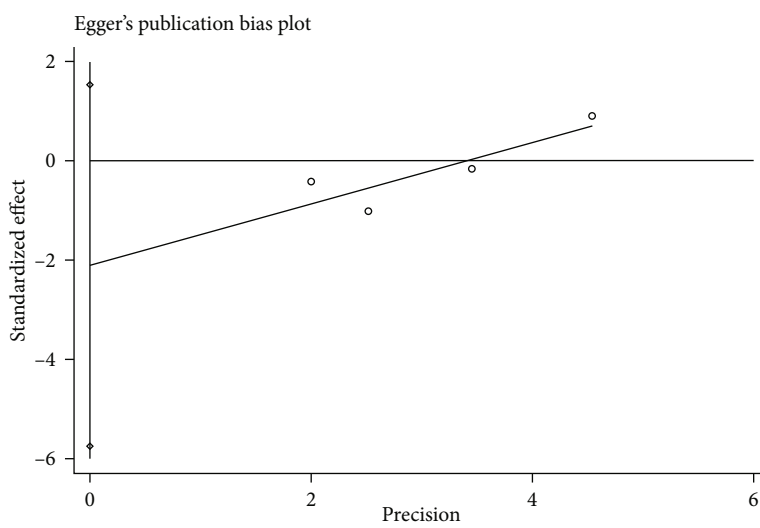
the hidden predictive value of GPS was demonstrated among osteosarcoma patients. One study speculates that GPS shows inflammation status and nutritional status of cancer patients as a better predictor of prognosing cancer than CRP [10]. Hence, this systematic examination and



(a)



(b)



(c)

FIGURE 6: Egger's test of the association of NLR (a), CRP (b), and GPS (c) levels with the OS of patients with osteosarcoma.

meta-analysis shall be made to draw more reliable conclusions on the effect of GPS on osteosarcoma. In this meta-analysis, measuring GPS was an effective way to predict prognosis among patients suffering from osteosarcoma. Additionally, according to the pooled results, GPS is significantly associated with shortening of OS in patients with osteosarcoma (HR = 2.54, 95% CI: 1.95-3.31), demonstrating that high level of GPS before treatment may also be a negative prognostic element for patients with osteosarcoma.

The prognostic value of PLR and LMR for other tumors shows different conclusions from this article. In the latest study, PLR is thought to be inversely associated with the prognosis of breast cancer [48], and LMR is considered as a risk factor for gastric cancer [49]. The pooled results show that there is no significant relationship between PLR or LMR and OS of patients with osteosarcoma. This anomaly of LMR may be related to the insufficient number of included studies; in addition to this, there remains a study for PLR showing that the predictive value of high PLR in terms of overall survival is greater in cancer patients with comorbidities, especially those with metabolic syndrome [50] which may not be consistent with patients with osteosarcoma. In addition, due to the error of measurement results and the influence of other unrelated confounding factors, some research results may be ignored and reported, resulting in the trend of the prognostic value of these two inflammatory markers for osteosarcoma is not obvious. However, specific conclusions need to be supported by further research results.

Different types of treatment and osteosarcoma may have different overall survival times, which may contribute to high heterogeneity. Due to the differences between individuals and groups, patients of different races, regions, and ages may have different degrees of disease or disease tendency, resulting in different treatment methods. This leads to the blending of various factors, which we cannot distinguish in detail for the time being. We believe that there will be more scientific statistical methods and more rigorous experimental design to solve these problems in the future.

In addition to the above problems, this meta-analysis does have several limitations. First, most of the included studies were retrospectively designed, which increased the risk of bias due to inadequate random blinding. Second, even though subgroup analyses were performed, there was an obvious heterogeneity in this meta-analysis, but at present, we have not yet found a clear cause for the heterogeneity. Third, the overall results may be overestimated because of negative data from unpublished studies. Fourth, restricted by insufficient number of literature and the original data, the reliability of the results may be shortened and we cannot draw receiver operating characteristic curves (ROC curves) to study the prognostic value of each marker, further. We can only expect more studies to be carried out so that we can update this meta-analysis. Finally, sensitivity analysis and funnel plots showed potential publication bias in some researches. After ignoring these researches, the distribution of OS in the remaining studies was more symmetrical. This bias may be due to differences in baseline characteristics and study regimen-related protocols among patients. Moreover, the differences in detection methods and data storage

may have resulted in heterogeneity. Although the random effects model reduced the effect of heterogeneity, the heterogeneity between studies was not abolished. In view of the above limitations, it is recommended to prospectively recruit subjects in future studies. At the same time, researchers may consider combining multiple inflammatory markers to explore their common prognostic value and make the results more sensitive.

5. Conclusion

For patients with osteosarcoma, meta-analysis performed in this paper demonstrated that high great contents of NLR, CRP, and GPS before treatment may be a negative prognostic element, and ethnicity, histology, and metastasis all have an impact on its prognosis of patients with osteosarcoma; however, PLR and LMR might have nothing to do with it. In conclusion, the measurement of these inflammatory markers' levels can provide the basis for clinicians to judge the outcome of prognosis.

Data Availability

The datasets are available from the corresponding author on reasonable request.

Additional Points

Code Availability. Microsoft Excel 2010; Microsoft, Redmond, WA, USA. STATA meta. Ado module (version 15.1; College Station, TX, USA).

Conflicts of Interest

The authors declare that they have no conflicts of interest.

Authors' Contributions

Xiaotong Song and Hao Zhang wrote the manuscript; Yanshuo Han and Xiaotong Song conceived the manuscript; Xiaotong Song, Jinzhu Liu, and Yanshuo Han participated in data collection; all authors have read and approved the final manuscript. Xiaotong Song and Hao Zhang are co-first authors in this study and they contributed equally to this work.

Acknowledgments

This work was supported by the Fundamental Research Funds for the Central Universities (grant number: DUT19RC(3)076), the National Natural Science Foundation of China (grant number: 81600370), and the China Postdoctoral Science Foundation (grant number: 2018M640270).

Supplementary Materials

Supplementary File 1: search strategy for Medline database. Supplementary File 2: sensitivity analysis of the association of NLR, CRP, LMR, GRS, and PLR levels with the OS of patients with osteosarcoma. Supplementary File 3: Begg's

funnel plot of the association of NLR, CRP, and GPS levels with the OS of patients with osteosarcoma. (*Supplementary Materials*)

References

- [1] L. Mirabello, R. J. Troisi, and S. A. Savage, "Osteosarcoma incidence and survival rates from 1973 to 2004," *Cancer*, vol. 115, no. 7, pp. 1531–1543, 2009.
- [2] I. Lilienthal and N. Herold, "Targeting molecular mechanisms underlying treatment efficacy and resistance in osteosarcoma: a review of current and future strategies," *International Journal of Molecular Sciences*, vol. 21, no. 18, p. 6885, 2020.
- [3] C. A. Stiller, "International patterns of cancer incidence in adolescents," *Cancer Treatment Reviews*, vol. 33, no. 7, pp. 631–645, 2007.
- [4] S. S. Nathan and J. H. Healey, "Demographic determinants of survival in osteosarcoma," *Annals of the Academy of Medicine, Singapore*, vol. 41, no. 9, pp. 390–399, 2012.
- [5] Y. J. Li, Y. L. Dai, Y. S. Cheng, W. B. Zhang, and C. Q. Tu, "Positron emission tomography (18)F-fluorodeoxyglucose uptake and prognosis in patients with bone and soft tissue sarcoma: a meta-analysis," *European Journal of Surgical Oncology*, vol. 42, no. 8, pp. 1103–1114, 2016.
- [6] K. J. Halazun, A. Aldoori, H. Z. Malik et al., "Elevated preoperative neutrophil to lymphocyte ratio predicts survival following hepatic resection for colorectal liver metastases," *European Journal of Surgical Oncology*, vol. 34, no. 1, pp. 55–60, 2008.
- [7] P. I. Karakiewicz, G. C. Hutterer, Q. D. Trinh et al., "C-reactive protein is an informative predictor of renal cell carcinoma-specific mortality," *Cancer*, vol. 110, no. 6, pp. 1241–1247, 2007.
- [8] L. M. Forrest, D. C. McMillan, C. S. McArdle, W. J. Angerson, K. Dagg, and H. R. Scott, "A prospective longitudinal study of performance status, an inflammation-based score (GPS) and survival in patients with inoperable non-small-cell lung cancer," *British Journal of Cancer*, vol. 92, no. 10, pp. 1834–1836, 2005.
- [9] Q. Deng, B. He, X. Liu et al., "Prognostic value of pre-operative inflammatory response biomarkers in gastric cancer patients and the construction of a predictive model," *Journal of Translational Medicine*, vol. 13, no. 1, p. 66, 2015.
- [10] B. Liu, Y. Huang, Y. Sun et al., "Prognostic value of inflammation-based scores in patients with osteosarcoma," *Scientific Reports*, vol. 6, no. 1, p. 39862, 2016.
- [11] W. K. Xia, Z. L. Liu, D. Shen, Q. F. Lin, J. Su, and W. D. Mao, "Prognostic performance of pre-treatment NLR and PLR in patients suffering from osteosarcoma," *World Journal of Surgical Oncology*, vol. 14, no. 1, 2016.
- [12] X. Huang, H. Hu, W. Zhang, and Z. Shao, "Prognostic value of prognostic nutritional index and systemic immune-inflammation index in patients with osteosarcoma," *Journal of Cellular Physiology*, vol. 234, no. 10, pp. 18408–18414, 2019.
- [13] X. Li, F. Tian, F. Wang, and Y. Li, "Serum C-reactive protein and overall survival of patients with osteosarcoma," *Tumor Biology*, vol. 36, no. 7, pp. 5663–5666, 2015.
- [14] D. Moher, A. Liberati, J. Tetzlaff, D. G. Altman, and The PRISMA Group, "Preferred reporting items for systematic reviews and meta-analyses: the PRISMA statement," *PLoS Medicine*, vol. 6, no. 7, article e1000097, 2009.
- [15] D. A. Cook and D. A. Reed, "Appraising the quality of medical education research methods," *Academic Medicine*, vol. 90, no. 8, pp. 1067–1076, 2015.
- [16] C. B. Begg and M. Mazumdar, "Operating characteristics of a rank correlation test for publication bias," *Biometrics*, vol. 50, no. 4, pp. 1088–1101, 1994.
- [17] M. Borenstein, L. V. Hedges, J. P. Higgins, and H. R. Rothstein, "A basic introduction to fixed-effect and random-effects models for meta-analysis," *Research Synthesis Methods*, vol. 1, no. 2, pp. 97–111, 2010.
- [18] P. T. Funovics, G. Edelhauser, M. A. Funovics et al., "Pre-operative serum C-reactive protein as independent prognostic factor for survival but not infection in patients with high-grade osteosarcoma," *International Orthopaedics*, vol. 35, no. 10, pp. 1529–1536, 2011.
- [19] T. Nakamura, R. J. Grimer, C. L. Gaston, M. Watanuki, A. Sudo, and L. Jeys, "The prognostic value of the serum level of C-reactive protein for the survival of patients with a primary sarcoma of bone," *Bone Joint J*, vol. 95-b, no. 3, pp. 411–418, 2013.
- [20] T. Liu, X. C. Fang, Z. Ding, Z. G. Sun, L. M. Sun, and Y. L. Wang, "Pre-operative lymphocyte-to-monocyte ratio as a predictor of overall survival in patients suffering from osteosarcoma," *FEBS Open Bio*, vol. 5, no. 1, pp. 682–687, 2015.
- [21] N. Aggerholm-Pedersen, K. Maretty-Kongstad, J. Keller, S. Baerentzen, and A. Safwat, "The prognostic value of serum biomarkers in localized bone sarcoma," *Translational Oncology*, vol. 9, no. 4, pp. 322–328, 2016.
- [22] Y. J. Li, K. Yao, M. X. Lu, W. B. Zhang, C. Xiao, and C. Q. Tu, "Prognostic value of the C-reactive protein to albumin ratio: a novel inflammation-based prognostic indicator in osteosarcoma," *Oncotargets and Therapy*, vol. Volume 10, pp. 5255–5261, 2017.
- [23] P. Jettoo, G. J. S. Tan, C. H. Gerrand, and K. S. Rankin, "Role of routine blood tests for predicting clinical outcomes in osteosarcoma patients," *Journal of Orthopaedic Surgery*, vol. 27, no. 2, p. 230949901983829, 2019.
- [24] H. Zhenhua, Y. Chen, L. Yuling, D. Qiong, and R. Xiaoxiang, "Role of systemic inflammatory response in evaluating the prognosis of patients with osteosarcoma," *The Journal of Practical Medicine*, vol. 34, no. 20, pp. 3410–3414, 2018.
- [25] H. Hu, X. Deng, Q. Song et al., "Prognostic value of the preoperative lymphocyte-to-c-reactive protein ratio and albumin-to-globulin ratio in patients with osteosarcoma," *Oncotargets and Therapy*, vol. Volume 13, pp. 12673–12681, 2020.
- [26] M. L. Pot, J. C. Giltay, A. van Wilsen, and E. J. Breslau-Siderius, "Unbalanced karyotype, dup 14(q13-q22), in a mother and her two children," *Clinical Genetics*, vol. 50, no. 5, pp. 398–402, 1996.
- [27] A. Mantovani, P. Allavena, A. Sica, and F. Balkwill, "Cancer-related inflammation," *Nature*, vol. 454, no. 7203, pp. 436–444, 2008.
- [28] C. I. Diakos, K. A. Charles, D. C. McMillan, and S. J. Clarke, "Cancer-related inflammation and treatment effectiveness," *The Lancet Oncology*, vol. 15, no. 11, pp. e493–e503, 2014.
- [29] E. Elinav, R. Nowarski, C. A. Thaiss, B. Hu, C. Jin, and R. A. Flavell, "Inflammation-induced cancer: crosstalk between tumours, immune cells and microorganisms," *Nature Reviews Cancer*, vol. 13, no. 11, pp. 759–771, 2013.

- [30] J. Candido and T. Hagemann, "Cancer-related inflammation," *Journal of Clinical Immunology*, vol. 33, no. 1, pp. S79–S84, 2013.
- [31] B. Azab, N. Jaglall, J. P. Atallah et al., "Neutrophil-lymphocyte ratio as a predictor of adverse outcomes of acute pancreatitis," *Pancreatology*, vol. 11, no. 4, pp. 445–452, 2011.
- [32] A. C. Sawant, P. Adhikari, S. R. Narra, S. S. Srivatsa, P. K. Mills, and S. S. Srivatsa, "Neutrophil to lymphocyte ratio predicts short- and long-term mortality following revascularization therapy for ST elevation myocardial infarction," *Cardiology Journal*, vol. 21, no. 5, pp. 500–508, 2014.
- [33] O. F. Cirakoglu and A. S. Yilmaz, "Systemic immune-inflammation index is associated with increased carotid intima-media thickness in hypertensive patients," *Clinical and Experimental Hypertension*, vol. 43, no. 6, pp. 565–571, 2021.
- [34] B. Azab, N. Shah, J. Radbel et al., "Pretreatment neutrophil/lymphocyte ratio is superior to platelet/lymphocyte ratio as a predictor of long-term mortality in breast cancer patients," *Medical Oncology*, vol. 30, no. 1, p. 432, 2013.
- [35] M. J. Proctor, D. S. Morrison, D. Talwar et al., "A comparison of inflammation-based prognostic scores in patients with cancer. A Glasgow Inflammation Outcome Study," *European Journal of Cancer*, vol. 47, no. 17, pp. 2633–2641, 2011.
- [36] C. S. Roxburgh and D. C. McMillan, "Role of systemic inflammatory response in predicting survival in patients with primary operable cancer," *Future Oncology*, vol. 6, no. 1, pp. 149–163, 2010.
- [37] G. Morris-Stiff, D. Gomez, and K. R. Prasad, "C-reactive protein in liver cancer surgery," *European Journal of Surgical Oncology*, vol. 34, no. 7, pp. 727–729, 2008.
- [38] P. Libby, P. M. Ridker, and A. Maseri, "Inflammation and atherosclerosis," *Circulation*, vol. 105, no. 9, pp. 1135–1143, 2002.
- [39] N. S. Rost, P. A. Wolf, C. S. Kase et al., "Plasma concentration of C-reactive protein and risk of ischemic stroke and transient ischemic attack: the Framingham study," *Stroke*, vol. 32, no. 11, pp. 2575–2579, 2001.
- [40] K. W. Muir, C. J. Weir, W. Alwan, I. B. Squire, and K. R. Lees, "C-reactive protein and outcome after ischemic stroke," *Stroke*, vol. 30, no. 5, pp. 981–985, 1999.
- [41] F. Zhou, L. Zhou, T. Guo et al., "Plasma proteomics reveals coagulation, inflammation, and metabolic shifts in H-type hypertension patients with and without acute ischemic stroke," *Oncotarget*, vol. 8, no. 59, pp. 100384–100395, 2017.
- [42] P. M. Ridker, R. J. Glynn, and C. H. Hennekens, "C-reactive protein adds to the predictive value of total and HDL cholesterol in determining risk of first myocardial infarction," *Circulation*, vol. 97, no. 20, pp. 2007–2011, 1998.
- [43] K. Hashimoto, Y. Ikeda, D. Korenaga et al., "The impact of preoperative serum C-reactive protein on the prognosis of patients with hepatocellular carcinoma," *Cancer*, vol. 103, no. 9, pp. 1856–1864, 2005.
- [44] J. Szkandera, M. Stotz, G. Absenger et al., "Validation of C-reactive protein levels as a prognostic indicator for survival in a large cohort of pancreatic cancer patients," *British Journal of Cancer*, vol. 110, no. 1, pp. 183–188, 2014.
- [45] Y. Okugawa, Y. Shirai, Y. Toiyama et al., "Clinical burden of modified Glasgow prognostic scale in colorectal cancer," *Anticancer Research*, vol. 38, no. 3, pp. 1599–1610, 2018.
- [46] M. Tomita, T. Ayabe, E. Chosa, and K. Nakamura, "Prognostic significance of pre- and postoperative Glasgow prognostic score for patients with non-small cell lung cancer," *Anticancer Research*, vol. 34, no. 6, pp. 3137–3140, 2014.
- [47] A. G. Jiang, H. L. Chen, and H. Y. Lu, "Comparison of Glasgow prognostic score and prognostic index in patients with advanced non-small cell lung cancer," *Journal of Cancer Research and Clinical Oncology*, vol. 141, no. 3, pp. 563–568, 2015.
- [48] Q. Guo and Y. Hua, "The assessment of circulating cell-free DNA as a diagnostic tool for breast cancer: an updated systematic review and meta-analysis of quantitative and qualitative assays," *Clinical Chemistry and Laboratory Medicine*, vol. 59, no. 9, pp. 1479–1500, 2021.
- [49] K. Inagaki, M. Kanda, K. Nakanishi et al., "Accurate prediction of prognosis after radical resection of gastric cancer by the modified systemic inflammation score; a multicenter dataset analysis," *World Journal of Surgery*, vol. 45, no. 8, pp. 2513–2520, 2021.
- [50] J. You, H. Zhang, Y. Shen et al., "Impact of platelet to lymphocyte ratio and metabolic syndrome on the prognosis of colorectal cancer patients," *Oncotargets and Therapy*, vol. 10, pp. 2199–2208, 2017.

Research Article

The Upregulation of COX2 in Human Degenerated Nucleus Pulposus: The Association of Inflammation with Intervertebral Disc Degeneration

Chang Liu,¹ Guoyan Liang,² Zhantao Deng,² Jing Tan,¹ Qiujian Zheng,² and Feng-Juan Lyu ¹

¹Joint Center of South China University of Technology-The University of Western Australia for Regenerative Medicine Research, School of Medicine, South China University of Technology, Guangzhou 510006, China

²Department of Orthopedics, Guangdong Provincial People's Hospital, Guangdong Academy of Medical Sciences, Guangzhou 510080, China

Correspondence should be addressed to Feng-Juan Lyu; lufj0@scut.edu.cn

Received 5 June 2021; Revised 18 August 2021; Accepted 6 September 2021; Published 18 October 2021

Academic Editor: Zhenhan Deng

Copyright © 2021 Chang Liu et al. This is an open access article distributed under the Creative Commons Attribution License, which permits unrestricted use, distribution, and reproduction in any medium, provided the original work is properly cited.

Intervertebral disc degeneration (IVDD) is an important risk factor of low back pain. We previously found upregulated markers of fibrosis, the late stage of chronic inflammation, in degenerated IVD with a small number of clinical specimens. Here, we aimed to study on a larger scale the association of cyclooxygenase 2 (COX2), an inflammation and/or pain marker, with IVDD. This study involved 107 LBP participants. The IVD degeneration level was graded on a 1–5 scale according to the Pfirrmann classification system. Discs at grades 1-3 were further grouped as white discs with grades 4-5 as black discs. We recorded baseline information about age, gender, body mass index (BMI), diabetes history, smoking history, and magnetic resonance imaging (MRI). Their association with IVDD was statistically analyzed. The expression level of COX2 was investigated by immunohistochemistry. The total integrated COX2 optical density (IOD), number of COX2-positive cells, and total cell number of each image were counted and analyzed by Image-Pro Plus software. The IOD and number of COX2-positive cells were divided by the total cell number to obtain COX2 expression density (IOD/cell) and COX2 positivity (cell+/cell). As a result, among the baseline information investigated, only age was found to have a significant association with IVDD. The IOD/cell was found to be significantly increased from grade 2 to grade 5, as well as in black discs compared to white discs. The cell+/cell displayed the same trend that it increased in highly degenerative discs compared to their counterparts. In conclusion, the expression of COX2 is associated with IVDD, which highlights COX2 as a biomarker for IVD degeneration and indicates the involvement of inflammation and pain signaling in IVDD.

1. Introduction

Low back pain (LBP) imposes huge social and economic burdens [1, 2]. It is estimated that about 80% of the world's population suffer from low back pain at least once in their lifetime. In the United States, LBP is the fifth leading cause of patient visits and the third leading cause of surgery [3]. LBP caused by internal disc disruption is defined as discogenic low back pain and is an important cause of LBP, accounting for about 42% of LBP [4]. Imaging examination

shows that patients with low back pain are often accompanied by intervertebral disc degeneration (IVDD) [5, 6].

The intervertebral disc (IVD) is the main joint connecting two adjacent vertebral bones in the spine. It is composed of three closely connected parts: nucleus pulposus (NP), annulus fibrosus (AF), and cartilage endplate (EP). In the process of IVDD, the decrease in proteoglycan and collagen in the extracellular matrix (ECM) directly reduces the hydration capacity of IVD, leading to the decrease in water content in NP, which in turn leads to intervertebral disc

collapse and decreased disc height [7, 8]. Pfirrmann et al. [9] proposed the Pfirrmann classification of lumbar disc degeneration based on the characteristics of NP water content and disc height reflected in magnetic resonance imaging (MRI) T2WI images, which has been widely used in clinical practice. Studies have defined grade 4 and grade 5 discs (black discs) in Pfirrmann's grading system as degenerative discs, while those with grade 3 and below are defined as nondegenerative discs (white discs) [5, 10]. The cause of IVDD is not well known. In addition to age, IVDD is associated with obesity [11], smoking [12], and diabetes mellitus [10]. Genetic factors have also been shown to be associated with IVDD [13, 14]. Exploring the mechanism of IVD degeneration is helpful for the prevention and treatment of LBP, reducing social and economic burden and improving life quality.

IVDD is accompanied by molecular expressional changes which have the potential to serve as IVD degeneration markers, such as the downregulation of keratin 19 and N-cadherin [15, 16]. Increased inflammatory factors have also been found in degenerated IVDs [17]. Previous research reported that degenerated human IVDs are in a chronic inflammatory state [18, 19]. Studies have found increased expression of several proinflammatory factors in human degenerative IVDs such as interleukin-1 beta (IL-1 β) and tumor necrosis factor alpha (TNF- α) [20]. A number of studies have mimicked IVDD by adding proinflammatory factors in vitro and in vivo [21, 22]. Our previous study has found the upregulation of fibrosis markers [23, 24], the late stage of chronic inflammation, in degenerated IVDs. In the mouse and rabbit model, abnormal remodeling of the collagenous reticular tissue in the NP was observed [25, 26]. Overall, these evidences suggest degenerative IVDs in a chronic inflammatory environment.

Cyclooxygenase-2 (COX2) is an "inducible" isoform of COX enzymes. Unlike COX1, COX2 expression is usually minimal, but when activated COX2 regulates prostaglandin E2 (PGE2) production which is involved in neuronal, metabolic, and immune system function, COX2 is involved in inflammation and is a crucial mediator of pain conduction [27]. COX2 has been shown to be regulated by, or regulates, many other inflammatory factors. Studies have demonstrated that treatment of rat serosal connective tissue mast cells with NGF induced COX2 [28]. IL-1 β [29] treatment of human tendon cells and TNF- α treatment [30] of human lung fibroblasts both induced COX2 expression. IL-6 treatment of human NP cells induced PGE2 synthesis and COX2 expression [31]. Stimulation of COX2 also induced IL-8 production [32], suggesting that COX2 can further promote the inflammatory cascade. COX2 is also a critical pain mediator, and COX2-specific inhibitors have been used clinically for the treatment of painful conditions, including low back pain.

COX2 has been found to be induced in in vitro disc cell cultures by various degeneration inductors, such as TNF- α [33] and IL-1 β [34]. However, up to date, the evidence on how COX2 expression changes in the natural process of IVD degeneration in human is rare. In this study, we verified the expression of COX2 in a relatively large scale of human specimens who visit the clinics due to low back pain. Here,

we evaluated its expression by immunohistochemistry (IHC) and assessed its association with the degeneration grade of IVDs. We further analyzed the correlation of COX2 expression with the baseline information of the patients, as well as investigating the expression of COX2 in cultured human NP cells under the treatment with IL-1 β , a well-accepted inflammatory mediator [35, 36] in IVDD. The aim is to gain a further understanding of COX2 in different degrees of IVDD, which can contribute to the understanding of IVDD pathogenesis and potential development of blocking strategies.

2. Materials and Methods

2.1. Participants. This study was conducted in the Orthopedics Department of the First Affiliated Hospital of the South China University of Technology between August 2019 and November 2020 with ethical approval from the Medical Ethical Committee from the South China University of Technology. 107 LBP participants undergoing spinal surgery after no response to conservative treatments for at least 6 weeks were included with informed patient consent. All patients received transdiscoscopic discectomy or lumbar fusion. IVD removed from these patients during surgery were collected as approved by the institutional review board (IRB). Among these, patients with spinal tumor and/or tuberculosis were excluded from this study. The enrolled patients had different degrees of low back pain. The degeneration grade of IVD was evaluated on a 1–5 scale according to the Pfirrmann classification system based on MRI T2WI [9]. Data about age, gender, body mass index (BMI), diabetes history, smoking history, and radiological imaging (MRI) were also recorded.

2.2. Immunohistochemistry. The expression of COX2 in the collected IVDs was analyzed by IHC. Tissue samples were fixed with 10% formalin and embedded in paraffin, cut into 5 μ m sections, and transferred to adhesive-treated slides. These slides were dried for 2 hours at 60°C, dewaxed for three times with xylene, and subjected to rehydration. After that, the slides were placed in an antigen repair apparatus (PT Module, Thermo Fisher Scientific) filled with antigenic repair solution (citric acid, pH = 6.0) in a microwave oven for antigenic repair. After heating at 100°C for 20 minutes and natural cooling, the slides were washed with PBS (pH 7.4) on a decolorization shaker for 3 times, 5 min each. 3% hydrogen peroxide was incubated for 25 min at room temperature (RT) to block the endogenous peroxidase activity. Then, the slides were blocked in 3% BSA for 30 min at RT. Afterwards, the sections were incubated overnight at 4°C with a primary rabbit antibody against COX2 (Abcam, ab15191) diluted in an antibody diluent (Servicebio, G2025) at the concentrations of 1:150 and 1:300, respectively. Then, the slides were incubated with a mouse anti-rabbit secondary antibody (Servicebio, GB23303) at the concentration of 1:200 at RT for 50 minutes and developed with diaminobenzidine (DAB) (Solarbio, DA1010), counterstained with hematoxylin (Servicebio, G1004), dehydrated in graded ethanol, and sealed with neutral balsam (Solarbio,

96949-21-2). Diagnostic scanners (3DHISTECH, Panoramic MIDI) were used to randomly pick five microscopic images for each sample. The number of COX2-positive cells was manually counted, and the integrated optical density (IOD) and total cell number of each image were counted by using Image-Pro Plus (IPP6) software.

2.3. Degeneration Grading of the Clinical Samples. Two experienced trained staff independently graded the degeneration status of the patient IVDs based on sagittal MRI images (T2-weighted image (T2WI)) of the patient's spine according to the Pfirrmann grading system [9]. Images with conflicted judgments were evaluated again by working together until consensus was achieved for all patients.

2.4. Culture of Human Nucleus Pulposus Cells. The human nucleus pulposus cells used in this experiment were purchased from ScienCell. After defrosting, cells were inoculated into tissue culture dishes and cultured in DMEM complete medium supplemented with 1% penicillin-streptomycin, 1% L-glutamine, and 10% fetal calf serum in a 37°C humidified incubator. The cells were subcultured at a dilution of 1:3 when they reached 90% confluency. To test the induction of COX2 by IL-1 β , cells at P3 were subjected to the addition of IL1 β at the final concentration of 0, 5, 10, and 15 ng/ml for 24 hr. After 24 hr, the cells were harvested. RNA was isolated by using Trizol and assessed by using a Nanodrop bioanalyzer (Thermo Scientific, US). Reverse transcription of RNA to cDNA was done with an RNA to cDNA kit (Tsingke, PRC). Quantitative real-time PCR (qRT-PCR) of the expression of COX2 was performed on a StepOnePlus system (Applied Biosystems, Life technologies, US) using SYBR green real-time PCR master mixes (Tsingke, PRC). GAPDH was tested as an endogenous control. The relative quantification was achieved by the comparative CT method.

2.5. Statistical Evaluation. The normality of variables was assessed. For a comparison between two sets of data, data of normal distribution was expressed as mean \pm standard deviation and the differences were evaluated by the *t*-test. Data with nonnormal distributions are represented by median (25th-75th percentile), and the differences were evaluated by the Mann-Whitney *U* test. For comparison among multiple groups of data, an ordinary one-way ANOVA test was used for comparison following normal distribution; the Kruskal-Wallis test was used for those who did not follow the normal distribution. The Spearman coefficient was used to assess the correlation between COX2 expression and the baseline information in the IVDD samples. Significance was set at $P < 0.05$. All statistical analyses were performed with SPSS 23.0 software (IBM, Chicago, USA).

3. Results

3.1. Age Is Associated with IVDD in Population Baseline Information. According to the grading system, we graded the disc samples collected from 107 patients. We have 7, 38, 57, and 5 cases of intervertebral discs at grades 2, 3, 4, and 5, respectively. The MRI images of the patients classified

into Pfirrmann grades II to V are represented in Supplementary Figure 1. Apart from dividing the specimens into grades 2~5, we further adopted the grouping methods mentioned by Teraguchi et al. [5], which grouped grade 4 and 5 discs (black discs) as degenerative discs, while those with grade 3 and below were grouped as nondegenerative discs (white discs). Table 1 shows the characteristics of 107 patients, among whom 62 cases (57.9%) were degenerative (black) discs and 45 cases (42.1%) were nondegenerative (white) discs. The population information, including gender, age, body mass index (BMI), diabetes mellitus (DM) history, and smoking history, was compared between the patients with black discs and those with white discs. Patients with black discs were significantly older ($P < 0.001$) and tend to have higher prevalence of DM ($P = 0.051$) than their counterparts though not significant difference was found. This is consistent with the previous report [10]. Other than age and DM, the other population baseline parameters were not statistically different in black discs compared to white ones.

3.2. Optimization of the IHC Staining of COX2 in Human Specimens. We tested the staining effect of the COX2 antibody at 1:150 and 1:300 dilution, as shown in Figure 1. Staining at both antibody concentrations can yield similar positive signals, while the staining at 1:300 dilution is slightly clearer than that at 1:150 dilution. Therefore, we adopted 1:300 dilution for the following experiments.

3.3. Differential Expression of COX2 in Disc NP at Different Degeneration Grades. The staining results of COX2 in different degrees of IVDD are illustrated in Figure 2 and Supplementary Figure 2. The number of COX2-positive cells in grade 2 discs is low, which is increased in grade 3. In grade 4, the number of COX2-positive cells is significantly increased and the signal is enhanced. There is no visual difference in the number of COX2-positive cells and signal intensity between grade 5 and grade 4 NP.

3.4. Analysis of COX2 Expression in Human Discs at Pfirrmann Grades II to V. We use IPP6 software and two analyzing methods of IHC images to more accurately assess the expression of the target protein in human degenerative and nondegenerative NP tissues. The IOD/cell number represents the average COX2 signal intensity per cell, while the cell+/cell number represents the percentage of cells positive for COX2 expression. We conducted statistical analysis on the samples according to levels 2, 3, 4, and 5. The results are shown in Figure 3. COX2 positivity is highly significantly different between grades 3 and 4 ($P < 0.0001$) and grades 3 and 5 ($P = 0.0213$), respectively. COX2 expression density is highly significantly different between grades 3 and 4 ($P < 0.01$) and between grades 3 and 5 ($P < 0.01$), respectively. In summary, the expression levels of COX2 increase in high degenerative NP when compared to low/mild degenerative NP.

3.5. Analysis of COX2 Expression in Human Black and White Discs. Next, we grouped discs at grades 2 to 3 as white (nondegenerative) discs and discs at grades 4 to 5 as black

TABLE 1: Population baseline between human degenerated and nondegenerated discs of the study patients.

	Total	Nondegeneration	Degeneration	P value
Patients (n)	107 [100]	45 [42.1]	62 [57.9]	—
Gender (n [%])	107 [100]	45 [100]	62 [100]	
Male	70 [65.4]	34 [75.6]	36 [58.1]	
Female	37 [34.6]	11 [24.4]	26 [41.9]	0.06
Age (years)	43.0 ± 14.9	35.8 ± 13.3	48.3 ± 13.9	<0.001
BMI	23.4 ± 3.4	23.1 ± 3.9	23.6 ± 3.1	0.485
Height (m)	1.66 ± 0.08	1.67 ± 0.07	1.66 ± 0.09	0.363
Weight (kg)	65 (56-70)	63 (55.8-71.5)	65 (57-70)	0.75
Diabetes (yes vs. no)	107 [100]	45 [100]	62 [100]	
Yes	5 [4.7]	0 [0]	5 [8.1]	
No	102 [95.3]	45 [100]	57 [91.9]	0.051
History of smoking (yes vs. no)	107 [100]	45 [100]	62 [100]	
Yes	5 [4.7]	2 [4.4]	3 [4.8]	
No	102 [95.3]	43 [95.6]	59 [95.2]	0.924

*Values are expressed as mean ± standard deviation or number.

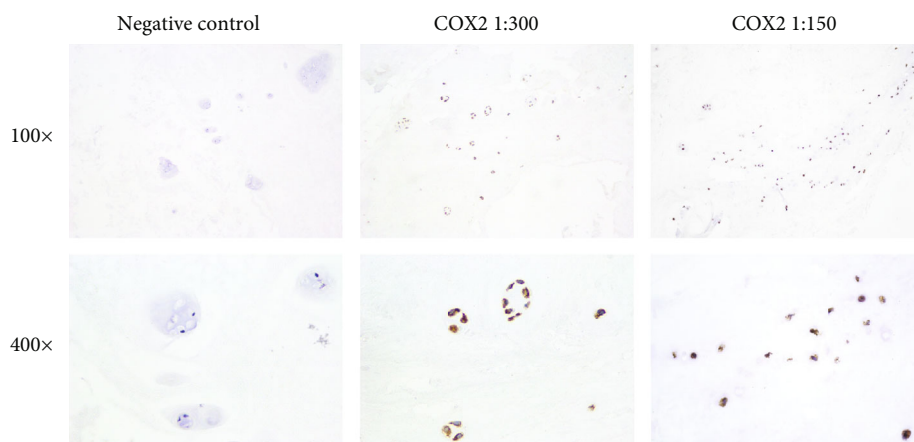


FIGURE 1: Illustration of the optimization of COX2 staining. IHC staining was performed with the COX2 antibody at 1:150 and 1:300 dilution. Negative control was obtained by omitting the primary antibody. Photos were taken at 100x and 400x magnification.

(degenerative) discs and compared the expression of COX2 among them. The results are shown in Figure 4. For COX2 positivity, degenerative NP had significantly higher COX2+ cell proportion (57.9% vs. 30.8%, $P < 0.001$) than nondegenerative NP, respectively. For the cellular COX2 expression intensity, degenerative NP exhibits significantly higher IOD/cell number of COX2 (3460.1 vs. 1192.2, $P < 0.001$) than nondegenerative ones.

3.6. Spearman Analysis of Correlation between COX2 Expression and Baseline Information. The correlation between COX2 expression and the baseline information of the patients was assessed by the Spearman analysis. As shown in Table 2, the expression intensity of COX2, as represented by IOD/cell number, and the COX2 positivity, as represented by the cell+/cell number, are both significantly correlated with diabetes history ($P = 0.031/P = 0.008$). Body weight is significantly correlated with COX2 positivity, but

not with COX2 expression intensity. Similarly, age is correlated with COX2 expression intensity but not with COX2 positivity. In summary, this indicates that COX2 expression is positively correlated with the occurrence of diabetes (Spearman correlation > 0), while it may have a correlation with age and weight.

3.7. IL-1 β Stimulated COX2 Expression in Cultured Human NP Cells. IL-1 β is known to induce inflammatory response in human or animal NP in the literature and has been widely utilized as an inflammation inducer in IVD in various studies [35, 36]. Here, we investigated whether the treatment of IL-1 β may inflect the expression of COX2 in human NP cells in vitro. As shown in Figure 5, COX2 expression in human NP cells was all significantly upregulated by IL-1 β at 5, 10, and 15 ng/ml within 24 hours. This result indicated that COX2 is involved in the inflammatory cascade induced by IL-1 β in the NP.

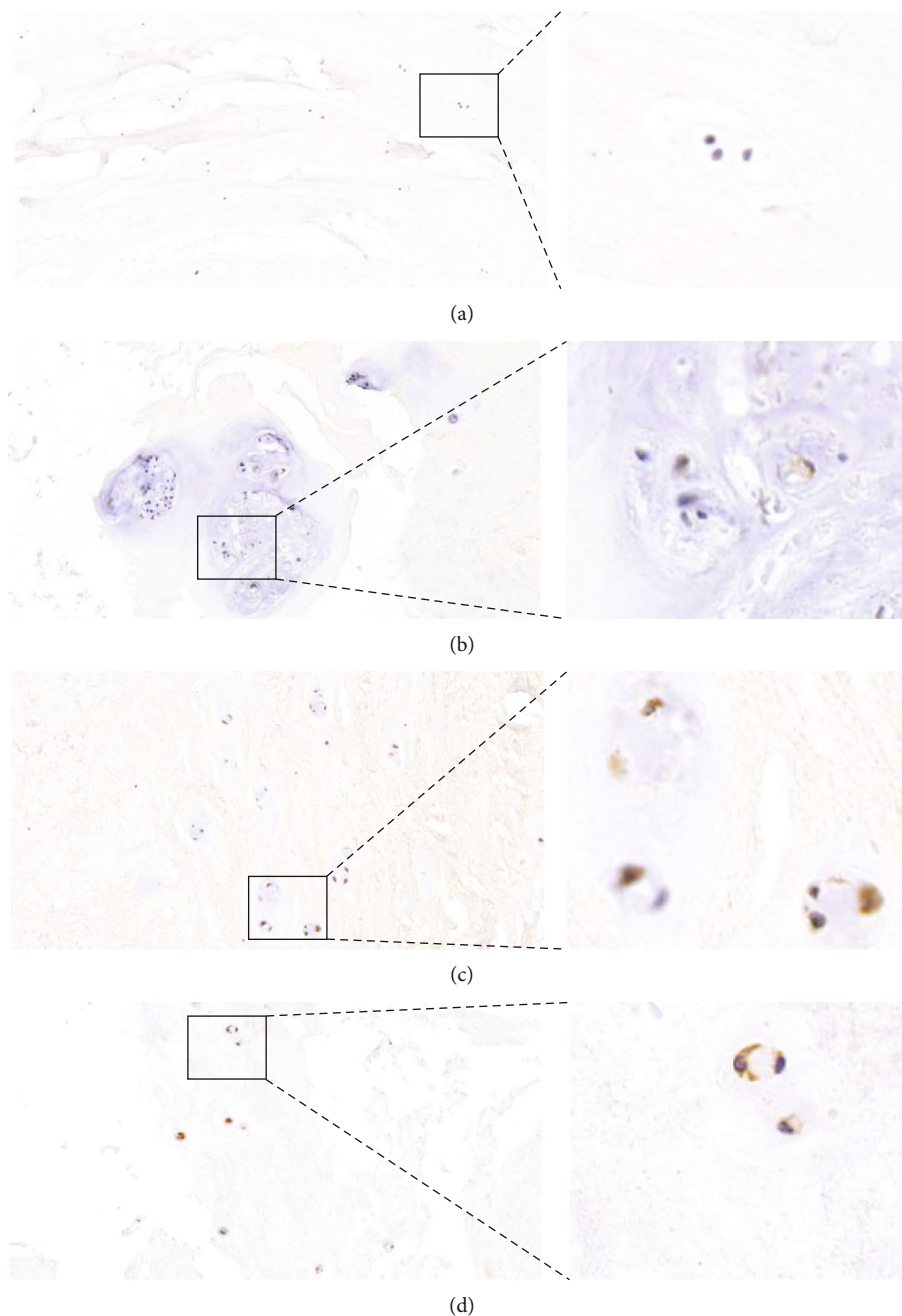
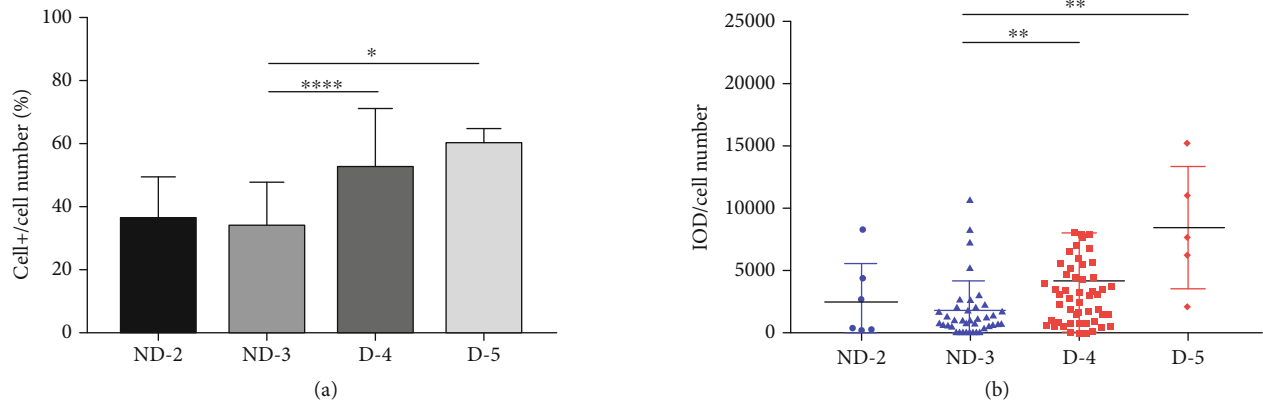


FIGURE 2: Immunohistochemical staining images of COX2 in human nucleus pulposus tissue. (a–d) The staining of NP at Pfirrmann grades II (a), III (b), IV (c), and V (d).

4. Discussion

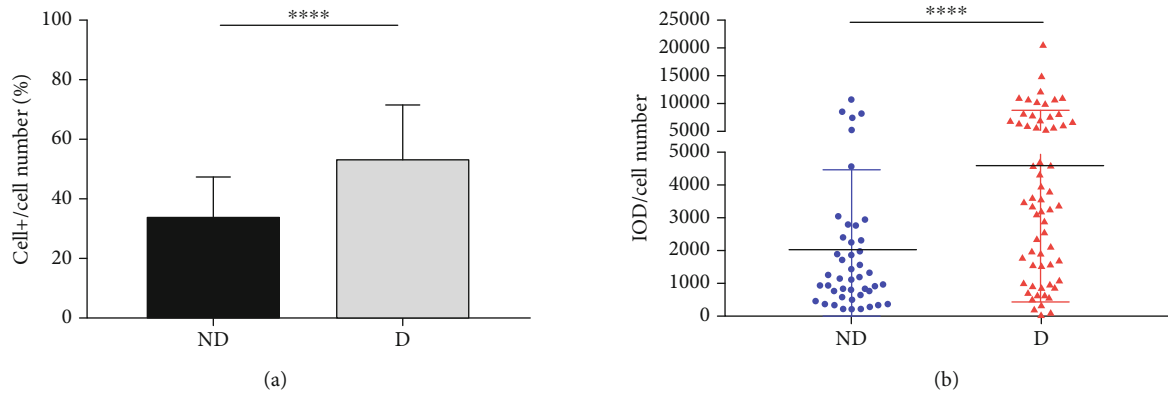
Not all IVD degeneration causes low back pain. While some degenerated IVDs cause discogenic LBP, some others are pain-free. A previous study has reported that none of the morphological changes, such as disc bulges, narrowing, Schmorl's nodes, or protrusions, can be distinguishable factors between asymptomatic and symptomatic patients [37, 38]. Inflammation is an important element of IVDD and might be the crucial factor distinguishing symptomatic and asymptomatic IVD degeneration [18].

COX2 is indicated in the inflammatory process in various tissues, such as Alzheimer's disease [39], Parkinson's disease [40], and diabetic kidney disease [41]. Its overexpression has been implicated as a biomarker for various types of cancers [42–44]. COX2 is also a crucial pain mediator. COX2 regulates the synthesis of prostaglandin E2 (PGE2), which plays an important role to induce radiculopathy. A COX2 selective inhibitor has been successfully developed as a commercially available drug to suppress pain. As a crucial mediator of pain and participant of inflammation signaling, COX2 may play an important role in IVDD and LBP



	Pfirrmann II group	Pfirrmann III group	Pfirrmann IV group	Pfirrmann V group	<i>p</i> value
COX2 (cell+/cell number) [%]	35.4(20.7-50.0)	30.5 (25.5-40.1)	54.0(34.4-66.7)	60.0 (55.3-63.6)	<0.001
COX2 (IOD/cell number)	1737.1(485.7-4591.9)	1182.0 (778.1-2304.7)	3381.5(1089.4-6042.9)	7734.9 (4288.6-13199.9)	<0.001

FIGURE 3: The expression of COX2 between grade 2, 3, 4, and 5 discs of the patients. (a) The percent of COX2+ cells in the total cell population in NP tissues at grades 2, 3, 4, and 5. (b) The IOD/cell number of COX2 in NP tissues at grades 2, 3, 4, and 5. * represents $P < 0.05$, ** represents $P < 0.01$, *** represents $P < 0.001$, and **** represents $P < 0.0001$.



	Total	Non-Degeneration	Degeneration	<i>p</i> -value
COX2 (IOD/cell number)	2016.8 (923.6-5337.6)	1192.2 (659.6-2368.4)	3460.1 (1474.0-6760.0)	<0.001
COX2 (cell+/cell number) [%]	40.4 (26.7-60)	30.8 (24.6-40.3)	57.0 (36.2-66.7)	<0.001

FIGURE 4: The expression of COX2 between human white and black discs of the patients. (a) The percent of COX2+ cells in total cell population between human degenerated and nondegenerated NP tissues. (b) The IOD/cell number of COX2 between human degenerated and nondegenerated NP tissues. D: degenerative (black) discs; ND: nondegenerative (white) discs. *** represents $P < 0.001$, and **** represents $P < 0.0001$.

development. Currently, the knowledge about the involvement of COX2 with IVDD is relatively low. A few studies have investigated the association of COX2 with IVDD in animal models and in vitro cell culture. In rat [45] and dog [46] models with induced IVD degeneration, increased expression of COX2 has been found in degenerated discs. In disc cell culture, IL-1 β [34, 47] and TNF- α [48] have been found to elevate inflammatory gene expression including

COX2. However, the information about COX2 expression in native human IVD at different degeneration grades is still scarce.

In this study, we looked into the baseline information of patients with different degrees of IVDD. We explored the association of COX2 with IVD degeneration with a relatively large scale of clinical human specimens. As a result, among all the baseline information investigated, none but age is

TABLE 2: Spearman analysis of correlation between COX2 and baseline information.

	COX2 positivity (cell+/cell number)		COX2 intensity (IOD/cell number)	
	Spearman correlation	<i>P</i> value	Spearman correlation	<i>P</i> value
Gender (<i>n</i> [%])	0.068	0.488	0.054	0.58
Age (years)	0.177	0.069	0.313	0.001
BMI	0.14	0.15	0.123	0.206
Height (m)	0.077	0.433	0.018	0.851
Weight (kg)	0.193	0.047	0.131	0.178
Diabetes history (yes or no)	0.209	0.031	0.254	0.008
Smoking history (yes or no)	-0.079	0.419	0.049	0.618

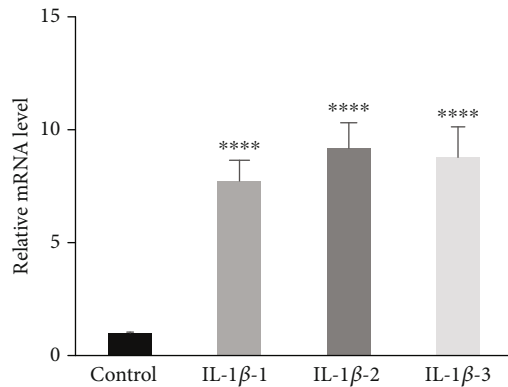


FIGURE 5: Expression of COX2 after treatment with IL-1 β on human nucleus pulposus cells. The expressions of COX2 in each group were normalized to the expression of COX2 in the control group with no IL-1 β treatment. IL-1 β -1: 5 ng/ml, IL-1 β -2: 10 ng/ml, and IL-1 β -3: 15 ng/ml. COX2: cyclooxygenase 2; IL-1 β : interleukin 1 β . **** represents $P < 0.0001$.

shown to be associated with IVDD. The expression intensity of COX2 increased from grade 2 to grade 5, and the same trend is detected when comparing white discs to black discs. Consistently, cell positivity of COX2 also increases in more degenerative NP when compared to NP at lower degenerative grades. We further checked the expression of COX2 in cell culture in vitro and found that IL-1 β treatment could upregulate COX2 expression in human NP cells, which is consistent with other findings [34, 47]. This indicates that COX2 is involved in the IL-1 β -induced inflammatory process. In conclusion, the expression of COX2 is positively correlated with the degree of IVD degeneration and confirms the onset of inflammation in degenerated IVD. However, this study has its limitations in that it is an observational study to reveal the expressional changes of COX2 in different degeneration levels of human IVD only. We have not performed investigations of its expression in animal models of IVDD, which will be beneficial for consolidating the association of COX2 with IVDD.

The incidence of IVDD is high and age-dependent. A study showed that the prevalence rates of IVDD in the whole spine are 71% in men and 77% in women at age 50-, while the rates are over 90% at age 50+ both in men and women [5]. A large population-based study in South China showed that 40% of people under 30 suffer from lumbar disc degen-

eration, but the proportion in the 60+ group is approximately 100% [49]. In recent years, a young population showed an increased incidence rate. Makino et al. [50] reported that 31% of people under 20 at their first MRI examination were found to have IVDD. A recent review has evaluated the occurrence of IVDD ranging from kindergarten- to middle school-aged children and shows that LBP is rare in preschoolers and then increases until it becomes similar to that of adults at age 18 [51]. In our study, it is found that the age of patients in the IVDD group is significantly higher than that in the non-IVDD group, which is consistent with a number of previous reports. We did not find any association of BMI or smoking with IVDD in this study. Since the pathogenesis of the type I and type II diabetes is different, we further looked into the patient information and found that all the 5 patients involved in this study have type II diabetes. We did not find association of type II diabetes with IVDD in these patients. The possible reason is that the sample sizes of patients with diabetes or smoking history (5 each) in this study are too small to study the association of diabetes or smoking with IVDD. It is the same for our study that though COX2 expression is found to be positively correlated with diabetes through the Spearman analysis, the scientific significance of their association is undermined by the small sample size of diabetes patients in this study. Body weight has a correlation with COX2 cellular positivity, while age has an association with COX2 expression intensity, which indicates that COX2 expression may be connected with the body weight and age of the patients.

We realize that though the sample size was relatively large, due to the difficulty in obtaining healthy IVD samples, only degenerative IVDs at grades 2 to 5 of the Pfirrmann grading system were obtained. To solve this, apart from directly comparing the discs at different degeneration grades, we also adopted the criteria by Teraguchi et al. [5] to have the white disc group and black disc group to allow multiple examination of their association with IVDD. Also, this is only an observational study on COX2 expression in IVDD. Though we showed that IL-1 β can regulate COX2 expression in the NP, much detail is lacking to reveal the upstream and downstream signaling of COX2 in IVDD. Further investigation on their roles in IVD inflammation and degeneration would help to understand the pathogenesis of IVDD in more detail and facilitate the development of repairing strategies.

In addition, the recent identification of endogenous progenitor cells with mesenchymal stem cell-like properties [52] in the IVD [53] brings forward a question of how IVD progenitor cells are involved in or respond to IVD inflammation. Further investigation on the association of IVD progenitor cells with IVD inflammation would be desirable.

5. Conclusion

The expression of COX2 increased with the degree of IVD degeneration, which highlights COX2 as a biomarker for IVD degeneration. Furthermore, IL-1 β regulates COX2 expression in the NP, which indicates the possible involvement of inflammation and pain signaling in the process of IVD degeneration. Further investigation into the function of COX2 during IVDD is required to reveal its role in IVDD.

Data Availability

The data used to support the findings of this study are available from the corresponding author upon request.

Conflicts of Interest

The authors declare no conflicting personal or financial interests.

Authors' Contributions

Liu C., Liang G., and Deng Z. contributed equally to this work and shared the co-first authorship.

Acknowledgments

This study is supported by the Natural Science Foundation of Guangdong Province (2020A1515011031, 2020A1515010268, and 2021A1515011008), the Guangzhou Science and Technology Program Key Projects (2021053000053), the National Natural Science Foundation of China (81702191, 81802217, and 81802222), and the Fundamental Research Funds for the Central Universities (2020ZYGXZR010).

Supplementary Materials

Supplementary Figure 1: MRI images of human intervertebral discs of Pfirrmann grades II to V. The red arrow indicates the harvested IVD level for the Pfirrmann classification. Supplementary Figure 2: representative COX2 immunohistochemical staining results of several human nucleus pulposus specimens at Pfirrmann grades II (line 1), III (line 2), IV (line 3), and V (line 4). (*Supplementary Materials*)

References

- [1] C. J. Murray, R. M. Barber, K. J. Foreman et al., "Global, regional, and national disability-adjusted life years (DALYs) for 306 diseases and injuries and healthy life expectancy (HALE) for 188 countries, 1990-2013: quantifying the epidemiological transition," *Lancet*, vol. 386, no. 10009, pp. 2145–2191, 2015.
- [2] C. J. Murray, J. Abraham, M. K. Ali et al., "The state of US health, 1990-2010," *JAMA*, vol. 310, no. 6, pp. 591–608, 2013.
- [3] L. G. Hart, R. A. Deyo, and D. C. Cherkin, "Physician office visits for low back Pain," *Spine*, vol. 20, no. 1, pp. 11–19, 1995.
- [4] M. J. DePalma, J. M. Ketchum, and T. Saullo, "What is the source of chronic low back pain and does age play a role?," *Pain Medicine*, vol. 12, no. 2, pp. 224–233, 2011.
- [5] M. Teraguchi, N. Yoshimura, H. Hashizume et al., "Prevalence and distribution of intervertebral disc degeneration over the entire spine in a population-based cohort: the Wakayama Spine Study," *Osteoarthritis and Cartilage*, vol. 22, no. 1, pp. 104–110, 2014.
- [6] M. Teraguchi, N. Yoshimura, H. Hashizume et al., "The association of combination of disc degeneration, end plate signal change, and Schmorl node with low back pain in a large population study: the Wakayama Spine Study," *The Spine Journal*, vol. 15, no. 4, pp. 622–628, 2015.
- [7] K. Luoma, T. Vehmas, H. Riihimäki, and R. Raininko, "Disc height and signal intensity of the nucleus pulposus on magnetic resonance imaging as indicators of lumbar disc degeneration," *Spine (Phila Pa 1976)*, vol. 26, no. 6, pp. 680–686, 2001.
- [8] A. M. Wang, P. Cao, A. Yee, D. Chan, and E. X. Wu, "Detection of extracellular matrix degradation in intervertebral disc degeneration by diffusion magnetic resonance spectroscopy," *Magnetic Resonance in Medicine*, vol. 73, no. 5, pp. 1703–1712, 2015.
- [9] C. W. Pfirrmann, A. Metzdorf, M. Zanetti, J. Hodler, and N. Boos, "Magnetic resonance classification of lumbar intervertebral disc degeneration," *Spine (Phila Pa 1976)*, vol. 26, no. 17, pp. 1873–1878, 2001.
- [10] M. Teraguchi, N. Yoshimura, H. Hashizume et al., "Progression, incidence, and risk factors for intervertebral disc degeneration in a longitudinal population-based cohort: the Wakayama Spine Study," *Osteoarthritis and Cartilage*, vol. 25, no. 7, pp. 1122–1131, 2017.
- [11] D. Samartzis, J. Karppinen, F. Mok, D. Y. T. Fong, K. D. K. Luk, and K. M. C. Cheung, "A population-based study of juvenile disc degeneration and its association with overweight and obesity, low back pain, and diminished functional status," *The Journal of Bone and Joint Surgery. American Volume*, vol. 93, no. 7, pp. 662–670, 2011.
- [12] D. Wang, L. A. Nasto, P. Roughley et al., "Spine degeneration in a murine model of chronic human tobacco smokers," *Osteoarthritis and Cartilage*, vol. 20, no. 8, pp. 896–905, 2012.
- [13] R. Jing, Y. Liu, P. Guo et al., "Evaluation of common variants in matrix metalloproteinase-9 gene with lumbar disc herniation in Han Chinese population," *Genetic Testing and Molecular Biomarkers*, vol. 22, no. 10, pp. 622–629, 2018.
- [14] A. Saberi, Z. Salehi, B. Naderinabi, S. H. Ansari, and S. Mashayekhi, "Genetic dimension of intervertebral disc degeneration: polymorphism of matrix metalloproteinase 1 and 3 in the north Iranian population," *Turkish Neurosurgery*, vol. 28, no. 3, pp. 447–453, 2018.
- [15] F. Lv, V. Y. L. Leung, S. Huang, Y. Huang, Y. Sun, and K. M. C. Cheung, "In search of nucleus pulposus-specific molecular markers," *Rheumatology (Oxford)*, vol. 53, no. 4, pp. 600–610, 2014.
- [16] F. Lv, V. Y. L. Leung, and K. M. C. Cheung, "The expression of keratin 19 in intervertebral disc degeneration and aging,"

- Global Spine Journal*, vol. 6, article s-0036-1582624, 1_suppl, 2016.
- [17] F. J. Lyu, H. Cui, H. Pan et al., "Painful intervertebral disc degeneration and inflammation: from laboratory evidence to clinical interventions," *Bone Research*, vol. 9, no. 1, p. 7, 2021.
- [18] Y. Peng and F. J. Lv, "Symptomatic versus asymptomatic intervertebral disc degeneration: is inflammation the key?," *Critical Reviews in Eukaryotic Gene Expression*, vol. 25, no. 1, pp. 13–21, 2015.
- [19] S. E. Navone, G. Marfia, A. Giannoni et al., "Inflammatory mediators and signalling pathways controlling intervertebral disc degeneration," *Histology and Histopathology*, vol. 32, no. 6, pp. 523–542, 2017.
- [20] C. L. Le Maitre, J. A. Hoyland, and A. J. Freemont, "Catabolic cytokine expression in degenerate and herniated human intervertebral discs: IL-1 β and TNF α expression profile," *Arthritis Research & Therapy*, vol. 9, no. 4, p. R77, 2007.
- [21] P. Tang, J. M. Gu, Z. A. Xie et al., "Honokiol alleviates the degeneration of intervertebral disc via suppressing the activation of TXNIP-NLRP3 inflammasome signal pathway," *Free Radical Biology & Medicine*, vol. 120, pp. 368–379, 2018.
- [22] E. Mavrogenatou, M. T. Angelopoulou, and D. Kletsas, "The catabolic effect of TNF α on bovine nucleus pulposus intervertebral disc cells and the restraining role of glucosamine sulfate in the TNF α -mediated up-regulation of MMP-3," *Journal of Orthopaedic Research*, vol. 32, no. 12, pp. 1701–1707, 2014.
- [23] F. J. Lv, Y. Peng, F. L. Lim et al., "Matrix metalloproteinase 12 is an indicator of intervertebral disc degeneration co-expressed with fibrotic markers," *Osteoarthritis and Cartilage*, vol. 24, no. 10, pp. 1826–1836, 2016.
- [24] F. Lv, F. Lim, V. Y. Leung, and K. M. Cheung, "Degenerated intervertebral discs contain increased proportion of α -smooth muscle actin positive cells," *Osteoarthritis and Cartilage*, vol. 24, pp. S481–S482, 2016.
- [25] V. Y. Leung, D. M. K. Aladin, F. Lv et al., "Mesenchymal stem cells reduce intervertebral disc fibrosis and facilitate repair," *Stem Cells*, vol. 32, no. 8, pp. 2164–2177, 2014.
- [26] F. Yang, V. Y. L. Leung, K. D. K. Luk, D. Chan, and K. M. C. Cheung, "Injury-induced sequential transformation of notochordal nucleus pulposus to chondrogenic and fibrocartilaginous phenotype in the mouse," *The Journal of Pathology*, vol. 218, no. 1, pp. 113–121, 2009.
- [27] K. Tsuge, T. Inazumi, A. Shimamoto, and Y. Sugimoto, "Molecular mechanisms underlying prostaglandin E₂-exacerbated inflammation and immune diseases," *International Immunology*, vol. 31, no. 9, pp. 597–606, 2019.
- [28] K. Tada, M. Murakami, T. Kambe, and I. Kudo, "Induction of cyclooxygenase-2 by secretory phospholipase A₂ in nerve growth factor-stimulated rat serosal mast cells is facilitated by interaction with fibroblasts and mediated by a mechanism independent of their enzymatic functions," *Journal of Immunology*, vol. 161, no. 9, pp. 5008–5015, 1998.
- [29] M. Tsuzaki, G. Guyton, W. Garrett et al., "IL-1 β induces COX2, MMP-1, -3 and -13, ADAMTS-4, IL-1 β and IL-6 in human tendon cells," *Journal of Orthopaedic Research*, vol. 21, no. 2, pp. 256–264, 2003.
- [30] A. Diaz, K. P. Chepenik, J. H. Korn, A. M. Reginato, and S. A. Jimenez, "Differential Regulation of Cyclooxygenases 1 and 2 by Interleukin-1 β , Tumor Necrosis Factor- α , and Transforming Growth Factor- β 1 in Human Lung Fibroblasts," *Experimental Cell Research*, vol. 241, no. 1, pp. 222–229, 1998.
- [31] R. K. Studer, N. Vo, G. Sowa, C. Ondeck, and J. Kang, "Human nucleus pulposus cells react to IL-6," *Spine (Phila Pa 1976)*, vol. 36, no. 8, pp. 593–599, 2011.
- [32] B. Singh, J. A. Berry, L. E. Vincent, and A. Lucci, "Involvement of IL-8 in COX-2-mediated bone metastases from breast cancer," *The Journal of Surgical Research*, vol. 134, no. 1, pp. 44–51, 2006.
- [33] J. du, J. J. Pfannkuche, G. Lang et al., "Proinflammatory intervertebral disc cell and organ culture models induced by tumor necrosis factor alpha," *JOR Spine*, vol. 3, no. 3, article e1104, 2020.
- [34] W. J. Zhang, Y. Liu, J. S. Wei, and Y. L. Wu, "Ginsenoside Rd inhibits IL-1 β -induced inflammation and degradation of intervertebral disc chondrocytes by increasing IL1RAP ubiquitination," *Brazilian Journal of Medical and Biological Research*, vol. 52, no. 9, article e8525, 2019.
- [35] K. L. Phillips, K. Cullen, N. Chiverton et al., "Potential roles of cytokines and chemokines in human intervertebral disc degeneration: interleukin-1 is a master regulator of catabolic processes," *Osteoarthritis and Cartilage*, vol. 23, no. 7, pp. 1165–1177, 2015.
- [36] C. le Maitre, A. J. Freemont, and J. A. Hoyland, "The role of interleukin-1 in the pathogenesis of human intervertebral disc degeneration," *Arthritis Research & Therapy*, vol. 7, no. 4, pp. R732–R745, 2005.
- [37] D. Gopal, A. L. Ho, A. Shah, and J. H. Chi, "Molecular basis of intervertebral disc degeneration," *Advances in Experimental Medicine and Biology*, vol. 760, pp. 114–133, 2012.
- [38] C. K. Kepler, R. K. Ponnappan, C. A. Tannoury, M. V. Risbud, and D. G. Anderson, "The molecular basis of intervertebral disc degeneration," *The Spine Journal*, vol. 13, no. 3, pp. 318–330, 2013.
- [39] P. P. Guan and P. Wang, "Integrated communications between cyclooxygenase-2 and Alzheimer's disease," *The FASEB Journal*, vol. 33, no. 1, pp. 13–33, 2019.
- [40] C. Pochard, L. Leclair-Visonneau, E. Coron, M. Neunlist, M. Rolli-Derkinderen, and P. Derkinderen, "Cyclooxygenase 2 is upregulated in the gastrointestinal tract in Parkinson's disease," *Movement Disorders*, vol. 33, no. 3, pp. 493–494, 2018.
- [41] L. Wang, Y. Sha, J. Bai et al., "Podocyte-specific knockout of cyclooxygenase 2 exacerbates diabetic kidney disease," *American Journal of Physiology. Renal Physiology*, vol. 313, no. 2, pp. F430–F439, 2017.
- [42] M. Szweda, A. Rychlik, I. Babińska, and A. Pomianowski, "Cyclooxygenase-2 as a biomarker with diagnostic, therapeutic, prognostic, and predictive relevance in small animal oncology," *Journal of Veterinary Research*, vol. 64, no. 1, pp. 151–160, 2020.
- [43] T. L. Silveira, E. S. Veloso, I. N. N. Gonçalves et al., "Cyclooxygenase-2 expression is associated with infiltration of inflammatory cells in oral and skin canine melanomas," *Veterinary and Comparative Oncology*, vol. 18, no. 4, pp. 727–738, 2020.
- [44] Y. Elborai, A. Elgammal, A. Salama et al., "Cyclooxygenase-2 expression as a prognostic factor in pediatric classical Hodgkin lymphoma," *Clinical & Translational Oncology*, vol. 22, no. 9, pp. 1539–1547, 2020.
- [45] F. Ding and X. Li, "Apigenin mitigates intervertebral disc degeneration through the amelioration of tumor necrosis

- factor alpha (TNF-alpha) signaling pathway," *Medical Science Monitor*, vol. 26, article e924587, 2020.
- [46] N. Willems, A. R. Tellegen, N. Bergknut et al., "Inflammatory profiles in canine intervertebral disc degeneration," *BMC Veterinary Research*, vol. 12, no. 1, p. 10, 2016.
- [47] J. Chen, J. Xuan, Y. T. Gu et al., "Celastrol reduces IL-1 β induced matrix catabolism, oxidative stress and inflammation in human nucleus pulposus cells and attenuates rat intervertebral disc degeneration in vivo," *Biomedicine & Pharmacotherapy*, vol. 91, pp. 208–219, 2017.
- [48] T. Yamamoto, S. Suzuki, T. Fujii et al., "Efficacy of hyaluronic acid on intervertebral disc inflammation: an in vitro study using notochordal cell lines and human disc cells," *Journal of Orthopaedic Research*, vol. 39, no. 10, pp. 2197–2208, 2021.
- [49] K. M. Cheung, J. Karppinen, D. Chan et al., "Prevalence and pattern of lumbar magnetic resonance imaging changes in a population study of one thousand forty-three individuals," *Spine (Phila Pa 1976)*, vol. 34, no. 9, pp. 934–940, 2009.
- [50] H. Makino, Y. Kawaguchi, S. Seki et al., "Lumbar disc degeneration progression in young women in their 20's: a prospective ten-year follow up," *Journal of Orthopaedic Science*, vol. 22, no. 4, pp. 635–640, 2017.
- [51] J. MacDonald, E. Stuart, and R. Rodenberg, "Musculoskeletal low back pain in school-aged Children," *JAMA Pediatrics*, vol. 171, no. 3, pp. 280–287, 2017.
- [52] F. J. Lv, R. S. Tuan, K. M. C. Cheung, and V. Y. L. Leung, "Concise review: the surface markers and identity of human mesenchymal stem cells," *Stem Cells*, vol. 32, no. 6, pp. 1408–1419, 2014.
- [53] F. J. Lyu, K. M. Cheung, Z. Zheng, H. Wang, D. Sakai, and V. Y. Leung, "IVD progenitor cells: a new horizon for understanding disc homeostasis and repair," *Nature Reviews Rheumatology*, vol. 15, no. 2, pp. 102–112, 2019.

Review Article

Tryptophan-Kynurenine Pathway in COVID-19-Dependent Musculoskeletal Pathology: A Minireview

Sagar Vyavahare,¹ Sandeep Kumar,¹ Nicholas Cantu,² Ravindra Kolhe,³ Wendy B. Bollag,^{4,5} Meghan E. McGee-Lawrence,^{1,5} William D. Hill,⁶ Mark W. Hamrick ,^{1,5} Carlos M. Isales,^{2,5} and Sadanand Fulzele ^{1,2,5}

¹Department of Cell Biology and Anatomy, Augusta University, Augusta, GA, USA

²Department of Medicine, Augusta University, Augusta, GA, USA

³Department of Pathology, Augusta University, Augusta, GA, USA

⁴Department of Physiology, Augusta University, Augusta, GA, USA

⁵Center for Healthy Aging, Augusta University, Augusta, GA, USA

⁶Department of Pathology, Medical University of South Carolina, Charleston, SC, USA

Correspondence should be addressed to Sadanand Fulzele; sfulzele@augusta.edu

Received 10 August 2021; Revised 9 September 2021; Accepted 21 September 2021; Published 5 October 2021

Academic Editor: zhenhan deng

Copyright © 2021 Sagar Vyavahare et al. This is an open access article distributed under the Creative Commons Attribution License, which permits unrestricted use, distribution, and reproduction in any medium, provided the original work is properly cited.

Severe acute respiratory syndrome coronavirus 2 (SARS-CoV-2) causes coronavirus disease 2019 (COVID-19), affecting multiple organ systems, including the respiratory tract and lungs. Several studies have reported that the tryptophan-kynurenine pathway is altered in COVID-19 patients. The tryptophan-kynurenine pathway plays a vital role in regulating inflammation, metabolism, immune responses, and musculoskeletal system biology. In this minireview, we surmise the effects of the kynurenine pathway in COVID-19 patients and how this pathway might impact muscle and bone biology.

1. Introduction

Severe acute respiratory syndrome coronavirus 2 (SARS-CoV-2) is responsible for the current pandemic, suspected to originate from infected bats [1]. Coronavirus disease 2019 (COVID-19), caused by SARS-CoV-2, has turned out to be a major global catastrophe affecting millions of individuals across the globe [2]. In the United States, as of today, more than 30 million lives have been affected by COVID-19, and over six hundred thousand Americans have lost their lives, according to the Johns Hopkins Coronavirus Resource Center [3]. COVID-19 can present a wide spectrum of symptoms such as cough, fever, shortness of breath, muscle pain, and loss of taste and smell [4]. Mild to severely affected patients may experience elevated proinflammatory cytokines such as IL-1, TNF- α , and IL-6 [5], which negatively affect human health (Figure 1). Excessive activation of these proin-

flammatory cytokines (cytokine storm) leads to the alteration of several metabolic signaling pathways (e.g., the tryptophan-kynurenine pathway).

Recent studies have shown that the tryptophan-kynurenine pathway (Trp-Kyn) is altered in COVID-19 patients. A study conducted by Thomas et al. analyzed serum metabolites of COVID-19 patients and found that tryptophan (Trp) levels were reduced, and L-kynurenine (Kyn) was elevated [5]. A study performed by Fraser et al. reported similar findings (elevated levels of Kyn in COVID-19 patients) [6]. Another study reported that Kyn levels were elevated, along with kynurenic acid (Kyn-A) and quinolinic acid (QA) in the serum of COVID-19 patients [7]. The study conducted by Lawler et al. demonstrated elevated levels of QA in the blood plasma of COVID-19 patients [8]. Sex-specific differences have also been reported in the levels of Kyn-A and QA metabolites

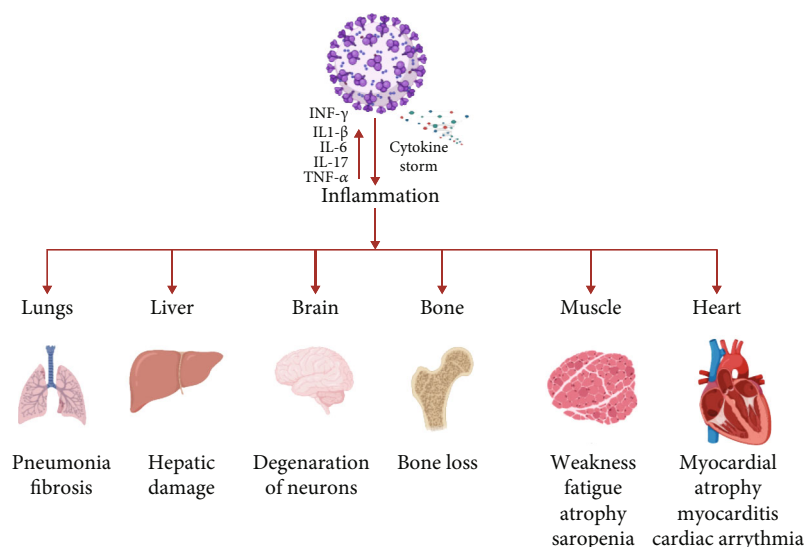


FIGURE 1: Illustration of impact of COVID-19 caused by infection with SARS-CoV-2 on various human organs-lungs, liver, brain, bone, muscle, and heart. (Figure is created by using <http://BioRinder.com>.)

in COVID-19 patients. Serum metabolic analyses performed by Cai et al. reported elevated levels of Kyn-A in male patients compared to female patients [9]. Lionetto et al. assessed serum metabolites in COVID-19 patients and found that Kyn/Trp levels were elevated in male patients [10]. Moreover, Cai et al. (2020) reported an elevated Kyn-A: L-Kyn was associated with increased severity of COVID-19 infection in male patients [9]. The studies mentioned above indicate that activation of the tryptophan-kynurenine pathway might be one of the reasons for the increased susceptibility of males to COVID-19 infection.

Several studies also reported elevated levels of genes involved in tryptophan metabolic pathways [11, 12]. The study conducted by Policard et al. reported that indoleamine-pyrrole 2,3-dioxygenase (IDO-1) is significantly upregulated in COVID-19 patients [11]. Another study also reported similar findings showing elevated levels of IDO-1 in COVID-19 patients [12]. The study conducted by Grunewald et al. in the murine model demonstrated that IDO-1, IDO-2, and TDO-2 were significantly upregulated in murine coronavirus infection [13]. The prevalence and severity of COVID-19 disease are directly associated with age and the underlying condition, such as diabetes, obesity, and cardiovascular disorders [14, 15]. It is well known that the tryptophan-kynurenine pathway elevated with age and above mentioned underlying conditions [16].

The findings from these studies strongly indicate that the Trp-Kyn pathway is altered in COVID-19 patients, leading to a decrease in Trp levels and an increase in Kyn and its metabolites. Recent studies also demonstrated reduced muscle mass and bone loss in COVID-19 patients [17–20]. Based on the findings from our group and published literature, we came up with a novel perspective suggesting that the activation of the Trp-Kyn pathway in COVID-19 patients might be involved in bone and muscle loss.

2. The Tryptophan-Kynurenine (Trp-Kyn) Pathway

Tryptophan (Trp) is an essential amino acid that plays a vital role in protein synthesis, growth, mental health, and immune responses [21]. As age advances, proinflammatory cytokines, such as IL-6, IL-1 β , and IFN- γ , lead to the activation of indoleamine 2,3-dioxygenase (IDO-1) [22]. An increase in levels/activity of IDO-1 along with inflammaging further leads to immunosuppression, neurodegenerative disorders, cardiovascular diseases, and fragility [21–24]. Augmentation of the levels/activity of IDO-1 decreases Trp levels and leads to the generation of several Trp intermediate metabolites [25]. Trp is catabolized by rate-limiting enzymes such as indoleamine 2,3-dioxygenase-1 (IDO-1), indoleamine 2,3-dioxygenase-2 (IDO-2), and tryptophan 2,3-dioxygenase-2 (TDO-2) into N-formylkynurenine and Kyn [26]. Further, Kyn is broken down into Kyn-A and 3-hydroxykynurenine by kynurenine aminotransferases (KAT) and kynurenine 3-monooxygenase (KMO) [27]. Trp also acts as a substrate for the generation of nicotinamide adenine dinucleotide (NAD⁺) through the conversion of quinolinic acid. NAD⁺ plays a crucial role in regulating several cellular processes, including energy production, chromosome stability, immune cell signaling, longevity mechanisms, and DNA repair [28, 29]. The Kyn and its metabolites induce downstream signaling by directly activating Ahr signaling [30] and/or indirect activation of the MEK- (mitogen-activated protein kinase (MAPK)/extracellular signal-regulated kinase (ERK) kinase-) ERK1/2 MAPK signaling pathway [31, 32].

IDO-1 is a master regulator of the Kyn pathway and downstream regulator of interferon signaling [33], which is activated during viral infection [34]. On the other hand, it has been reported that interferon- γ stimulates the expression of ACE2 (the receptor for SARS-CoV-2) in COVID-19 infection [35]. Hence, the interferon- γ signaling cascade

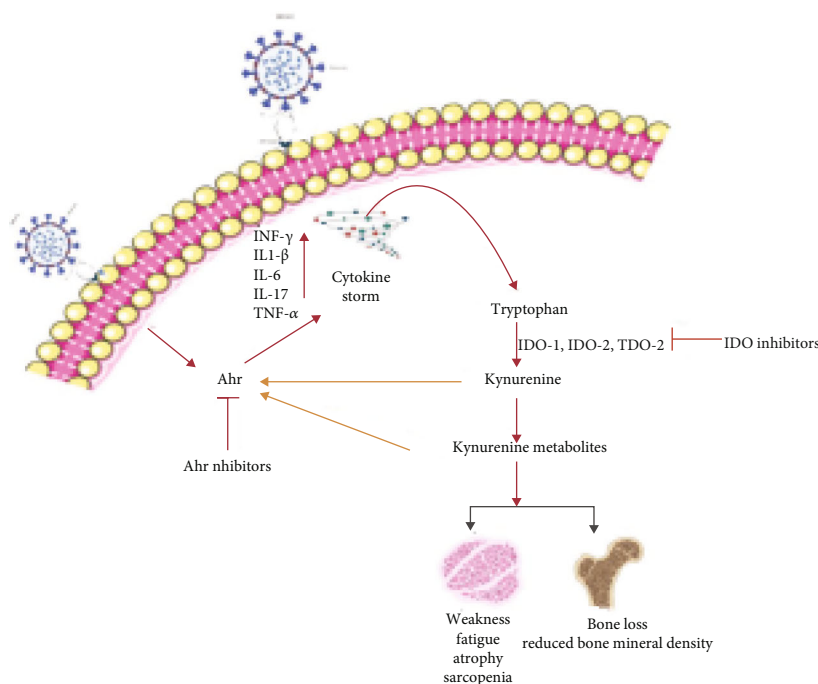


FIGURE 2: Overview of effects of SARS-CoV-2 infection on the muscle and bone. The SARS-CoV-2 infection elicits systemic inflammation (Cytokine storm), which activates the tryptophan-kynurenine pathway. Kynurenine is broken down into several downstream metabolites, which further activates AhR signaling, affecting the integrity and structure of the musculoskeletal system. (Figure is created by using <http://BioRinder.com>.)

potentiates inflammation in SARS-CoV-2 pathology [5]. Enhanced inflammation further leads to an increase in IDO-1 activity followed by enhanced degradation of Trp into Kyn and its metabolites. Our group identified the Trp-Kyn catabolic pathway as a novel causal mechanism in age-associated musculoskeletal complications (stem cell dysfunction and muscle and bone loss). We hypothesized that elevated levels of Kyn and its metabolites might be involved in COVID-19 musculoskeletal pathophysiology (Figure 2).

3. The Try-Kyn Pathway in COVID-19-Induced Musculoskeletal Pathophysiology

Kyn is known to increase with age and is involved in deleterious effects on the musculoskeletal system [24, 36–38]. Recently published data have demonstrated a loss of bone and muscle in COVID-19 patients [17–20]. We hypothesize that an increase in cytokine levels leads to activation of the IDO-Kyn pathway, which raises the levels of Kyn and its metabolites, leading to activation of the aryl hydrocarbon receptor (AhR) and downstream signaling. Induction of AhR signaling directly by viral particles [39] or by Kyn metabolites leads to bone and muscle loss. Viral infection activates AhR through an IDO1-AhR-IDO1-positive feedback loop, which eventually causes upregulation of downstream effectors, such as TCDD-inducible PARP (TiPARP), and enhances the expression of cytokines (e.g., interleukin IL-1β, IL-10, and TNF-α) [39]. Therefore, we hypothesize that elevations in the cytokine expression elicit IDO-Kyn-AhR activation that results in bone and muscle loss.

There is conclusive evidence demonstrating that Kyn increases bone resorption by activating the AhR signaling pathway [38, 40, 41]. An increase in Kyn levels accelerates skeletal aging, leading to decreased osteoblast numbers and increased osteoclast numbers and activity, resulting in bone loss via decreased formation and enhanced resorption [42]. The study performed by our group analyzed the direct effects of feeding Kyn on bone mass and also evaluated the short-term effects of intraperitoneal injection of Kyn on bone turnover in CD-1 mice [24]. Micro-CT analysis revealed a significant bone loss upon Kyn feeding in adult mice, and serum analysis revealed an increase in the levels of osteoclastogenic markers such as RANKL and pyridinoline crosslinks (PYD) [24]. Our study also reported an increase in bone marrow adiposity with Kyn treatment. Moreover, bone marrow stromal cells isolated from Kyn-injected mice showed a decrease in the expression of Hdac-3 and its cofactor NcoR1 and augmentation of the expression of lipid storage genes such as Cidec and Plin1 [24], suggesting a phenotype similar to accelerated aging since such changes are also observed in aged bone marrow cells [43]. A study conducted by Kalaska et al. revealed that elevated Kyn levels decrease bone strength in rats [44]. Kyn metabolites may also exert effects on bone: a study performed by Darlington et al. measured the ratio of 3-hydroxyanthranilic acid to anthranilic acid and found that anthranilic acid levels were increased, and 3-hydroxyanthranilic acid levels were decreased in osteoporotic patients [45].

Studies performed by our group have shown that *in vitro* treatment of RAW264.7 cells, a macrophage-like cells line,

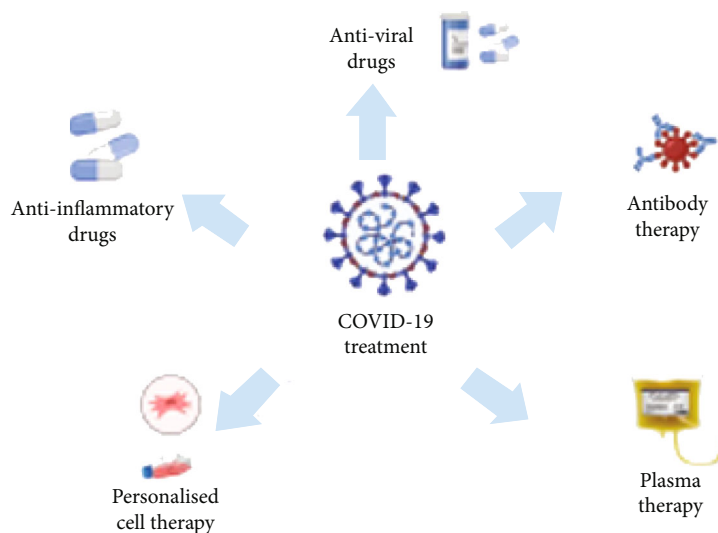


FIGURE 3: Illustration of various strategies used for COVID-19 treatment. (Figure is created by using <http://BioRinder.com>.)

with Kyn induces osteoclastogenesis by upregulating osteoclast transcription factors (such as c-fos and NFATc1) which leads to an increase in TRAP⁺ osteoclasts [40]. Another metabolite, Kyn-A, inhibits the differentiation of osteoblasts and increases osteoclastogenesis through the extracellular signal-regulated kinase (ERK) pathway [36, 46]. Another study conducted by our group demonstrated that Kyn treatment of human and mouse myoblasts increases reactive oxygen species formation [47]. Consistent with this in vitro studies, in vivo treatment of mice with Kyn leads to increased lipid peroxidation accompanied by reduced muscle size and muscle strength [47]. Several Trp downstream metabolites such as Kyn, Kyn-A, and 3-hydroxykynurenine are endogenous AhR ligands likely to induce musculoskeletal damage [38, 40, 41, 48].

The decline in tryptophan levels and elevated levels of Kyn and its metabolites postcovid will affect not only musculoskeletal health but also accelerate other age-related diseases (such as Alzheimer and Parkinson). The decline in tryptophan levels will impair the serotonin and melatonin pathway, which leads to the development of neurological disorders such as depression, cognitive impairment, sleep disorder, Alzheimer, and Parkinson's [49]. Moreover, a decrease in tryptophan levels will also affect protein synthesis leading to weight loss and muscular atrophy [50]. Some of the comorbidities that have been associated with severe COVID-19 are aging, diabetes, hypertension, chronic lung disease, cancer, and HIV. It is well known that the tryptophan-Kyn pathway is activated in the abovementioned conditions [51–55].

Inhibiting Trp-Kyn and/or AhR signaling may represent a novel therapeutic approach for preventing COVID-19-dependent musculoskeletal health and other age-related diseases. There are several Trp-Kyn/AhR inhibitors that are undergoing clinical trials for various diseased conditions [56]. Currently, indoximod (IDO inhibitor), epacadostat (IDO inhibitor), and IK175 (AhR inhibitor) are being used for inhibiting Trp-Kyn-AhR signaling [26].

4. Conclusion

Current studies regarding the activation of the IDO-Kyn-AhR pathway in COVID-19 patients have opened up a new frontier for the scientific research community. Based on the available literature, it seems inevitable that activation of the IDO-Kyn-AhR pathway in COVID-19 patients should lead to bone and muscle loss, inducing significant musculoskeletal damage. However, there is currently advancement in COVID-19 therapies (Figure 3), but no strategies are available to address musculoskeletal-related issues. Given that the IDO-Kyn-AhR pathway is activated in COVID-19 patients, the use of inhibitors of IDO and/or AhR might be beneficial to reduce or prevent bone and muscle loss in this disease. IDO1 inhibitors (such as indoximod) and AhR inhibitors (e.g., IK 175) may help prevent bone and muscle loss. Some of these inhibitors are currently in clinical trials to treat several cancers and related complications. However, we suggest the necessity of conducting detailed clinical studies to design therapeutic strategies using these inhibitors to prevent bone and muscle loss in COVID-19 patients. The above-discussed literature is based on old variants of COVID-19. It will be interesting to know how delta and other recent variants circulating in the population will affect the IDO-Kyn-AhR pathway.

Data Availability

The data supporting this review are from previously reported studies and datasets, which have been cited.

Conflicts of Interest

The authors also declare that there is no other conflict of interest regarding the publication of this manuscript. The abovementioned funding did not lead to any conflict of interest regarding the publication of this manuscript.

Authors' Contributions

Conceptualization was contributed by SF. Methodology was contributed by SF, SV, CN, SK, and RK. Formal analysis was contributed by CN, SV, SK, RK, MML, and WDH. Resources were contributed by SF, CI, MML, and WDH. MWH. Original draft preparation was contributed by SF and SV. Writing—review and editing was contributed by SF, SV, CN, CI, MWH, and WBB. Funding acquisition was contributed by SF, CI, MML, WDH, MWH, and WBB.

Acknowledgments

This publication is based upon work supported in part by the National Institutes of Health, AG036675 (National Institute on Aging-AG036675 S. F, MML, W.D.H, M. H, C.I.).

References

- [1] K. Sharun, K. Dhama, A. M. Pawde et al., "SARS-CoV-2 in animals: potential for unknown reservoir hosts and public health implications," *Veterinary Quarterly*, vol. 41, no. 1, pp. 181–201, 2021.
- [2] S. A. M. Saghir, N. A. AlGabri, M. M. Alagawany et al., "Chloroquine and Hydroxychloroquine for the prevention and treatment of COVID-19: a fiction, Hope or hype? An updated review," *Therapeutics and Clinical Risk Management*, vol. 17, pp. 371–387, 2021.
- [3] E. Dong, H. Du, and L. Gardner, "An interactive web-based dashboard to track COVID-19 in real time," *The Lancet Infectious Diseases*, vol. 20, no. 5, pp. 533–534, 2020.
- [4] L. Mao, H. Jin, M. Wang et al., "Neurologic manifestations of hospitalized patients with coronavirus disease 2019 in Wuhan, China," *JAMA Neurology*, vol. 77, no. 6, pp. 683–690, 2020.
- [5] T. Thomas, D. Stefanoni, J. A. Reisz et al., "COVID-19 infection alters kynurenine and fatty acid metabolism, correlating with IL-6 levels and renal status," *JCI Insight*, vol. 5, no. 14, article e140327, 2020.
- [6] D. D. Fraser, M. Slessarev, C. M. Martin et al., "Metabolomics profiling of critically ill coronavirus disease 2019 patients: identification of diagnostic and prognostic biomarkers," *Critical Care Explorations*, vol. 2, no. 10, article e0272, 2020.
- [7] B. Shen, X. Yi, Y. Sun et al., "Proteomic and metabolomic characterization of COVID-19 patient sera," *Cell*, vol. 182, no. 1, pp. 59–72.e15, 2020.
- [8] N. G. Lawler, N. Gray, T. Kimhofer et al., "Systemic perturbations in amine and kynurenine metabolism associated with acute SARS-CoV-2 infection and inflammatory cytokine responses," *Journal of Proteome Research*, vol. 20, no. 5, pp. 2796–2811, 2021.
- [9] Y. Cai, D. J. Kim, T. Takahashi et al., "Kynurenic acid underlies sex-specific immune responses to COVID-19," *medRxiv*, 2020.
- [10] L. Lionetto, M. Ulivieri, M. Capi et al., "Increased kynurenine-to-tryptophan ratio in the serum of patients infected with SARS-CoV2: An observational cohort study," *Biochimica et Biophysica Acta - Molecular Basis of Disease*, vol. 1867, no. 3, article 166042, 2021.
- [11] M. Policard, S. Jain, S. Rego, and S. Dakshanamurthy, "Immune characterization and profiles of SARS-CoV-2 infected patients reveals potential host therapeutic targets and SARS-CoV-2 oncogenesis mechanism," *bioRxiv*, 2021.
- [12] W. Sungnak, N. Huang, C. Bécavin et al., "SARS-CoV-2 entry factors are highly expressed in nasal epithelial cells together with innate immune genes," *Nature Medicine*, vol. 26, no. 5, pp. 681–687, 2020.
- [13] M. E. Grunewald, M. G. Shaban, S. R. Mackin, A. R. Fehr, and S. Perlman, "Murine coronavirus infection activates the aryl hydrocarbon receptor in an indoleamine 2,3-dioxygenase-independent manner, contributing to cytokine modulation and proviral TCDD-inducible-PARP expression," *Journal of Virology*, vol. 94, 2020.
- [14] A. Gasmi, M. Peana, L. Pivina et al., "Interrelations between COVID-19 and other disorders," *Clinical Immunology*, vol. 224, article 108651, 2021.
- [15] M. O'Hearn, J. Liu, F. Cudhea, R. Micha, and D. Mozaffarian, "Coronavirus disease 2019 hospitalizations attributable to cardiometabolic conditions in the United States: a comparative risk assessment analysis," *Journal of the American Heart Association*, vol. 10, no. 5, article e019259, 2021.
- [16] G. Oxenkrug, "Insulin resistance and dysregulation of tryptophan-kynurenine and kynurenine-nicotinamide adenine dinucleotide metabolic pathways," *Molecular Neurobiology*, vol. 48, no. 2, pp. 294–301, 2013.
- [17] R. R. Narla and R. A. Adler, "Osteoporosis care amidst the prolonged pandemic," *Journal of Endocrinological Investigation*, vol. 44, no. 7, pp. 1353–1361, 2021.
- [18] S. L. Ramani, J. Samet, C. K. Franz et al., "Musculoskeletal involvement of COVID-19: review of imaging," *Skeletal Radiology*, vol. 50, no. 9, pp. 1763–1773, 2021.
- [19] C. Giraud, G. Librizzi, G. Fichera et al., "Reduced muscle mass as predictor of intensive care unit hospitalization in COVID-19 patients," *PLoS One*, vol. 16, no. 6, article e0253433, 2021.
- [20] M. A. Lim and A. A. Kurniawan, "Dreadful Consequences of Sarcopenia and Osteoporosis Due to COVID-19 Containment," *Geriatric Orthopaedic Surgery & Rehabilitation*, vol. 12, 2021.
- [21] L. Palego, L. Betti, A. Rossi, and G. Giannaccini, "Tryptophan biochemistry: structural, nutritional, metabolic, and medical aspects in humans," *Amino Acids*, vol. 2016, article 8952520, pp. 1–13, 2016.
- [22] Y. Zhan, Y. Zhou, W. Zheng et al., "Alterations of multiple peripheral inflammatory cytokine levels after repeated ketamine infusions in major depressive disorder," *Translational Psychiatry*, vol. 10, no. 1, p. 246, 2020.
- [23] M. D. Lovelace, B. Varney, G. Sundaram et al., "Recent evidence for an expanded role of the kynurenine pathway of tryptophan metabolism in neurological diseases," *Neuropharmacology*, vol. 112, Part B, pp. 373–388, 2017.
- [24] M. E. Refaey, M. E. McGee-Lawrence, S. Fulzele et al., "Kynurenine, a tryptophan metabolite that accumulates with age, induces bone loss," *Journal of Bone and Mineral Research*, vol. 32, no. 11, pp. 2182–2193, 2017.
- [25] M. Platten, E. A. A. Nollen, U. F. Röhrig, F. Fallarino, and C. A. Opitz, "Tryptophan metabolism as a common therapeutic target in cancer, neurodegeneration and beyond," *Nature Reviews. Drug Discovery*, vol. 18, no. 5, pp. 379–401, 2019.
- [26] K. Tang, Y. H. Wu, Y. Song, and B. Yu, "Indoleamine 2,3-dioxygenase 1 (IDO1) inhibitors in clinical trials for cancer immunotherapy," *Journal of Hematology & Oncology*, vol. 14, no. 1, p. 68, 2021.

- [27] J. Kindler, C. K. Lim, C. S. Weickert et al., "Dysregulation of kynurenine metabolism is related to proinflammatory cytokines, attention, and prefrontal cortex volume in schizophrenia," *Molecular Psychiatry*, vol. 25, no. 11, pp. 2860–2872, 2020.
- [28] W. Ying, "NAD⁺/NADH and NADP⁺/NADPH in cellular functions and cell death: regulation and biological consequences," *Antioxidants & Redox Signaling*, vol. 10, no. 2, pp. 179–206, 2008.
- [29] L. Fania, C. Mazzanti, E. Campione, E. Candi, D. Abeni, and E. Dellambra, "Role of nicotinamide in genomic stability and skin cancer chemoprevention," *International Journal of Molecular Sciences*, vol. 20, no. 23, p. 5946, 2019.
- [30] H. Wang, D. C. Do, J. Liu et al., "Functional role of kynurenine and aryl hydrocarbon receptor axis in chronic rhinosinusitis with nasal polyps," *Journal of Allergy and Clinical Immunology*, vol. 141, no. 2, pp. 586–600.e6, 2018.
- [31] Y. Li, R. T. Kilani, E. Rahmani-Neishaboob, R. B. Jalili, and A. Ghahary, "Kynurenine increases matrix metalloproteinase-1 and -3 expression in cultured dermal fibroblasts and improves scarring _in vivo_," *The Journal of Investigative Dermatology*, vol. 134, no. 3, pp. 643–650, 2014.
- [32] H. J. Lee, J. H. Bach, H. S. Chae et al., "Mitogen-activated protein kinase/extracellular signal-regulated kinase attenuates 3-hydroxykynurenine-induced neuronal cell death," *Journal of Neurochemistry*, vol. 88, no. 3, pp. 647–656, 2004.
- [33] R. K. Powers, R. Culp-Hill, M. P. Ludwig et al., "Trisomy 21 activates the kynurenine pathway via increased dosage of interferon receptors," *Nature Communications*, vol. 10, no. 1, p. 4766, 2019.
- [34] K. B. Nguyen, W. T. Watford, R. Salomon et al., "Critical role for STAT4 activation by type I interferons in the interferon gamma response to viral infection," *Science*, vol. 297, no. 5589, pp. 2063–2066, 2002.
- [35] O. O. Onabajo, A. R. Banday, M. L. Stanifer et al., "Interferons and viruses induce a novel truncated ACE2 isoform and not the full-length SARS-CoV-2 receptor," *Nature Genetics*, vol. 52, no. 12, pp. 1283–1293, 2020.
- [36] T. H. Lin, R. S. Yang, C. H. Tang, M. Y. Wu, and W. M. Fu, "Regulation of the maturation of osteoblasts and osteoclastogenesis by glutamate," *European Journal of Pharmacology*, vol. 589, no. 1–3, pp. 37–44, 2008.
- [37] K. S. Martin, M. Azzolini, and J. Lira Ruas, "The kynurenine connection: how exercise shifts muscle tryptophan metabolism and affects energy homeostasis, the immune system, and the brain," *American Journal of Physiology-Cell Physiology*, vol. 318, no. 5, pp. C818–C830, 2020.
- [38] D. Kondrikov, A. Elmansi, R. T. Bragg et al., "Kynurenine inhibits autophagy and promotes senescence in aged bone marrow mesenchymal stem cells through the aryl hydrocarbon receptor pathway," *Exp Gerontol.*, vol. 130, article 110805, 2020.
- [39] W. A. Turski, A. Wnorowski, G. N. Turski, C. A. Turski, and L. Turski, "AhR and IDO1 in pathogenesis of Covid-19 and the "systemic AhR activation syndrome": a translational review and therapeutic perspectives," *Restorative Neurology and Neuroscience*, vol. 38, no. 4, pp. 343–354, 2020.
- [40] N. H. Eisa, S. V. Reddy, A. M. Elmansi et al., "Kynurenine promotes RANKL-induced osteoclastogenesis in vitro by activating the aryl hydrocarbon receptor pathway," *International Journal of Molecular Sciences*, vol. 21, no. 21, p. 7931, 2020.
- [41] Z. Duan and J. Lu, "Involvement of aryl hydrocarbon receptor in L-kynurenine-mediated parathyroid hormone-related peptide expression," *Hormones and Cancer*, vol. 10, no. 2-3, pp. 89–96, 2019.
- [42] B.-J. Kim, M. W. Hamrick, H. J. Yoo et al., "The detrimental effects of kynurenine, a tryptophan metabolite, on human bone metabolism," *The Journal of Clinical Endocrinology & Metabolism*, vol. 104, no. 6, pp. 2334–2342, 2019.
- [43] M. E. McGee-Lawrence, L. R. Carpio, R. J. Schulze et al., "Hdac3 deficiency increases marrow adiposity and induces lipid storage and glucocorticoid metabolism in osteochondroprogenitor cells," *Journal of Bone and Mineral Research*, vol. 31, no. 1, pp. 116–128, 2016.
- [44] B. Kalaska, K. Pawlak, T. Domaniewski et al., "Elevated levels of peripheral kynurenine decrease bone strength in rats with chronic kidney disease," *Frontiers in Physiology*, vol. 8, p. 836, 2017.
- [45] L. G. Darlington, C. M. Forrest, G. M. Mackay et al., "On the biological importance of the 3-hydroxyanthranilic acid: anthranilic acid ratio," *International Journal of Tryptophan Research*, vol. 3, pp. 51–59, 2010.
- [46] T. W. Stone, N. Stoy, and L. G. Darlington, "An expanding range of targets for kynurenine metabolites of tryptophan," *Trends in Pharmacological Sciences*, vol. 34, no. 2, pp. 136–143, 2013.
- [47] H. Kaiser, K. Yu, C. Pandya et al., "Kynurenine, a Tryptophan Metabolite That Increases with Age, Induces Muscle Atrophy and Lipid Peroxidation," *Oxidative Medicine and Cellular Longevity*, vol. 2019, 9894239 pages, 2019.
- [48] A. Al Saedi, S. Sharma, M. A. Summers, K. Nurgali, and G. Duque, "The multiple faces of tryptophan in bone biology," *Experimental Gerontology*, vol. 129, pp. 110778–115565, 2020.
- [49] D. M. Richard, M. A. Dawes, C. W. Mathias, A. Acheson, N. Hill-Kapturczak, and D. M. Dougherty, "L-tryptophan: basic metabolic functions, behavioral research and therapeutic indications," *International Journal of Tryptophan Research*, vol. 2, pp. 45–60, 2009.
- [50] S. Ninomiya, N. Nakamura, H. Nakamura et al., "Low levels of serum tryptophan underlie skeletal muscle atrophy," *Nutrients*, vol. 12, no. 4, p. 978, 2020.
- [51] W. H. Hoffman, S. A. Whelan, and N. Lee, "Tryptophan, kynurenine pathway, and diabetic ketoacidosis in type 1 diabetes," *PLoS One*, vol. 16, no. 7, article e0254116, 2021.
- [52] S. Cussotto, I. Delgado, A. Anesi et al., "Tryptophan metabolic pathways are altered in obesity and are associated with systemic inflammation," *Frontiers in Immunology*, vol. 11, p. 557, 2020.
- [53] S. Naz, M. Bhat, S. Ståhl et al., "Dysregulation of the tryptophan pathway evidences gender differences in COPD," *Metabolites*, vol. 9, no. 10, p. 212, 2019.
- [54] A. Mor, A. Tankiewicz-Kwedlo, and D. Pawlak, "Kynurenines as a novel target for the treatment of malignancies," *Pharmaceuticals*, vol. 14, no. 7, p. 606, 2021.
- [55] Y. H. Zhou, L. Sun, J. Chen et al., "Tryptophan metabolism activates aryl hydrocarbon receptor-mediated pathway to promote HIV-1 infection and reactivation," *mBio*, vol. 10, no. 6, 2019.
- [56] C. A. Opitz, L. F. Somarrivas Patterson, S. R. Mohapatra et al., "The therapeutic potential of targeting tryptophan catabolism in cancer," *British Journal of Cancer*, vol. 122, no. 1, pp. 30–44, 2020.

Research Article

Extracorporeal Shockwave Therapy Modulates the Expressions of Proinflammatory Cytokines IL33 and IL17A, and Their Receptors ST2 and IL17RA, within the Articular Cartilage in Early Avascular Necrosis of the Femoral Head in a Rat Model

Jai-Hong Cheng ^{1,2,3}, Shun-Wun Jhan,^{1,4} Chieh-Cheng Hsu,^{1,4} Hung-Wen Chiu,^{1,4}
and Shan-Ling Hsu ^{1,4,5}

¹Center for Shockwave Medicine and Tissue Engineering, Kaohsiung Chang Gung Memorial Hospital and Chang Gung University College of Medicine, Kaohsiung 833, Taiwan

²Medical Research, Kaohsiung Chang Gung Memorial Hospital and Chang Gung University College of Medicine, Kaohsiung 833, Taiwan

³Department of Leisure and Sports Management, Cheng Shiu University, Kaohsiung 833, Taiwan

⁴Department of Orthopedic Surgery, Sports Medicine, Kaohsiung Chang Gung Memorial Hospital and Chang Gung University College of Medicine, Kaohsiung 833, Taiwan

⁵Fooyin University, School of Nursing, Kaohsiung 831, Taiwan

Correspondence should be addressed to Jai-Hong Cheng; cjh1106@cgmh.org.tw and Shan-Ling Hsu; hsishanlin@yahoo.com.tw

Received 11 March 2021; Revised 6 May 2021; Accepted 11 June 2021; Published 9 July 2021

Academic Editor: Fangjie Zhang

Copyright © 2021 Jai-Hong Cheng et al. This is an open access article distributed under the Creative Commons Attribution License, which permits unrestricted use, distribution, and reproduction in any medium, provided the original work is properly cited.

Avascular necrosis (AVN) of the femoral head (AVNFH) is a disease caused by injury to the blood supply of the femoral head, resulting in a collapse with osteonecrosis and damage to the articular cartilage. Extracorporeal shockwave therapy (ESWT) has been demonstrated to improve AVNFH owing to its anti-inflammation activity, angiogenesis effect, and tissue regeneration in clinical treatment. However, there are still so many pieces of the jigsaw that need to be fit into place in order to ascertain the mechanism of ESWT for the treatment of AVNFH. The study demonstrated that ESWT significantly protected the trabecular bone volume fraction BV/TV ($P < 0.01$) and the trabecular thickness ($P < 0.001$), while in contrast, the trabecular number and trabecular separation were not significantly different after treatment as compared with AVNFH. ESWT protected the articular cartilage in animal model of AVNFH. The levels of IL1- β and IL33 were significantly induced in the AVNFH group ($P < 0.001$) as compared with Sham and ESWT groups and reduced in ESWT group ($P < 0.001$) as compared with AVNFH group. In addition, the expression of the receptor of IL33, ST2, was reduced in AVNFH and induced after ESWT ($P < 0.001$). The expression of IL17A was induced in the AVNFH group ($P < 0.001$) and reduced in the ESWT group ($P < 0.001$). Further, the expression of the receptor of IL17A, IL17RA, was reduced in the AVNFH group ($P < 0.001$) and improved to a normal level in the ESWT group as compared with Sham group ($P < 0.001$). Taken together, the results of the study indicated that ESWT modulated the expression of IL1- β , pro-inflammatory cytokines IL33 and IL17A, and their receptors ST2 and IL17RA, to protect against loss of the extracellular matrix in the articular cartilage of early AVNFH.

1. Introduction

Avascular necrosis (AVN) or osteonecrosis of the femoral head (AVNFH) is a major, painful hip joint disorder that causes severe hip disability, requiring total hip arthroplasty

(THA). The quality of life of patients is seriously affected by this disease, especially in younger patients [1]. Although the survival rate of THA patients has improved over the past few years, its durability is still limited, and treatment for joint preservation is preferred. Traditional treatment for AVNFH

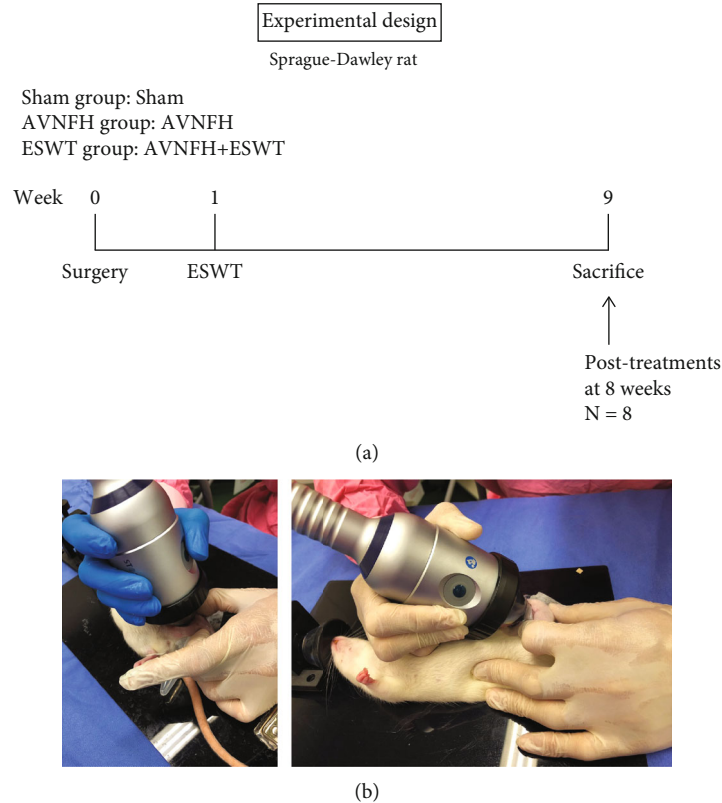


FIGURE 1: The study design and application of shockwave therapy. (a) The graph displayed the study design of the experiment, including ONFH surgery, shockwave application, and sacrificed animals. (b) The two focal points were approximately 0.5 cm apart and the corresponding locations on the skin in the groin area to make with a marker. Each of the two points was treated with 2000 impulses of shockwaves at 0.25 mJ/mm^2 energy flux density and total of 4000 impulses of shockwaves were applied to the affected femoral head. $N = 8$ for all groups.

is recommended within the early stages and includes nonsteroid drugs, protected weight-bearing, and physical treatments, but the outcomes are often disappointing [2, 3]. Surgical interventions in symptomatic hips are preceded by core decompression, muscle pedicle grafts, nonvascularized or vascularized bone grafts, and derotational osteotomy [4–7]. However, to date, the outcomes of all methods are varying and unreliable; therefore, a new and effective treatment for AVNFH is needed.

Pathologically, AVNFH is characterized by the destruction of blood flow to the femoral head, which induces bone damage and necrosis [8, 9]. If the healing process of reparative tissue from necrosis of bone does not overcome the damage caused, further collapse of the head and joint in the femur could occur [10]. Prevention of progressive degradation of AVNFH is difficult. Core decompression is a well-known technique that has been used to treat AVNFH for more than three decades [11], and core decompression and avascular or vascularized bone grafting have been demonstrated to achieve good and moderate results for early AVNFH. However, the variability of core decompression in terms of the clinical success rate was reported to be only 63%, and the rate of subsequent joint replacement surgery or hip salvage surgery was reported to be approximately 33% of patients [12–14]. Complications of core decompression include donor site

morbidity and nerve palsy [15]. One physical method, a non-invasive treatment, is extracorporeal shockwave therapy (ESWT), which has been demonstrated to be safe for the treatment of AVNFH.

ESWT has been shown to be effective in the treatment of musculoskeletal disorders, including nonunion and tendinopathy of the shoulder, elbow, knee, and heel [16–22]. Many studies have reported that ESWT also exerts beneficial effects in osteonecrosis. There are many varieties of growth factors and tissue repair factors that are induced by ESWT, such as vascular endothelial growth factor (VEGF), insulin-like growth factor- (IGF-) I, transforming growth factor- (TGF-) beta, epithelial growth factor (EGF), fibroblast growth factor (FGF), platelet-derived growth factor (PDGF), proliferating cell nuclear antigen (PCNA), von Willebrand factor (vWF), Wnts, endothelial nitric oxide synthase (eNOS), and osteocalcin and bone morphogenetic proteins (BMPs) [19, 20, 23, 24]. The results of animal studies have shown that ESWT promotes bone remodeling and tissue regeneration with ingrowth of angiogenic and osteogenic growth factors [24, 25]. Recently, many clinical studies have revealed that ESWT appears to be effective for the treatment of early AVNFH [20]. ESWT is reported to result in clinical improvement in 79% of AVNFH patients; however, only 39% of patients achieved regression of the lesion according to

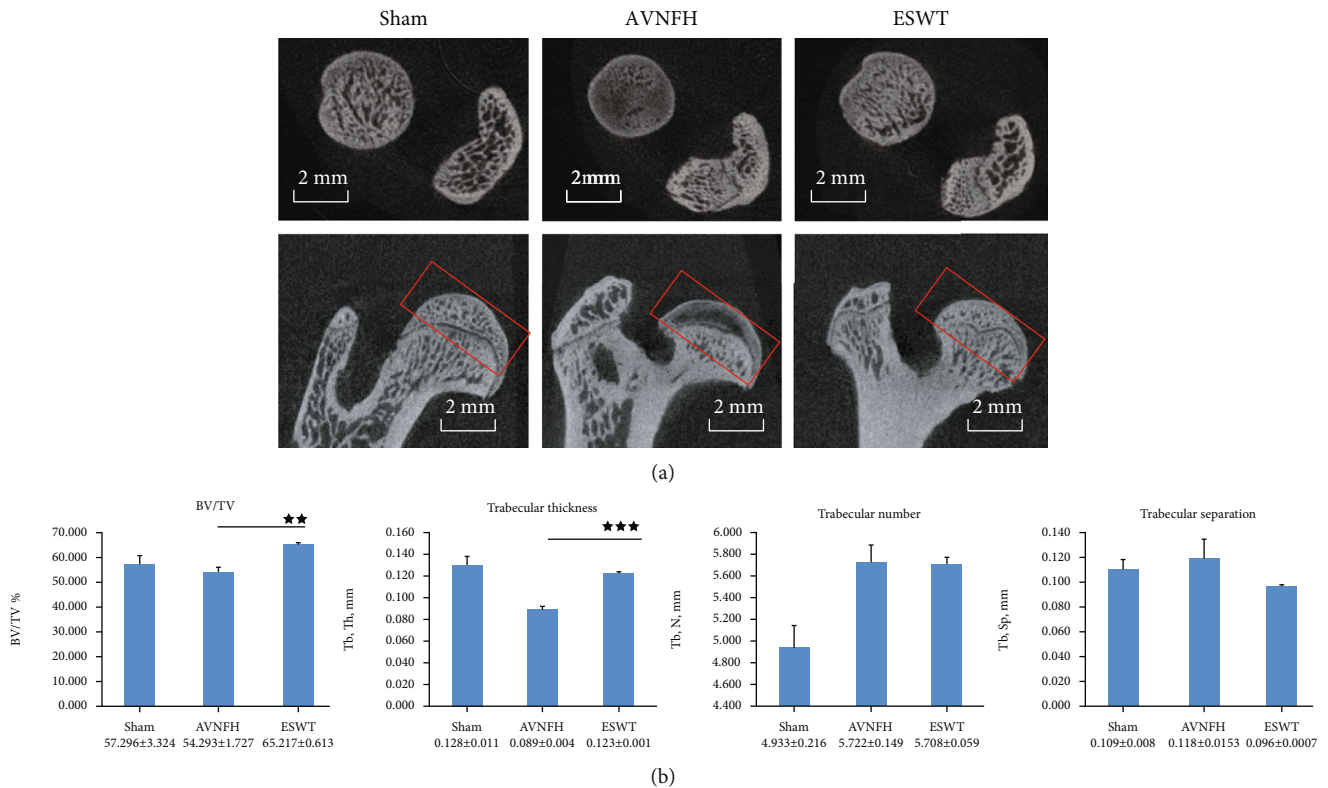


FIGURE 2: Micro-CT scan of the left femur of subchondral bone in different groups. (a) The results showed photomicrographs of the femur head in sagittal and transverse views from micro-CT. The region of interesting was indicated by a red rectangle. (b) The data of subchondral bone of femur head displayed the graphic illustrations of the trabecular bone volume fraction (BV/TV), trabecular thickness, trabecular number, and trabecular separation. $^{**}P < 0.01$ and $^{***}P < 0.001$ as compared with the AVNFH group. The scale bar was 2 mm. $N = 8$ for all groups.

magnetic resonance imaging (MRI) [26]. The results showed that twenty-three patients with stage I, II, or III lesions treated with ESWT and seven patients for whom THA was performed due to failure of treatment saw no improvement, or worsened. Another long-term follow-up study of the outcomes of ESWT for early AVNFH revealed that the necessity for THA increased with time, and 24% (7 of 29) of patients underwent surgery at 8-9 years after ESWT [27]; three patients (four hips) received a second course of shockwave treatment, and three hips eventually underwent THA. Therefore, most clinic studies demonstrated that ESWT is more effective than surgical intervention in early phase treatment.

In recent studies, pro-inflammatory cytokines, interleukin 33 (IL33), and interleukin 17A (IL17A), which are members of the interleukin 1 (IL1) family, play roles in osteonecrosis [28, 29]. Expressions of IL33 and IL17A have been observed in the serum and inflamed synovium of AVNFH patients [29, 30]. These results indicate that IL33 and IL17A may be involved in the development of this disease and could represent treatment targets. ESWT has been reported to exert immunomodulatory effects in the inflammatory disease [23, 31, 32]. In this study, we attempted to elucidate the expressions of pro-inflammatory cytokines IL33 and IL17A, and their receptors ST2 and IL17RA, in the articular cartilage of the animal model of AVNFH after ESWT.

2. Materials and Methods

2.1. Animals. The twenty-four rats were obtained and treated humanely according to the Guide for the Care and Use of Laboratory Animals. The IACUC protocol of the animal study was approved by the Animal Care Committee of Kaohsiung Chang Gung Memorial Hospital, and the approval number was 2019031801. The animals were maintained and cared for before and after the experiments in the Center for Laboratory Animals; they were housed at $23 \pm 1^\circ\text{C}$ with a 12-hour light and dark cycle and given food and water.

2.2. Study Design. The twenty-four rats were randomized into three groups for experiments (Figure 1(a)). The Sham group was the sham control, without surgery or treatment. In the AVNFH group, AVNFH was induced in the rats by anterior hip arthrotomy, transection of the ligamentum teres and vascular deprivation of femoral neck by electrocoagulation on left hips. Finally, in the ESWT group, AVNFH rats received shockwave therapy ($0.25 \text{ mJ}/\text{mm}^2$ with 4000 impulses, 4 Hz) to the neck of left femur one week postsurgery. All rats were sacrificed at 9 weeks post-surgery.

2.3. Avascular Necrosis of Femoral Head Rat Model. Sprague-Dawley rats (night weeks of age, 220 g) were anesthetized using Zoletil (25 mg/kg) and Xylazine (10 mg/kg). The left

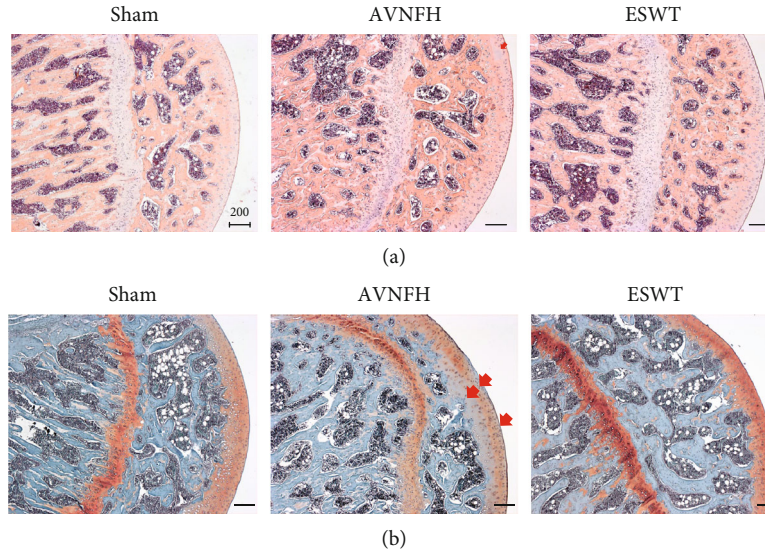


FIGURE 3: The microphotographs of the left femur head showed the changes of articular cartilage in the Sham, AVNFH, and ESWT groups. Some areas of disorganization, loss of extracellular matrix, and decreased number of chondrocytes are presented (arrow) and are protected in the ESWT group by (a) hematoxylin-eosin and (b) safranin-O stain. The scale bar was 200 μm . $N = 8$ for all groups.

hips of rats were subjected to surgery and opened the capsule without remove the muscles by comprising anterior hip arthrotomy. The ligamentum teres of hips were transected and periosteum was removed carefully. The blood vessel around the femoral neck was deprived by using electrocoagulation to induce AVNFH. The ampicillin (25 mg/kg) and ketorolac (1 mg/kg/day) were administered to prevent infection and reduce pain for 5 days after surgery. All rats were allowed unrestricted weight-bearing and activity.

2.4. Shockwave Treatment. The animals in the AVNFH group that received shockwave therapy at one week postsurgery comprised the ESWT group. Shockwaves were generated using a DUOLITH SD1 device (Storz Medical AG, Tägerwil, Switzerland). We selected two focal points, approximately 0.5 cm apart, and the corresponding locations on the skin in the groin area were marked with a marker pen. Each of the two points were subjected to 2000 impulses of shockwaves at an energy flux density of 0.25 mJ/mm^2 , and in total, 4000 impulses of shockwaves were applied to the affected femoral head, as shown in Figure 1(b).

2.5. Micro-CT Analysis. Harvested lower-limb specimens were subjected to micro-CT scanning (SkyScan, 1176, Kartuizersweg 3B 2550 Kontich, Belgium): filter A1 0.5 mm, exposure 270 ms, isotopic pixel size $18 \times 18 \times 18 \mu\text{m}$, X-ray voltage 50 kV, 500 μA . The left hip of the rat was prepared and sized prior to micro-CT for scanning. Image reconstruction was performed, and a series of planar transverse grey images were generated using NRecon software (Skyscan). The region of interest (ROI) of the bone morphometry was selected, and the trabecular volume fraction (BV/TV), trabecular thickness (Tb.Th), trabecular number (Tb.N), and trabecular separation (Tb.Sp) were obtained using the Sky-scan CT-analyser program.

TABLE 1: OARSJ score of the articular cartilage in Sham, AVNFH and ESWT groups.

	Average	Standard error	P value*
Sham	0	0	0
AVNFH	1.28	0.19	$P < 0.001$
ESWT	1.08	0.13	$P < 0.001$

*The $P < 0.001$ was as compared with the Sham group.

2.6. Histopathological Examination. Specimens were performed for histopathological examination. The left hips of the rats were fixed in 4% PBS-buffered formaldehyde at 4°C for one day and decalcified in 10% PBS-buffered EDTA at 4°C for one month. Decalcified hips were fixed and embedded to paraffin wax, and sliced into 5- μm -thick sections. The samples were then stained with hematoxylin-eosin (HE) and safranin-O. The level of damage to the degenerative cartilage was assessed from the results of safranin-O staining using the Osteoarthritis Research Society International (OARSJ) cartilage OA grading system; scores were obtained on a 0-to-24 scale by multiplying the index of the grades with the stage.

2.7. Immunohistochemical Analysis. The articular cartilage of femur heads was further analyzed with specific antibodies for immunohistochemical analysis, as follows: IL1- β (Abcam, USA, Ab-9787, 1:200), IL33 (Biorbyt, USA, orb6205, 1:200), ST2 (Proteintech, USA, 11920-1-AP, 1:150), type II collagen (Santa Cruz Biotechnology, USA, Sc-52658, 1:100), IL17A (Invitrogen, USA, PA5-79470, 1:200), and IL17RA (Abcam, USA, ab218249, 1:200). Sections of the samples were probed with specific proteins for anti-rat IL1- β , IL33, ST2, type II collagen, IL17A, and IL17RA to identify protein markers in the articular cartilage of the rats. The

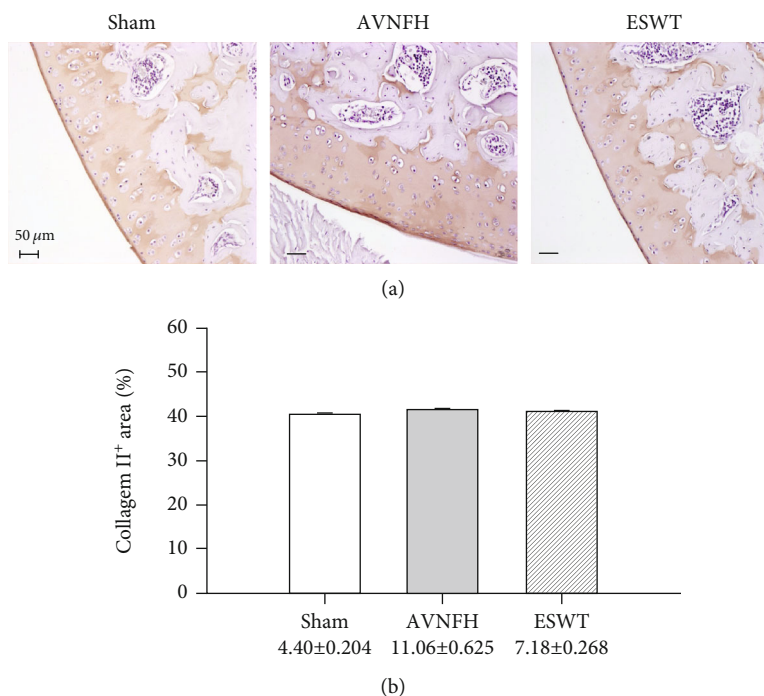


FIGURE 4: Immunohistochemical analysis for type II collagen in the articular cartilage of the left femur head (a) and the level of expression was measured after treatment (b). The scale bar was 50 μm. $N = 8$ for all groups.

immunoreactivity of samples was assessed using a HRP-DAB Cell and Tissue Staining Kit (R & D Systems, USA). The immunoreactivities were quantified from five areas in three sections of the same specimen using a Zeiss Axioskop II plus microscope (Carl Zeiss, Germany). Images were captured using a Cool CCD camera (SNAP-Pro c.f. Digital kit; Media Cybernetics, USA) and analysed using the Image-Pro® Plus software (Media Cybernetics, USA). The percentage of positive signals in each area was calculated, and the average of each sample was used as the result for analysis.

2.8. Statistical Analysis. Statistical software SPSS version 17.0 (SPSS Inc., Chicago, IL, USA; <http://www.ibm.com/tw-zh/analytics/spss-trials>) was employed for statistical analysis. Differences and significances of differences between groups were compared using one-way ANOVA for parametric data with $P < 0.05$, $P < 0.01$, and $P < 0.001$.

3. Results

3.1. ESWT Protected the Subchondral Bone in an Early AVNFH Rat Model. In the experiments, we established a rat AVNFH model and applied ESWT to the femur head of AVNFH rat to establish the ESWT group (Figure 1). The rats in each group were sacrificed posttreatment at 8 weeks. Via micro-CT scanning, the subchondral bone of the left femur head was observed to have been protected against damage after ESWT as compared with the AVNFH group (Figure 2(a), sagittal and transverse views). The results showed that ESWT protected the damage of bone in the femur head of AVNFH.

Micro-CT data showed that ESWT significantly increased the trabecular bone volume fraction BV/TV ($P < 0.01$) and trabecular thickness ($P < 0.001$) in the subchondral bone of the left femur head as compared with the AVNFH group (Figure 2(b)). The trabecular number and trabecular separation were not significantly different after ESWT.

3.2. ESWT Protected the Articular Cartilage in Early AVNFH. Pathological changes were measured using HE and safranin-O staining in the Sham, AVNFH, and ESWT groups (Figure 3). ESWT prevented the loss of the cellular matrix and chondrocytes of the articular cartilage of the hip joint as compared with the Sham and AVNFH groups posttreatment at 8 weeks according to the results of HE and safranin-O staining (Figures 3(a) and 3(b)). Some loss of cellular matrix tissues were observed in the articular cartilage of the AVNFH group as compared with Sham group (Figure 3(a), AVNFH group: red arrow). The recovered in the ESWT groups was obviously in safranin-O staining as compared with AVNFH group (Figure 3(b), AVNFH group: red arrow); however, the damage to cellular matrix tissue was not severe enough to increase the OARSI score greatly, and no significant difference was observed between the AVNFH and ESWT groups (Table 1). The expressed level of type II collagen was also measured in the Sham, AVNFH, and ESWT groups, and no significant differences were observed among the three groups (Figure 4). The results showed minor damages and pathological changes in the articular cartilage of AVNFH group at the end of the experiment duration, which recovered after ESWT.

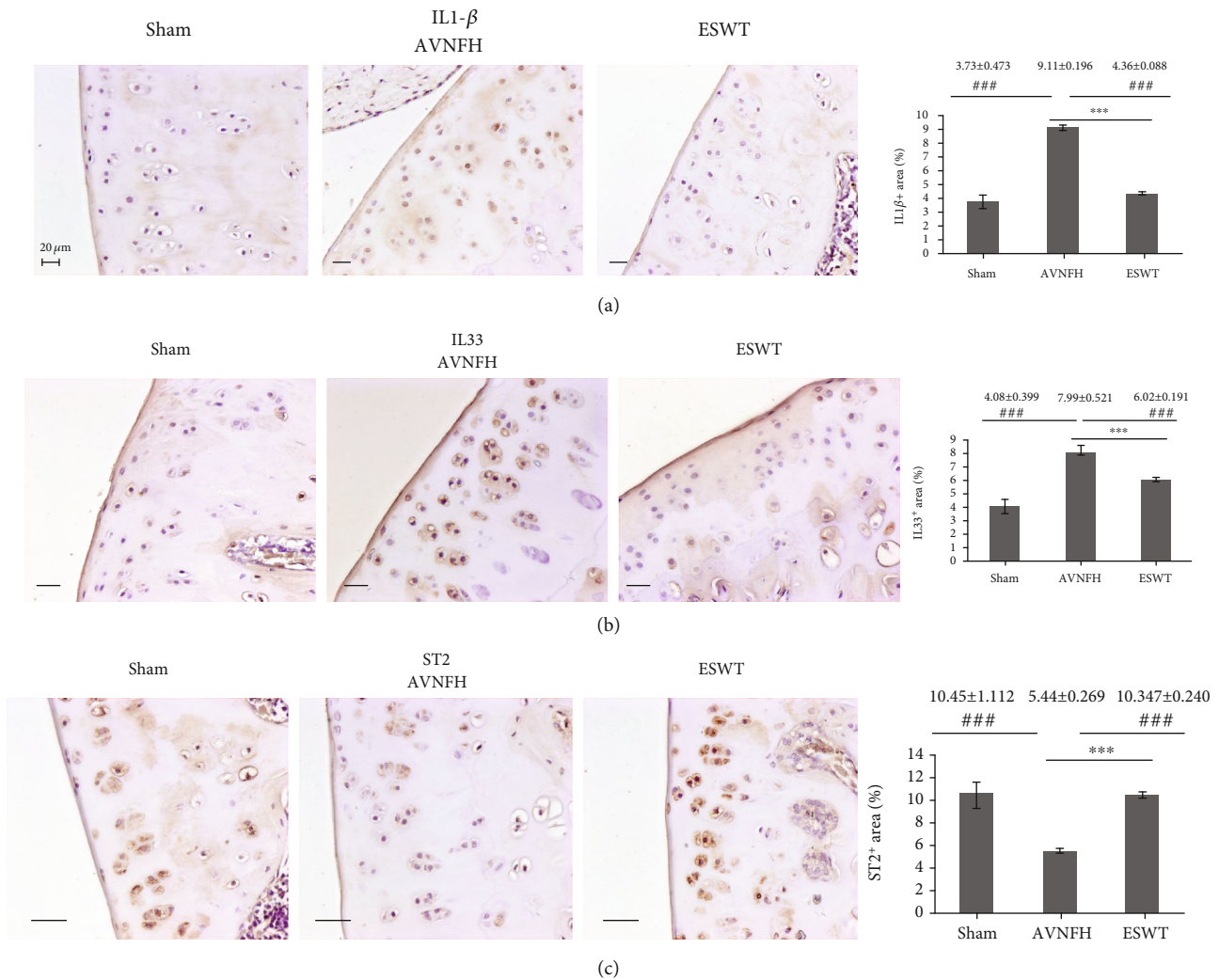


FIGURE 5: Immunohistochemical analysis for (a) IL1- β , (b) IL33, and (c) ST2 in the articular cartilage of the left femur head (right) and the level of expression was measured after treatment (left). *** $P < 0.001$ as compared with ESWT group and ### $P < 0.001$ as compared with AVNFH group. The scale bar was 20 μm . $N = 8$ for all groups.

3.3. ESWT Modulated the Expression of IL1- β , Th2-Oriented Cytokine IL33, and Receptor ST2 in the Articular Cartilage of Early AVNFH. In the experiment, the protein expression levels of IL1- β , IL33, and ST2 were surveyed by immunohistochemical analysis in the articular cartilage in the Sham, AVNFH, and ESWT groups (Figure 5). IL1- β and IL33 were significantly induced in the AVNFH group as compared with the Sham group and ESWT group ($P < 0.001$) and were reduced in the ESWT group as compared with the AVNFH group ($P < 0.001$). In addition, expression of the receptor of IL33, ST2, was reduced in the AVNFH group as compared with Sham and ESWT groups ($P < 0.001$) and increased after ESWT as compared with AVNFH ($P < 0.001$). The results demonstrated that ESWT modulates the inflammatory key factors IL1- β , Th2-oriented cytokine IL33, and receptor ST2 during cartilage repair in the treatment of AVNFH.

3.4. ESWT Modulated the Expression of pro-Inflammatory Cytokine IL17A and Receptor IL17RA in the Articular Cartilage of Early AVNFH. Immunohistochemical images

displayed the levels of IL17A and receptor IL17RA in the articular cartilage of the Sham, AVNFH, and ESWT groups (Figure 6). The expression of IL17A was induced in the AVNFH group as compared with the Sham and ESWT groups ($P < 0.001$) and was reduced in the ESWT group as compared with AVNFH groups ($P < 0.001$). In addition, the receptor of IL17A, IL17RA, was obviously reduced in the AVNFH group as compared with the Sham and ESWT groups ($P < 0.001$) and improved to a normal level in the ESWT group as compared with AVNFH group ($P < 0.001$). These results demonstrated that ESWT modulates the key factors of pro-inflammation IL17A and receptor IL17RA for AVNFH cartilage repair.

4. Discussion

In the current study, ESWT for AVNFH induced modulation of pro-inflammatory cytokines and protection of the articular cartilage of the hip with avascularity of the femoral head. ESWT significantly protected the articular cartilage and

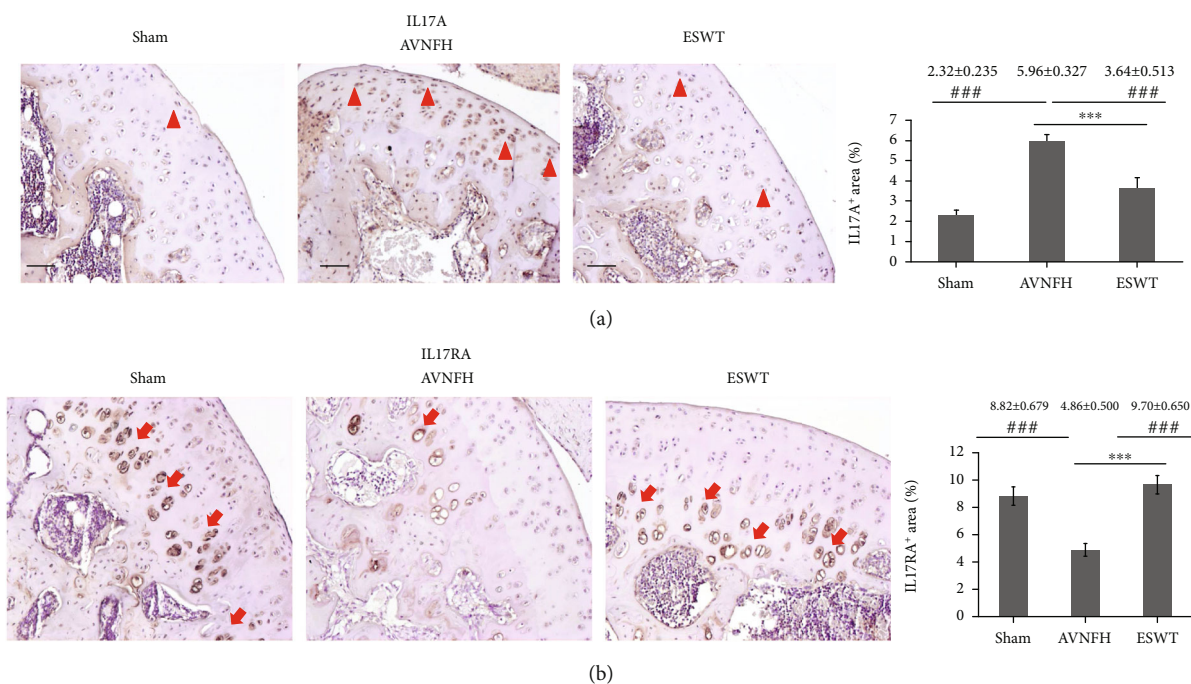


FIGURE 6: Immunohistochemical analysis for (a) IL17, (b) IL17RA in the articular cartilage of the left femur head (right), and the level of expression was measured after treatment (left). The expression of IL17A was major in superficial zone and proliferation zone (arrowhead), while IL17RA was major expressed in the hypertrophic chondrocytes of the calcified cartilage zone (arrow). *** $P < 0.001$ as compared with the ESWT group and ### $P < 0.001$ as compared with the AVNFH group. The scale bar was $50 \mu\text{m}$. $N = 8$ for all groups.

subchondral bone in AVNFH. The results of this study displayed that the expressions of inflammatory cytokines IL1- β , IL33, and IL17A were induced in AVNFH and were reduced after ESWT; in contrast, the receptors of IL33 and IL17A, ST2 and IL17RA, were reduced in the AVNFH and were induced after ESWT. The expressions of IL1- β , IL33, and IL17A cytokines, and their receptors ST2 and IL17RA, were elucidated in the articular cartilage of the AVNFH rat model following ESWT.

In the clinical studies, ESWT was demonstrated to promote bone repair and protect the femoral head in early-stage osteonecrosis [20, 33]. ESWT has been shown to increase osteogenic factors such as bone morphogenic proteins (BMPs), osteocalcin, alkaline phosphatase, and insulin-like growth factor, as well as osteogenic transcription factors such as core-binding factor crl-1 , Runt-related transcription factor 2, hypoxia-inducible factor 1- α , and vascular endothelial growth factor for bone remodeling [23, 24]. ESWT has also been shown to exert chondroprotective effects safely in animal models and in the clinical treatment of arthritis [25, 34]. The expressions of extracellular matrix proteins of the articular cartilage, including type II collagen, aggrecan, tenascin-C, and chitinase 3-like protein 1, are increased and the expression of the matrix metalloproteinases reduced after ESWT [25, 35]. In this study, the cellular matrix of the articular cartilage in AVNFH was protected by ESWT in a rat model (Figure 3). However, the collapse of the articular cartilage and repair in AVNFH rats after ESWT was not observed within the duration of this experiment; further study is required to elucidate and molecular mechanism of ESWT on the articular cartilage in AVNFH.

It has been reported that arthritis-related genes of IL1 β , IL6, and TNF α are expressed in the cartilage in AVNFH and could be potential biomarkers for AVNFH [36]. IL33 is a member of the IL1 family, and the level of IL33 in the serum has been reported to be related to the progression of AVNFH [37]. IL33 has also been proposed to be a key molecule in arthritis [38]; however, the expression of IL33 and its receptor ST2 in the articular cartilage of AVNFH are still unclear. The expressions of IL33 and ST2 in the articular cartilage of AVNFH and after ESWT were elucidated in this study. In addition, a high level of IL33 induces the expression of inflammatory cytokines IL1- β , IL6, IL13, and IL17, as well as matrix metalloproteinase (MMP)-3 and MMP-9 in arthritis [39]. The expression of ST2 affects the hypertrophic differentiation of chondrocyte and the expressions of hypertrophic markers such as Col X, OSC, VEGF, and MMP-13 [40]. Our results indicated that IL33 may induce an imbalance of cartilage anabolism in AVNFH, which is restored by ESWT. Further, ESWT could modulate the expression of ST2 to affect the function of hypertrophic chondrocyte in AVNFH. However, a detailed overview of the functions of IL33 and ST2 in the pathogenesis of AVNFH is still required for further investigation.

Recently, IL33 has been reported to be linked with IL17 in terms of contributing to immunological dysfunction in inflammatory diseases [41, 42]. The IL17 receptor is a complex that consists of IL17RA, IL17RB, IL17RC, IL17RD, and IL17RE [43]. IL17RA is a key component required for IL17A activity, and blocking of IL17 binding by IL17RA could inhibit the expression of IL-6 to prevent synovial inflammation in arthritis [44]. A high expression of IL17A

contributes to cartilage degradation by inducing disintegrin-like and metalloproteinase with thrombospondin motifs (ADAMTS) protease and matrix metalloprotease in the articular cartilage in arthritis [43]. A high expression of IL17A was observed in the hyaline cartilage, and receptor IL17RA was evaluated with regards to hypertrophy chondrocyte (Figure 6). It has been reported that IL17A is expressed in a paracrine manner in proliferating chondrocytes and spreads out to prehypertrophic cells during fracture healing [45]. However, IL17 receptor is mainly expressed in prehypertrophic chondrocytes during bone fracture healing. The different localizations of expressions of IL17A and IL17RA may be due to the repair mechanisms in different diseases, such as bone fracture healing or cartilage regeneration. There are few studies of the functions of IL17 and IL17RA axial signaling in the articular cartilage in AVNFB and after ESWT, and additional studies are needed to further validate their functions. Finally, this study was the first to show that ESWT modulated the expressions of IL33 and IL17A and their receptors ST2 and IL17RA, for repairing articular cartilage defects in AVNFB.

5. Conclusions

ESWT has been reported to have a good efficacy and safety for the clinical treatment of early AVNFB [46]; however, the mechanism of ESWT in the treatment of AVNFB is still unclear, especially with regard to immunomodulation. The results of this study displayed that ESWT affected the repair of the subchondral bone and articular cartilage in an animal model of AVNFB. In addition, ESWT modulated the expressions of IL1- β , pro-inflammatory cytokines IL33 and receptor ST2, and IL17A and receptor IL17RA to protect against loss of the extracellular matrix in the articular cartilage of AVNFB.

Data Availability

The data used to support the findings of this study are included within the article.

Conflicts of Interest

All authors declare that they have no conflict of interest.

Authors' Contributions

All authors were involved in drafting the article or revising it critically for important intellectual content, and all authors approved the final version to be published. JH Cheng and SL Shu conceptualized the study design and supervised the study. SW Jhan and HW Chiu performed the methodology and experiments. JH Cheng, CC Hsu, and HW Chiu analyzed the data and prepared the figures. JH Cheng and SL Shu wrote the manuscript and revised the manuscript.

Acknowledgments

We are grateful to the Center for Shockwave Medicine and Tissue Engineering and Department of Medical Research,

Kaohsiung Chang Gung Memorial Hospital, for supporting this work. Fund was received in total support for the research or clinical study presented in this article. The funding sources were from Chang Gung Research Fund (CMRPG8J0671, CLRPG8E0131).

References

- [1] Y. Zhang, L. Li, Z. J. Shi, J. Wang, and Z. H. Li, "Porous tantalum rod implant is an effective and safe choice for early-stage femoral head necrosis: a meta-analysis of clinical trials," *European Journal of Orthopaedic Surgery and Traumatology*, vol. 23, no. 2, pp. 211–217, 2013.
- [2] A. Rajpura, A. C. Wright, and T. N. Board, "Medical management of osteonecrosis of the hip: a review," *Hip International*, vol. 21, no. 4, pp. 385–392, 2011.
- [3] J. M. Aldridge 3rd and J. R. Urbaniak, "A vascular necrosis of the femoral head: etiology, pathophysiology, classification, and current treatment guidelines," *American Journal of Orthopedics (Belle Mead, N.J.)*, vol. 33, no. 7, pp. 327–332, 2004.
- [4] D. S. Hungerford, "Role of core decompression as treatment method for ischemic femur head necrosis," *Orthopade*, vol. 19, no. 4, pp. 219–223, 1990.
- [5] M. Ishizaka, M. Sofue, Y. Dohmae, N. Endo, and H. E. Takahashi, "Vascularized iliac bone graft for avascular necrosis of the femoral head," *Clinical Orthopaedics and Related Research*, vol. 337, pp. 140–148, 1997.
- [6] S. Y. Kim, Y. G. Kim, P. T. Kim, J. C. Ihn, B. C. Cho, and K. H. Koo, "Vascularized compared with nonvascularized fibular grafts for large osteonecrotic lesions of the femoral head," *The Journal of Bone and Joint Surgery. American Volume*, vol. 87, no. 9, pp. 2012–2018, 2005.
- [7] Y. Yasunaga, M. Ochi, Y. Ikuta, K. Shimogaki, and D. Dohi, "Rotational acetabular osteotomies: a rabbit model," *Archives of Orthopaedic and Trauma Surgery*, vol. 116, no. 1–2, pp. 74–76, 1997.
- [8] R. T. Steffen, N. A. Athanasou, H. S. Gill, and D. W. Murray, "Avascular necrosis associated with fracture of the femoral neck after hip resurfacing: histological assessment of femoral bone from retrieval specimens," *Journal of Bone and Joint Surgery. British Volume (London)*, vol. 92, no. 6, pp. 787–793, 2010.
- [9] A. P. Kaushik, A. Das, and Q. Cui, "Osteonecrosis of the femoral head: an update in year 2012," *World Journal of Orthopedics*, vol. 3, no. 5, pp. 49–57, 2012.
- [10] W. Fukushima, M. Fujioka, T. Kubo, A. Tamakoshi, M. Nagai, and Y. Hirota, "Nationwide epidemiologic survey of idiopathic osteonecrosis of the femoral head," *Clinical Orthopaedics and Related Research*, vol. 468, no. 10, pp. 2715–2724, 2010.
- [11] P. Yang, C. Bian, X. Huang, A. Shi, C. Wang, and K. Wang, "Core decompression in combination with nano-hydroxyapatite/polyamide 66 rod for the treatment of osteonecrosis of the femoral head," *Archives of Orthopaedic and Trauma Surgery*, vol. 134, no. 1, pp. 103–112, 2014.
- [12] M. A. Mont, J. J. Carbone, and A. C. Fairbank, "Core decompression versus nonoperative management for osteonecrosis of the hip," *Clin Orthop Relat Res*, vol. 324, pp. 169–178, 1996.
- [13] D. Liu, Q. Chen, Y. Chen, and Y. Liu, "Long-term follow-up of early-middle stage avascular necrosis of femoral head with core decompression and bone grafting," *Zhongguo Xiu Fu Chong Jian Wai Ke Za Zhi*, vol. 26, no. 10, pp. 1165–1168, 2012.

- [14] D. R. Marker, T. M. Seyler, S. D. Ulrich, S. Srivastava, and M. A. Mont, "Do modern techniques improve core decompression outcomes for hip osteonecrosis?," *Clinical Orthopaedics and Related Research*, vol. 466, no. 5, pp. 1093–1103, 2008.
- [15] M. C. Yoo, K. I. Kim, C. S. Hahn, and J. Parvizi, "Long-term followup of vascularized fibular grafting for femoral head necrosis," *Clinical Orthopaedics and Related Research*, vol. 466, no. 5, pp. 1133–1140, 2008.
- [16] T. Decker, B. Kuhne, and F. Gobel, "Extracorporeal shockwave therapy (ESWT) in epicondylitis humeri radialis. Short-term and intermediate-term results," *Orthopade*, vol. 31, no. 7, pp. 633–636, 2002.
- [17] J. Taylor, S. Dunkerley, D. Silver et al., "Extracorporeal shockwave therapy (ESWT) for refractory Achilles tendinopathy: a prospective audit with 2-year follow up," *The Foot*, vol. 26, pp. 23–29, 2016.
- [18] H. van der Worp, I. van den Akker-Scheek, H. van Schie, and J. Zwerver, "ESWT for tendinopathy: technology and clinical implications," *Knee Surgery, Sports Traumatology, Arthroscopy*, vol. 21, no. 6, pp. 1451–1458, 2013.
- [19] C.-J. Wang, "Extracorporeal shockwave therapy in musculoskeletal disorders," *Journal of Orthopaedic Surgery and Research*, vol. 7, no. 1, p. 11, 2012.
- [20] C. J. Wang, J. H. Cheng, C. C. Huang, H. K. Yip, and S. Russo, "Extracorporeal shockwave therapy for avascular necrosis of femoral head," *International Journal of Surgery*, vol. 24, no. - Part B, pp. 184–187, 2015.
- [21] C. J. Wang, J. H. Cheng, Y. R. Kuo, W. Schaden, and R. Mittermayr, "Extracorporeal shockwave therapy in diabetic foot ulcers," *International Journal of Surgery*, vol. 24, no. Part B, pp. 207–209, 2015.
- [22] G. Metzner, C. Dohnalek, and E. Aigner, "High-Energy extracorporeal shock-wave therapy (ESWT) for the treatment of chronic plantar fasciitis," *Foot & Ankle International*, vol. 31, no. 9, pp. 790–796, 2010.
- [23] D. Moya, S. Ramón, W. Schaden, C. J. Wang, L. Guiloff, and J. H. Cheng, "The role of extracorporeal shockwave treatment in musculoskeletal disorders," *Journal of Bone and Joint Surgery*, vol. 100, no. 3, pp. 251–263, 2018.
- [24] J.-H. Cheng and C.-J. Wang, "Biological mechanism of shockwave in bone," *International Journal of Surgery*, vol. 24, no. - Part B, pp. 143–146, 2015.
- [25] C.-J. Wang, L.-H. Weng, J.-Y. Ko, Y. C. Sun, Y. J. Yang, and F. S. Wang, "Extracorporeal shockwave therapy shows chondroprotective effects in osteoarthritic rat knee," *Archives of Orthopaedic and Trauma Surgery*, vol. 131, no. 8, pp. 1153–1158, 2011.
- [26] C. J. Wang, F. S. Wang, J. Y. Ko et al., "Extracorporeal shockwave therapy shows regeneration in hip necrosis," *Rheumatology*, vol. 47, no. 4, pp. 542–546, 2007.
- [27] C.-J. Wang, C.-C. Huang, J.-W. Wang, T. Wong, and Y. J. Yang, "Long-term results of extracorporeal shockwave therapy and core decompression in osteonecrosis of the femoral head with eight- to nine-year follow-up," *Biomedical Journal*, vol. 35, no. 6, pp. 481–485, 2012.
- [28] S. Saidi and D. Magne, "Interleukin-33: a novel player in osteonecrosis of the femoral head?," *Joint, Bone, Spine*, vol. 78, no. 6, pp. 550–554, 2011.
- [29] D. Zou, K. Zhang, Y. Yang et al., "Th17 i IL-17 osiągnają wyższe stężenia w przebiegu martwicy głowy kości udowej i są dodatnio skorelowane z nasileniem bólu," *Endokrynologia Polska*, vol. 69, no. 3, pp. 283–290, 2018.
- [30] J. Ma, W. Guo, Z. Li, B. Wang, S. Li, and P. Wang, "Hip osteonecrosis is associated with increased plasma IL-33 level," *Mediators of Inflammation*, vol. 2017, Article ID 1732638, 6 pages, 2017.
- [31] N. G. Sukubo, E. Tibalt, S. Respizzi, M. Locati, and M. C. d'Agostino, "Effect of shock waves on macrophages: a possible role in tissue regeneration and remodeling," *International Journal of Surgery*, vol. 24, no. Part B, pp. 124–130, 2015.
- [32] L. Amengual-Peñafiel, M. Jara-Sepúlveda, L. Parada-Pozas, F. Marchesani-Carrasco, R. Cartes-Velásquez, and B. Galdames-Gutiérrez, "Immunomodulation of osseointegration through extracorporeal shock wave therapy," *Dental Hypotheses*, vol. 9, no. 2, p. 45, 2018.
- [33] J. Ludwig, S. Lauber, H.-J. Lauber, U. Dreisilker, R. Radel, and H. Hotzinger, "High-energy shock wave treatment of femoral head necrosis in adults," *Clinical Orthopaedics and Related Research*, vol. 387, pp. 119–126, 2001.
- [34] Y. C. Wang, H. T. Huang, P. J. Huang, Z. M. Liu, and C. L. Shih, "Efficacy and safety of extracorporeal shockwave therapy for treatment of knee osteoarthritis: a systematic review and meta-analysis," *Pain Medicine*, vol. 21, no. 4, pp. 822–835, 2020.
- [35] S. Mayer-Wagner, J. Ernst, M. Maier et al., "The effect of high-energy extracorporeal shock waves on hyaline cartilage of adult rats in vivo," *Journal of Orthopaedic Research*, vol. 28, no. 8, pp. 1050–1056, 2010.
- [36] G. Chen, L. Zhong, Q. Wang et al., "The expression of chondrogenesis-related and arthritis-related genes in human ONFH cartilage with different Ficat stages," *PeerJ*, vol. 7, article e6306, 2019.
- [37] L. Zheng, W. Wang, J. Ni et al., "Plasma interleukin 33 level in patients with osteonecrosis of femoral head: an alarmin for osteonecrosis of the femoral head?," *Journal of Investigative Medicine*, vol. 62, no. 3, pp. 635–637, 2015.
- [38] Y. Li, Y. Fu, H. Chen, X. Liu, and M. Li, "Blocking Interleukin-33 alleviates the joint inflammation and inhibits the development of collagen-induced arthritis in mice," *Journal of Immunology Research*, vol. 2020, Article ID 4297354, 8 pages, 2020.
- [39] A. M. Miller, "Role of IL-33 in inflammation and disease," *Journal of Inflammation*, vol. 8, no. 1, p. 22, 2011.
- [40] E. Bonyadi Rad, G. Musumeci, K. Pichler et al., "Runx2 mediated induction of novel targets ST2 and Runx3 leads to cooperative regulation of hypertrophic differentiation in ATDC5 chondrocytes," *Scientific Reports*, vol. 7, no. 1, p. 17947, 2017.
- [41] K. N. Morrow, C. M. Coopersmith, and M. L. Ford, "IL-17, IL-27, and IL-33: a novel axis linked to immunological dysfunction during sepsis," *Frontiers in Immunology*, vol. 10, 2019.
- [42] R. K. Gupta, K. Gupta, and P. D. Dwivedi, "Pathophysiology of IL-33 and IL-17 in allergic disorders," *Cytokine & Growth Factor Reviews*, vol. 38, pp. 22–36, 2017.
- [43] D. Sinkeviciute, A. Aspberg, Y. He, A. C. Bay-Jensen, and P. Önnérjford, "Characterization of the interleukin-17 effect on articular cartilage in a translational model: an explorative study," *BMC Rheumatology*, vol. 4, no. 1, 2020.
- [44] L. Chen, D. Q. Li, J. Zhong et al., "IL-17RA aptamer-mediated repression of IL-6 inhibits synovium inflammation in a murine model of osteoarthritis," *Osteoarthritis and Cartilage*, vol. 19, no. 6, pp. 711–718, 2011.

- [45] T. Kokubu, D. R. Haudenschild, T. A. Moseley, L. Rose, and A. H. Reddi, "Immunolocalization of IL-17A, IL-17B, and their receptors in chondrocytes during fracture healing," *Journal of Histochemistry & Cytochemistry*, vol. 56, no. 2, pp. 89–95, 2008.
- [46] Q. Zhang, L. Liu, W. Sun, F. Gao, L. Cheng, and Z. Li, "Extracorporeal shockwave therapy in osteonecrosis of femoral head," *Medicine*, vol. 96, no. 4, article e5897, 2017.